UNIVERSITY OF BIRMINGHAM

Biomedical multi-materials bone scaffolds with tuneable properties using additive manufacturing

By

Abdullah Hanafi Mohammed

A thesis submitted to The University of Birmingham for the degree of

DOCTOR OF PHILOSOPHY

The School of Engineering

College of Engineering and Physical Sciences

University of Birmingham

June 2023

Abstract

Bone tissue engineering is a promising field that focuses on developing new techniques and materials for repairing or replacing damaged bones with bone scaffolds. Recently, 3D printing technologies have emerged as a feasible alternative to conventional manufacturing techniques, enabling the customization of bone scaffolds to meet individual patient needs. This technology has the potential to overcome the shortcomings of traditional approaches and provide better solutions for bone injuries by allowing for customized geometries, materials, and pore structures.

The structural properties of bone scaffolds, such as pore size and porosity, play a crucial role in their functionality in both *in vitro* and *in vivo* environments. In general, interconnected porous bone scaffolds that promote cell migration and proliferation are highly desirable. Polylactic acid (PLA) is a widely used biodegradable polymer in tissue engineering applications due to its favourable biocompatibility and mechanical properties. Calcium peroxide (CPO), which can release oxygen upon contact with water, is a valuable component in bone tissue engineering as increased oxygen levels can aid in promoting bone growth and healing.

In this thesis, a novel Fused Deposition Modelling (FDM) PLA/CPO composite filament was created through wet solution mixing and hot melt extrusion. The filaments were produced with different CPO ratios ranging from 1.5% to 24% and subjected to various physical analyses, including X-ray diffraction, surface morphology assessment, evaluation of filament extrudability and printability, microstructural analysis, and examination of rheological and mechanical properties.

The findings of the study indicated that increasing the CPO content resulted in changes in viscosity and microstructure, thereby influencing the mechanical strength and ductility of the composite filaments. However, it was found that the filament with 6% CPO content exhibited promising properties, including acceptable surface morphology and strength, making it suitable for 3D printing applications.

Additionally, the release of oxygen and calcium ions, generated porosity, antibacterial activities and cell culturing of the PLA/CPO composite filaments were assessed. The results revealed that among all the CPO ratios

investigated, the 6% CPO content exhibited optimal outcomes, including higher oxygen and calcium ions release, effective bacterial inhibition and exhibited differentiation to bone. These findings suggest that the PLA/CPO composite filament with 6% CPO content holds significant potential for enhancing bone generation by improving oxygenation of bone cells and providing resistance against bacterial infections.

Acknowledgements

I am deeply grateful to everyone who has supported me throughout this research journey and made this dissertation a reality.

First and foremost, I want to express my heartfelt appreciation to my supervisors, Prof. Khamis Essa and Dr. Hany Hassanin. Their unwavering guidance, support, and scholarly expertise have been invaluable in the development of this dissertation. I consider myself incredibly fortunate to have had their mentorship and knowledge throughout this process.

I would also like to extend my sincere thanks to the faculty members and researchers at the Center of Nanotechnology, King Abdulaziz University, Jeddah, Saudi Arabia. Their dedication to knowledge and excellence has been a tremendous source of inspiration for me. I am grateful for their commitment to fostering an environment that encourages intellectual curiosity and the pursuit of academic greatness.

The administrative staff and administrators at the University of Birmingham have been instrumental in facilitating the smooth progression of my research. I am grateful for their support, prompt responses, and organizational skills in navigating various administrative procedures and logistical arrangements.

To my family and friends, I owe a debt of gratitude for their unwavering support and understanding throughout my academic journey. Their love, encouragement, and belief in my abilities have been a constant source of motivation during moments of doubt. I am truly thankful for their presence in my life.

I would also like to acknowledge my fellow classmates and colleagues for their contributions. Our shared knowledge, intellectual discussions, and collaborative efforts have enriched my research experience and broadened my perspectives.

Last but not least, I want to express my deep appreciation to the participants who took part in my study. Their willingness to share their time, experiences, and expertise has been essential in generating meaningful insights and findings for this research. I am truly grateful for their invaluable contributions.

In conclusion, this dissertation would not have been possible without the support and encouragement of all the individuals mentioned above. Their collective efforts have played a pivotal role in shaping this research and my growth as a scholar. I am sincerely thankful for their contributions, and I hope that this dissertation can serve as a token of my gratitude for their unwavering support.

Thank you.

Abdullah Hanafi Mohammed

Table of Contents

List of Figures

List of Tables

List of Abbreviations

°C - Degree Celsius

µm - Micrometre

3D - Three-Dimensional

ABS - Acrylonitrile Butadiene Styrene

AM - Additive Manufacturing

ASTM - American Society for Testing and Materials

BCP - biphasic calcium phosphate

Ca - Calcium

CAD - Computer-Aided Design

CALPHAD - Calculation of Phase Diagrams

CAM - Computer-Aided Manufacturing

CMCs - Ceramic-Matrix Composites

CO_2 - Carbon Dioxide

COL1A1 - Collagen type I alpha 1 chain

CPC - Calcium Phosphate Cement

CPO - Calcium peroxide

CVD - Chemical Vapor Deposition

DCM - Dichloromethane

DED - Directed energy deposition

DLP - Digital Light Processing

E. coli - Escherichia coli

EDC - 1-ethyl-3-(3-dimethylaminopropyl) carbodiimide

EDX - Energy-Dispersive X-ray Spectroscopy

EMI - Electromagnetic Interference

FDA - Food and Drug Administration

FDM - Fused Deposition Modelling

Fe3O4 - Ferromagnetic Material

Fe-Mn - Iron-Manganese

FESEM - Field emission scanning electron microscopy

FGF - Fibroblast Growth Factor

GAPDH - Glyceraldehyde 3-phosphate dehydrogenase

GO - Graphene Oxide

GPa - Gigapascal

H_2O_2 - Hydrogen Peroxide

HA - Hyaluronic Acid

HA - Hydroxyapatite

hMSCs - Human Mesenchymal stem cells

hPRP - Human Platelet-Rich Plasma

HR-3 - Hybrid Rheometer

ICP - Inductively coupled plasma

ISO - International Organization for Standardization

KOSR - KnockOut™ Serum Replacement

L-PBF - Laser Powder Bed Fusion

MPa - Megapascal

MRSA - Methicillin-resistant Staphylococcus aureus

MSCs - Mesenchymal Stem Cells

Mw - Molecular weight

NaCl - sodium chloride

nHA - Nano-Hydroxyapatite

nm - Nanometers

PA - Pseudomonas aeruginosa

PBS - Phosphate Buffered Saline

PC - Polycarbonate

PCL - Polycaprolactone

PDGF - Platelet-Derived Growth Factor

PEG - polyethene-glycol

PEI - Polyetherimide

PGA - Poly(glycolic acid)

PHB - Polyhydroxybutyrate

PLA - Poly(lactic acid)

PLGA - Poly(lactic-co-glycolic acid)

PLLA - poly (L-lactic acid)

PPF - Polypropylene fumarate

PPSF - Polyphenylsulfone

PRP - Platelet-Rich Plasma

qRT-PCR - Quantitative Reverse Transcriptase Polymerase Chain Reaction

RGO - Reduced Graphene Oxide

RNA - Ribonucleic Acid

RUNX2 - Runt-related transcription factor 2

SA - Staphylococcus aureus

SD - Standard Deviation

SEM - scanning electron microscope

SL - Sheet lamination

SLA - Stereolithography

SLM - Selective Laser Melting

SLS - Selective Laser Sintering

SP7 - Sp7 transcription factor

SPP1 - Secreted phosphoprotein 1

STM - Spatial-Temporal Modulation

TCP - Tricalcium Phosphate

UV - Ultraviolet

VEGF - Vascular Endothelial Growth Factor

w/v - weight/volume

XRD - X-ray Diffraction

XTT - 2,3-Bis-(2-Methoxy-4-Nitro-5-Sulfophenyl)-2H-Tetrazolium-5-Carboxanili

List of Publications

- Mohammed, A.; Jiménez, A.; Bidare, P.; Elshaer, A.; Memić, A.; Hassanin, H.; Essa, K. Review on Engineering of Bone Scaffolds Using Conventional and Additive Manufacturing Technologies. *3D PRINTING AND ADDITIVE MANUFACTURING* **2023**, 06, 0360. Published in print.

- Mohammed, A.; Saeed, A.; Elshaer, A.; Melaibari, A.A.; Memić, A.; Hassanin, H.; Essa, K. Fabrication and Characterization of Oxygen-Generating Polylactic Acid/Calcium Peroxide Composite Filaments for Bone Scaffolds. *Pharmaceuticals* **2023**, *16*, 627. Published in print.

- Mohammed, A.H.; Kovacev, N.; Elshaer, A.; Melaibari, A.A.; Iqbal, J.; Hassanin, H.; Essa, K.; Memić, A. Preparation of Polylactic Acid/Calcium Peroxide Composite Filaments for Fused Deposition Modelling. *Polymers* **2023**, *15*, 2229. Published in print.

- Mohammed, A.; Tirnoveanu, A.; Webb, W.R.; Aslam, M.; Elshaer, A.; Hassanin, H.; Essa, K. Preparation and Characterisation of Poly Lactic Acid/Calcium Peroxide Composite 3D printed scaffold for Bone Tissue Engineering. *Biocybernetics and Biomedical Engineering.* Under review.

1 Chapter One: General Introduction

1.1 Introduction

1.1.1 Background

3D printing, also known as additive manufacturing, is a process of creating three-dimensional objects from a digital model by adding layers of material until the final object is created [1]. The process typically involves creating a digital model of the object using computer-aided design (CAD) software, preparing the digital model for printing using slicing software, and sending the prepared file to the 3D printer, which prints the object layer by layer using a variety of materials such as plastics, metals, and ceramics. There are several types of 3D printing techniques available in the market, each with its own unique capabilities and limitations. The most common type of 3D printer is the Fused Deposition Modelling (FDM) printer, which uses a filament of thermoplastic material to create objects layer by layer [2]. Another type of 3D printer is the Stereolithography (SLA) printer, which uses a liquid resin that is cured using a laser to create objects with high levels of detail and accuracy [3]. Other types of 3D printers include Selective Laser Sintering (SLS), Digital Light Processing (DLP), and Binder Jetting printers, each of which uses a different method for creating objects [4]. The choice of 3D printer depends on the specific requirements of the project, such as the size and complexity of the object, the desired level of detail, and the materials used [4]. 3D printing has become increasingly popular in recent years due to its versatility and potential for customization. The technology has been used in a wide range of industries, including aerospace, automotive, healthcare, and architecture. In aerospace, 3D printing has been used to create lightweight and complex components for aircraft and spacecraft [5]. In architecture, 3D printing has been used to create intricate and innovative structures and building components [6]. In healthcare, 3D printing has been used to create custom prosthetics and bone scaffolds that are tailored to individual patients [4]. With its ability to create complex shapes and structures quickly and

accurately, 3D printing is expected to continue to have a significant impact on a variety of fields. 3D printing has become a promising technique for fabricating bone scaffolds due to its ability to create complex geometries and customizable structures. The 3D printing process enables precise control over the architecture, pore size, and interconnectivity of the scaffold, which can greatly influence its mechanical properties and biological performance. Various materials have been used to create 3D printed bone scaffolds, including biodegradable polymers, ceramics, and composites [7].

Among all the 3D printing technologies Fused Deposition Modelling (FDM) is one of the most commonly used 3D printing technologies in the field of biomedicine, due to it is low cost and high speed [4]. FDM printers work by melting a thermoplastic filament and depositing it layer by layer onto a build platform to create a three-dimensional object [4]. The thermoplastic filament is fed through a heated extruder, which melts the material and extrudes it through a nozzle that moves along the X, Y, and Z axes to deposit the material in a precise pattern (Figure 1.1). One of the advantages of FDM is its ability to use a wide range of thermoplastic materials, such as acrylonitrile butadiene styrene (ABS) ($(C_8H_8)_x \cdot (C_4H_6)_y \cdot (C_3H_3N)_z$), polylactic acid (PLA) ($(C_3H_4O_2)_n$), and Polycaprolactone (PCL) ($(C_6H_{10}O_2)_n$), among others [8]. This versatility in materials allows for a range of functional applications, including prototyping, tooling, and even end-use parts in some cases. However, FDM has some limitations, such as its relatively low printing resolution, which can result in visible layer lines on the finished object, and its limited ability to create objects with intricate details or overhangs [9]. Additionally, FDM-printed parts can be prone to warping or deformation if the material is not properly heated and cooled during the printing process [10]. Despite these limitations, FDM remains a popular choice for 3D printing due to its accessibility, affordability, and ease of use, making it a widely adopted technology for both hobbyist and industrial applications. In the field of biomedical engineering, FDM has been extensively utilized to fabricate a variety of

scaffolds for tissue engineering and regenerative medicine applications [11]. For example, FDM has been used to create porous polymer scaffolds for bone tissue engineering using materials such as polycaprolactone (PCL) and PLA [12, 13]. FDM has also been used to fabricate scaffolds for diaphragmatic muscle reconstruction using a combination of PCL and gelatin [14].

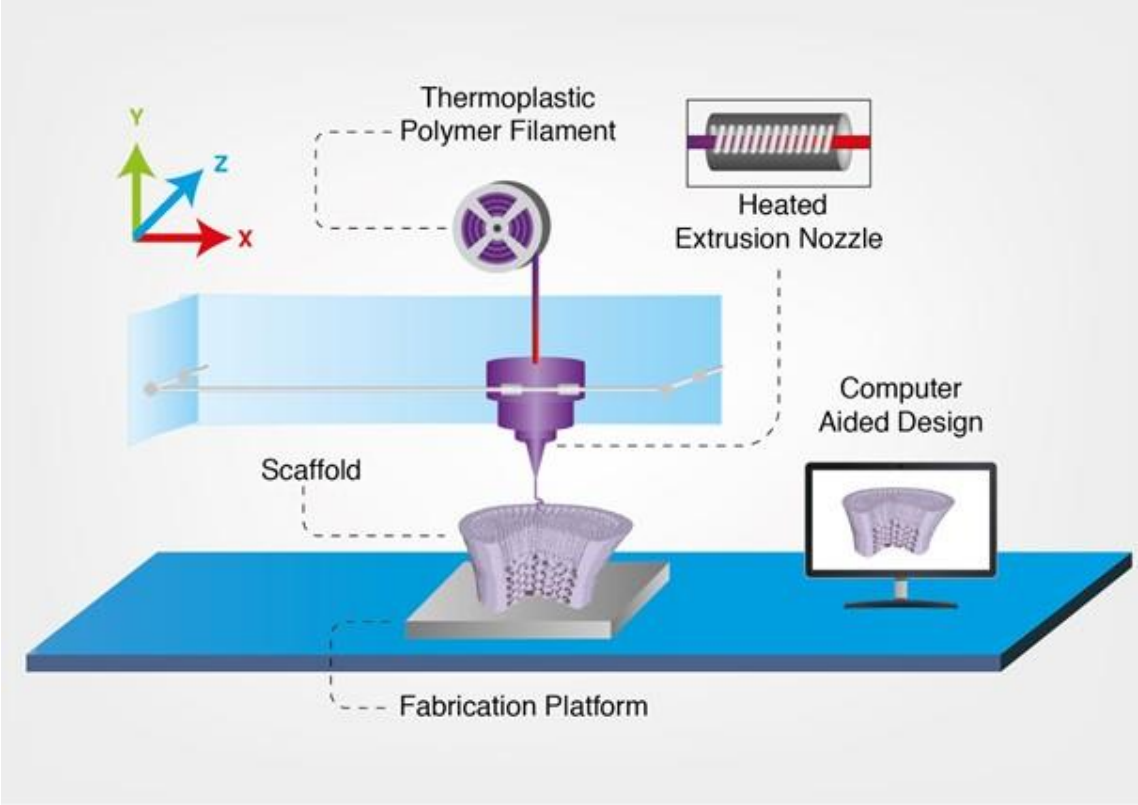

Figure 1.1. Fused Deposition Modelling (FDM) 3D printer process diagram.

Bone scaffolds are three-dimensional structures that are used to support and guide the growth of new bone tissue [15] . They are typically made of biocompatible materials and are designed to mimic the natural structure of bone (Figure 1.2). Bone scaffolds are important in bone tissue engineering because they can be used to repair or replace damaged or lost bone tissue. They provide a platform for cells to attach and grow, and they can be designed to degrade over time as new bone tissue forms. One major challenge is ensuring that the scaffold material is biocompatible and does not cause an immune response in the body [16]. Another challenge is

achieving the right balance between porosity and mechanical strength in the scaffold, which can influence the growth of new bone tissue [17]. Additionally, there is currently limited understanding of the long-term performance of 3D-printed bone scaffolds in the body [18]. The choice of material is critical to the success of 3D printing bone scaffolds, and several materials have been investigated for this purpose such as acrylonitrile butadiene styrene (ABS) ($(C_8H_8)_x \cdot (C_4H_6)_y \cdot (C_3H_3N)_z$), as polycaprolactone (PCL) ($(C_6H_{10}O_2)_n$) and polylactic acid (PLA) ($(C_3H_4O_2)_n$). PLA, in particular, has received considerable attention due to its biocompatibility, mechanical properties, and ease of use in FDM printing [19]. One study explored the use of PLA in combination with hydroxyapatite (HA) and tricalcium phosphate (TCP) to fabricate a 3D-printed scaffold for bone tissue engineering. The results showed that the addition of HA and TCP to other materials enhanced the mechanical properties and bioactivity of the scaffold, making it a promising candidate for bone tissue engineering applications [20]. Another study investigated the use of a PLA and PCL to create a composite scaffold with improved mechanical strength and biocompatibility for bone tissue engineering. The study results demonstrated that the composite scaffold showed enhanced cellular attachment and proliferation compared to pure PCL scaffolds [21]. Overall, the choice of material for 3D printing bone scaffolds must take into account factors such as biocompatibility, mechanical properties to be close to bone strength, and ability to be printed. PLA, with its favourable properties and ease of use, holds promise as a material for bone tissue engineering applications.

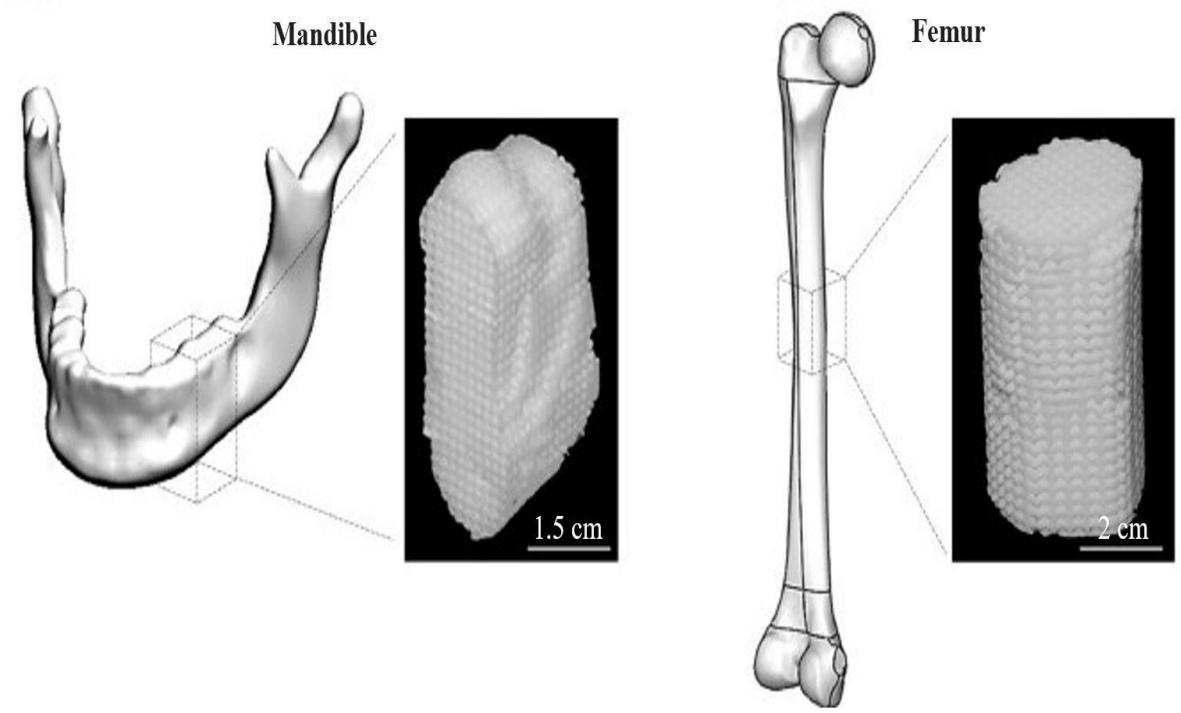

Figure 1.2. 3D printing of different parts of tissue engineering bone scaffold. Adopted from Mohammad Mirkhalaf [22].

1.1.2 Motivation

Bone scaffolds made from biodegradable polymers for tissue engineering have limitations in terms of mechanical strength and the promotion of vascularization. While existing 3D-printed bone scaffolds made from polymer materials such as polycaprolactone (PCL) ($(C_6H_{10}O_2)_n$), polyethylene glycol (PEG) ($C_{2n}H_{4n+2}O_{n+1}$), and poly(lactic-co-glycolic acid) (PLGA) ($C_5H_{10}O_6$) have shown promise in promoting vascularization, which is essential for supporting cell growth, they typically prioritize this function over mechanical strength, which is below 41 MPa [23]. For example, PCL-based scaffolds have good biocompatibility and can support cell growth, but their mechanical strength is limited [24]. On the other hand, PLA-based scaffolds have good mechanical strength of around 55 MPa, but may not support vascularization [25, 26]. Similarly, PLGA-based scaffolds have shown good biocompatibility, but their degradation may not be suitable for bone scaffolds applications [27]. Therefore, there is a clear need for a

biodegradable bone scaffold that can simultaneously promote mechanical strength and vascularization. Despite the promising outcomes in the field of bone scaffold research, its effectiveness is limited to addressing minor bone defects smaller than a few millimeters. This limitation primarily arises from inadequate vascularization, resulting in insufficient oxygen delivery [28]. In engineered tissues, the insufficient oxygen supply is a significant challenge, especially in the context of scaffold applications, where it is crucial for the viability and proliferation of cells attached to the scaffold [29]. Scientists have developed scaffolds that can generate oxygen by breaking down solid particles such as sodium percarbonate, magnesium peroxide, and calcium peroxide [29]. This study aims to address this challenge by developing a novel bone scaffold using PLA composed with calcium peroxide to enhance mechanical strength, while also promoting vascularization. The ultimate goal is to create a biodegradable bone scaffold that can support bone regeneration while also promoting vascularization, thus improving patient outcomes.

1.1.3 Aim and objectives

The aim of this research is to develop and optimize biodegradable composite materials filaments and a 3D printing method for creating bone scaffolds. Specifically, the study aims to investigate the impact of various material extruding and printing parameters such as temperature, speed, and infill density, as well as composite ratios on the mechanical properties and degradation behaviour of the printed scaffolds. Furthermore, the research seeks to evaluate the biocompatibility of the scaffolds with osteoblast cells and assess their potential for promoting bone tissue regeneration *in vitro*. Achieving these objectives will provide valuable insights into the development of effective and sustainable bone scaffolds for use in regenerative medicine applications.

1.1.3.1 Research objectives

1. Understanding the mechanism of bone fracture healing processes.
2. Defining the requirements for bone scaffold fabrication, such as materials, growth factors, designs, and manufacturing processes.
3. Identifying the appropriate bone scaffold materials and growth factor agents.
4. Identifying a 3D printing technique for bone scaffold fabrication.
5. Preparing the defined composite material.
6. Optimizing and characterizing the prepared composite material for morphological and mechanical properties.
7. Optimizing the 3D printing process for fabricating bone scaffold using the composite material.
8. Characterizing the printed scaffold for release, antibacterial activities and cell culturing.

The project's contributions are substantial and have the potential to bring about meaningful changes in the field of orthopaedic treatment. The development and refinement of materials and manufacturing processes used in orthopaedic treatments could lead to tangible improvements in patient outcomes. By finding innovative solutions for rigid orthopaedic treatments, the field of orthopaedics could experience advancements that may result in more comfortable and effective procedures for patients. In particular, the primary objective is to develop a new biodegradable bone scaffold that possesses superior mechanical strength and actively encourages vascularization. This innovative approach aims to create a biodegradable bone scaffold capable of not only facilitating bone regeneration but also promoting vascularization, with the ultimate goal of enhancing patient outcomes. One of the more

immediate and realistic outcomes of this project is the potential for cost reduction in orthopaedic treatments. The development of more efficient treatment methods can lead to cost savings for both healthcare institutions and patients. However, it's important to note that cost reduction is a complex process influenced by various factors, and achieving substantial changes may require a concerted effort across the healthcare system. In summary, while the project's contributions are promising, it's essential to acknowledge that real-world impacts often take time to materialize, and any advancements in the field of orthopaedics are likely to be gradual and incremental. Nonetheless, the potential benefits in terms of patient care and cost effectiveness make this research a worthwhile endeavour with the potential to make a positive difference in the future of orthopaedic treatment.

1.1.4 Thesis structure

The dissertation aims to investigate the development of biomedical implants using 3D printing technology for orthopaedic applications. The dissertation will be structured into six chapters. Chapter one will provide an introduction to the background and significance of the research, problem statement, aims, and objectives. Chapter two will review the literature on engineering of bone scaffolds using conventional and additive manufacturing technologies. This chapter is published and my contribution to this work was writing the original draft, conceptualization, methodology, formal analysis and data curation. The co-authors and other collaborators contributions were reviewing, conceptualization and supervision. Chapter three will be on investigation of fabricating composite filaments for Fused Deposition Modelling (FDM). This chapter is published and my contribution to this work was conceptualization, methodology, formal analysis, investigation, writing original draft and visualisation. The co-authors contributions were conceptualization, methodology, resources, writing-review, supervision and project administration. Other collaborators contributions were running some of the machines for characterisation under my supervision such as scanning electron microscope and

tensile testing machine. Chapter four will be on fabrication and characterization of oxygen generating poly(2-hydroxypropanoate)/calcium peroxide composite filaments for bone scaffolds. This chapter is published and my contribution to this work was conceptualization, methodology, formal analysis, investigation, writing original draft and visualisation. The co-authors contributions were conceptualization, methodology, resources, writing-review, supervision and project administration. Other collaborators contributions were running some of the machines for characterisation under my supervision such as scanning electron microscope and helping with preforming the antibacterial activity test. Chapter five will be on preparation and characterisation of poly lactic acid/calcium peroxide composite 3D printed scaffold for bone tissue engineering. This chapter is published and my contribution to this work was conceptualization, methodology, formal analysis, investigation, writing original draft and visualisation. The co-authors contributions were conceptualization, methodology, resources, writing-review, supervision and project administration. Other collaborators contributions were running some of the machines for characterisation under my supervision such as scanning electron microscope, tensile testing machine and helping with preforming the cells culturing for gene expansion experiment. Finally, the conclusion chapter will summarize the key findings of the research, highlight the contributions of the study, and discuss the potential for future research in the field.

1.2 References

[1] S. H. Huang, P. Liu, A. Mokasdar, and L. Hou, "Additive manufacturing and its societal impact: a literature review," *The International Journal of Advanced Manufacturing Technology,* vol. 67, no. 5, pp. 1191-1203, 2013/07/01 2013, doi: 10.1007/s00170-012-4558-5.

[2] N. R. Madhu, H. Erfani, S. Jadoun, M. Amir, Y. Thiagarajan, and N. P. S. Chauhan, "Fused deposition modelling approach using 3D printing and recycled industrial materials for a sustainable environment: a review," *The International Journal of Advanced Manufacturing Technology,* vol. 122, no. 5, pp. 2125-2138, 2022/09/01 2022, doi: 10.1007/s00170-022-10048-y.

[3] J. Huang, Q. Qin, and J. Wang, "A Review of Stereolithography: Processes and Systems," *Processes*, vol. 8, no. 9*,* doi: 10.3390/pr8091138.

[4] A. Mohammed, A. Elshaer, P. Sareh, M. Elsayed, and H. Hassanin, "Additive manufacturing technologies for drug delivery applications," *International Journal of Pharmaceutics,* vol. 580, p. 119245, 2020.

[5] M. S. Karkun and S. Dharmalingam, "3D Printing Technology in Aerospace Industry–A Review," *International Journal of Aviation, Aeronautics, and Aerospace,* vol. 9, no. 2, p. 4, 2022.

[6] M. Sakin and Y. C. Kiroglu, "3D Printing of Buildings: Construction of the Sustainable Houses of the Future by BIM," *Energy Procedia,* vol. 134, pp. 702-711, 2017/10/01/ 2017, doi: https://doi.org/10.1016/j.egypro.2017.09.562.

[7] M. Bahraminasab, "Challenges on optimization of 3D-printed bone scaffolds," *BioMedical Engineering OnLine,* vol. 19, no. 1, p. 69, 2020/09/03 2020, doi: 10.1186/s12938-020-00810-2.

[8] P. Dudek, "FDM 3D printing technology in manufacturing composite elements," *Archives of metallurgy and materials,* vol. 58, no. 4, pp. 1415--1418, 2013.

[9] R. F. Quero, G. D. da Silveira, J. A. F. da Silva, and D. P. de Jesus, "Understanding and improving FDM 3D printing to fabricate high-resolution and optically transparent microfluidic devices," *Lab on a Chip,* vol. 21, no. 19, pp. 3715-3729, 2021.

[10] J. Ramian, J. Ramian, and D. Dziob, "Thermal Deformations of Thermoplast during 3D Printing: Warping in the Case of ABS," (in eng), *Materials (Basel),* vol. 14, no. 22, Nov 21 2021, doi: 10.3390/ma14227070.

[11] R. Winarso, P. W. Anggoro, R. Ismail, J. Jamari, and A. P. Bayuseno, "Application of fused deposition modeling (FDM) on bone scaffold manufacturing process: A review," (in eng), *Heliyon,* vol. 8, no. 11, p. e11701, Nov 2022, doi: 10.1016/j.heliyon.2022.e11701.

[12] Z. Jiao, B. Luo, S. Xiang, H. Ma, Y. Yu, and W. Yang, "3D printing of HA / PCL composite tissue engineering scaffolds," *Advanced Industrial and Engineering Polymer Research,* vol. 2, no. 4, pp. 196-202, 2019/10/01/ 2019, doi: https://doi.org/10.1016/j.aiepr.2019.09.003.

[13] A. Grémare *et al.*, "Characterization of printed PLA scaffolds for bone tissue engineering," *Journal of Biomedical Materials Research Part A,* vol. 106, no. 4, pp. 887-894, 2018, doi: https://doi.org/10.1002/jbm.a.36289.

[14] T. Navaei, P. B. Milan, A. Samadikuchaksaraei, H. R. Davari, J. G. Hardy, and M. Mozafari, "Design and fabrication of polycaprolactone/gelatin composite scaffolds for diaphragmatic muscle reconstruction," *Journal of Tissue Engineering and Regenerative Medicine,* vol. 15, no. 1, pp. 78-87, 2021, doi: https://doi.org/10.1002/term.3151.

[15] A. G. Abdelaziz *et al.*, "A Review of 3D Polymeric Scaffolds for Bone Tissue Engineering: Principles, Fabrication Techniques, Immunomodulatory Roles, and Challenges," *Bioengineering*, vol. 10, no. 2*,* doi: 10.3390/bioengineering10020204.

[16] A. B. Gardner, S. K. Lee, E. C. Woods, and A. P. Acharya, "Biomaterials-based modulation of the immune system," (in eng), *Biomed Res Int,* vol. 2013, p. 732182, 2013, doi: 10.1155/2013/732182.

[17] Q. L. Loh and C. Choong, "Three-dimensional scaffolds for tissue engineering applications: role of porosity and pore size," (in eng), *Tissue Eng Part B Rev,* vol. 19, no. 6, pp. 485-502, Dec 2013, doi: 10.1089/ten.TEB.2012.0437.

[18] Z. Li, Q. Wang, and G. Liu, "A Review of 3D Printed Bone Implants," (in eng), *Micromachines (Basel),* vol. 13, no. 4, Mar 27 2022, doi: 10.3390/mi13040528.

[19] Y. Chen, T. Lu, L. Li, H. Zhang, H. Wang, and F. Ke, "Fully biodegradable PLA composite with improved mechanical properties via 3D printing," *Materials Letters,* vol. 331, p. 133543, 2023/01/15/ 2023, doi: https://doi.org/10.1016/j.matlet.2022.133543.

[20] E. H. Backes *et al.*, "Engineering 3D printed bioactive composite scaffolds based on the combination of aliphatic polyester and calcium phosphates for bone tissue regeneration," *Materials Science and Engineering: C,* vol. 122, p. 111928, 2021/03/01/ 2021, doi: https://doi.org/10.1016/j.msec.2021.111928.

[21] T. Patrício, M. Domingos, A. Gloria, U. D'Amora, J. F. Coelho, and P. J. Bártolo, "Fabrication and characterisation of PCL and PCL/PLA scaffolds for tissue engineering," *Rapid Prototyping Journal,* vol. 20, no. 2, pp. 145-156, 2014.

[22] M. Mirkhalaf, A. Dao, A. Schindeler, D. G. Little, C. R. Dunstan, and H. Zreiqat, "Personalized Baghdadite scaffolds: stereolithography, mechanics and in vivo testing," *Acta Biomaterialia,* vol. 132, pp. 217-226, 2021/09/15/ 2021, doi: https://doi.org/10.1016/j.actbio.2021.03.012.

[23] Z. Wang *et al.*, "Tough, Transparent, 3D-Printable, and Self-Healing Poly(ethylene glycol)-Gel (PEGgel)," *Advanced Materials,* vol. 34, no. 11, p. 2107791, 2022, doi: https://doi.org/10.1002/adma.202107791.

[24] M. Abedalwafa, F. Wang, L. Wang, and C. Li, "Biodegradable poly-epsilon-caprolactone (PCL) for tissue engineering applications: A review," *Rev. Adv. Mater. Sci,* vol. 34, no. 2, pp. 123-140, 2013.

[25] A. Gregor *et al.*, "Designing of PLA scaffolds for bone tissue replacement fabricated by ordinary commercial 3D printer," (in eng), *J Biol Eng,* vol. 11, p. 31, 2017, doi: 10.1186/s13036-017-0074-3.

[26] A. H. Mohammed *et al.*, "Preparation of polylactic acid/calcium peroxide composite filaments for fused deposition modelling," *Polymers,* vol. 15, no. 9, p. 2229, 2023.

[27] W. Ji *et al.*, "Biocompatibility and degradation characteristics of PLGA-based electrospun nanofibrous scaffolds with nanoapatite incorporation," *Biomaterials,* vol. 33, no. 28, pp. 6604-6614, 2012/10/01/ 2012, doi: https://doi.org/10.1016/j.biomaterials.2012.06.018.

[28] M. Gholipourmalekabadi, S. Zhao, B. S. Harrison, M. Mozafari, and A. M. Seifalian, "Oxygen-Generating Biomaterials: A New, Viable Paradigm for Tissue Engineering?," (in eng), Trends Biotechnol, vol. 34, no. 12, pp. 1010-1021, Dec 2016, doi: 10.1016/j.tibtech.2016.05.012.

[29] R. Augustine, M. Gezek, N. Seray Bostanci, A. Nguyen, and G. Camci-Unal, "Oxygen-Generating Scaffolds: One Step Closer to the Clinical Translation of Tissue Engineered Products," (in eng), Chem Eng J, vol. 455, no. Pt 2, Jan 1 2023, doi: 10.1016/j.cej.2022.140783.

2 Chapter Two: Review on Engineering of Bone Scaffolds Using Conventional and Additive Manufacturing Technologies

---

Abdullah Mohammed [1], Amaia Jiménez [2], Prveen Bidare [1], Amr Elshaer [3], Adnan Memic [4], Hany Hassanin [5], Khamis Essa [1*]

1. School of Engineering, University of Birmingham, Birmingham B15 2TT
2. Universidad de Navarra, TECNUN Escuela de Ingeniería, Manuel de Lardizábal 15, 20018, San Sebastián, Spain
3. Drug Discovery, Delivery and Patient Care (DDDPC), School of Life Sciences, Pharmacy and Chemistry, Kingston University London, Kingston Upon Thames, Surrey, KT1 2EE, UK
4. Center of Nanotechnology, King Abdulaziz University, Jeddah 21589, Saudi Arabia
5. School of Engineering, Technology, and Design, Canterbury Christ Church University, Canterbury CT1 1QU, UK

Authorship contribution statement

Abdullah Mohammed: Writing - Original Draft, Conceptualization, Methodology, Formal analysis, Data Curation. Amaia Jiménez: Writing - Review & Editing. Prveen Bidare: Writing - Review & Editing. Amr Elshaer: Conceptualization. Adnan Memic: Review Hany Hassanin: Supervision, Project administration. Khamis Essa: Supervision.

2.1 Abstract

Bone is a complex connective tissue that serves as mechanical and structural support for the human body. Bones' fractures are common, and the healing process is physiologically complex and involves both mechanical and biological aspects. Tissue engineering of bone scaffolds holds great promise for the future treatment of bone injuries. However, conventional technologies to prepare bone scaffolds can not provide the required properties of human bones. Over the past decade, three-dimensional printing or additive manufacturing technologies have enabled the control over the creation of bone scaffolds with personalized geometries, appropriate materials and tailored pores. This paper aims to review the recent advances in the fabrication of bone scaffolds for bone repair and regeneration. A detailed review of bone fracture repair and an in-depth discussion on conventional manufacturing and three-dimensional printing techniques are introduced with an emphasis on novel studies concepts, potentials and limitations.

2.2 Introduction

Bone injuries have recently increased due to ageing, traumatic injuries, and congenital diseases, making them a global health issue. It is estimated that the number of people aged more than 65 years will increase from 323 million to 1.55 billion by 2050 worldwide [1]. Age intensifies the risk of osteoporosis and consequently has dangerous effects on people's healthy life, disability, countries' healthcare systems, and loss of productivity. Globally, over 200 million people have osteoporosis, with an increased number of patients receiving hospital treatment every year due to fragility fractures and bone loss, accelerating the demand for bone tissue surgeries [2]. Efficient and cost-effective strategies to treat bone injuries will help to improve people's quality of life and relief the economic burden on governments [3].

A bone defect is generally defined as the lack of bone tissue in an area of the body, which results in pseudarthrosis. Usually, the human body is capable of self-repair, yet when a segmental bone fracture exceeds a size of 10 mm, the body fails to self-repair [4]. Therefore, external interventions are essential to assist in the self-repairing process by creating bone scaffolds. These scaffolds act as bridges over bone defect sites and facilitate repair [5]. The design of the bone substitutes must be controlled to avoid excessive bone tissue removal at defect sites and to allow cell activity and proliferation [3,5]. The latter is facilitated by designing a scaffold with a porous and linked pore structure. Thus, manufactured bone scaffolds are a promising solution for treating bone fractures, but this comes with some challenges.

Regarding bone scaffolds manufacturing techniques, several methods have been investigated to create porous scaffolds for bone repair, such as salt leaching, gas foaming, self-assembly, phase separation, electrospinning, and freeze drying methods. Although these approaches are capable of fabricating porous structures, they have certain drawbacks, such as restricted pore structure control and a limited ability to customise for particular defect sites [7]. Additionally, many of these techniques leave behind organic residues of the pore-forming agent, impairing the scaffolds' biological characteristics and lowering the quality of bone healing. Thus, developing fabrication techniques for scaffolds that are not restricted to obtaining the desired

external shape but also precisely control the pore structure is critical for their future orthopaedic application.

Given this context, additive manufacturing (AM) technologies are becoming a good alternative for manufacturing scaffolds as they can create porous scaffolds with customised external design and a porous inner structure [8]. The use of 3D printing technology for the generation of bone scaffolds has been gaining more attention from researchers and the biomedical industry

in recent years. The near future of bone regeneration and healing is closely linked to developments in tissue engineering. Polytherapy, which combines scaffolds, stem cells, and healing promoters with new advances in tissue-engineered constructs in three-dimensional printing, may be capable of overcoming current challenges in treating bone injuries. In this review paper, we will focus on scaffolds as an established treatment for bone fracture using 3D printing technologies and compare them with conventional manufacturing techniques (Figure 2.1).

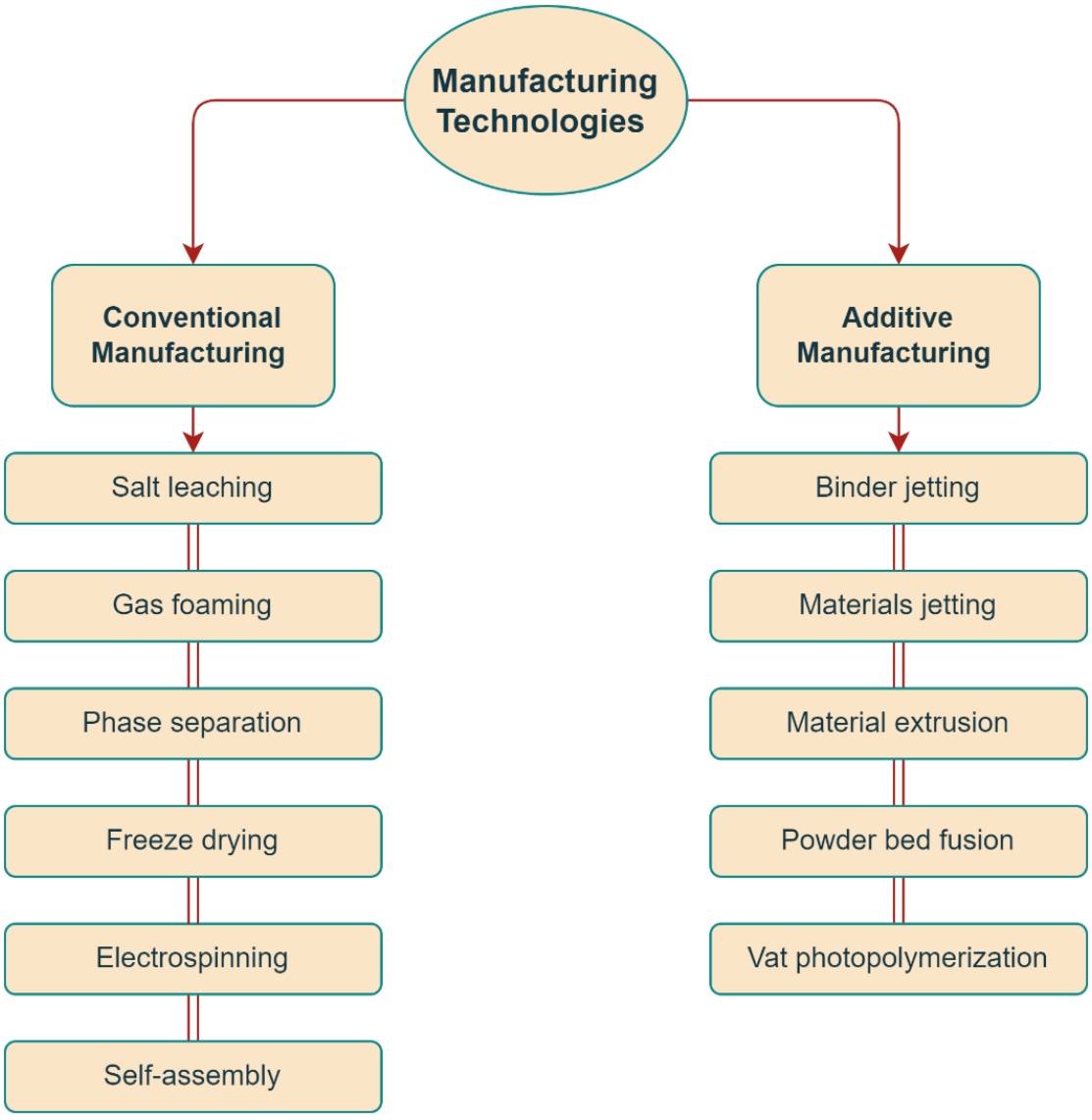

Figure 2.1. Flowchart of manufacturing technologies.

2.3 Bone Fracture Repair

Bone tissue can undergo biological remodelling as a function of a dynamic process that involves osteoclasts absorbing mature bone tissue and osteoblasts forming new bone tissue [9,10]. Bone is a complex connective tissue made up of osteoblasts, osteocytes, bone lining cells, and osteoclasts. The outer layers of bones are mineralised, giving them significant strength and rigidity to support the body structure and allow skeletal movement. Bones composition includes the inorganic phase (60% - 70% of the tissue), (22% - 35%) organic matrix and liquid (5% –8%), where collagen represents the majority of the organic matrix and only 10% non-collagenous proteins [11]. Bones strength and stiffness are mainly provided by hydroxyapatite crystal ($Ca_{10}(PO_4)_6(OH)_2$) with carbonate ions [12], which are found within and between collagen fibres in the form of needles, plates and rods with an average diameter of 20–80 nm and 2–5 nm in thickness [11]. Bone can also modify its structure according to body requirements, such as in repair, modelling, remodelling, and growth [13,14].

Bone tissues can be classified into cortical and trabecular (Figure 2.2). Both have the same matrix composition; however, they vary in structure and function as well as in relative distribution between bones. Cortical bone (dense or compact) is composed of layers surrounded by lamellar bone and vascular channels. This arrangement is known as the Haversian or osteon [15]. An osteon's central channel contains cells, vessels, nerves, and osteon-connecting Volkmann's channels [15]. On the other hand, trabecular bone (spongy or cancellous) is located in the epiphysis and metaphysis of long bones and inside small or flat bones. Trabecular bone has a wide network of individual trabeculae, small and interconnected plates and rods guided by external loading [15]. Typically, cortical and trabecular bones have Young's moduli of approximately 17 and 1 GPa, respectively [15]. Cortical bone is a dense structure representing about 80% of the total skeletal tissue. Yet, cortical bones have some microscopic pores (about 10% of the total cortical bone volume) to allow vascular and neural supply and enable the

delivery of nutrients [16]. The porosity of cortical bone is critical as an increase in intracortical porosity can reduce the bone strength and consequently increase the chances of fracture [17].

It is evident that cortical bone becomes more fragile at around 2% strain levels reflecting high-impact trauma (Figure 2.3) [15]. As the strain rate increases, cortical bone shows a ductile to brittle transition [18], and like any material, the cortical bone could be prone to fatigue failure.

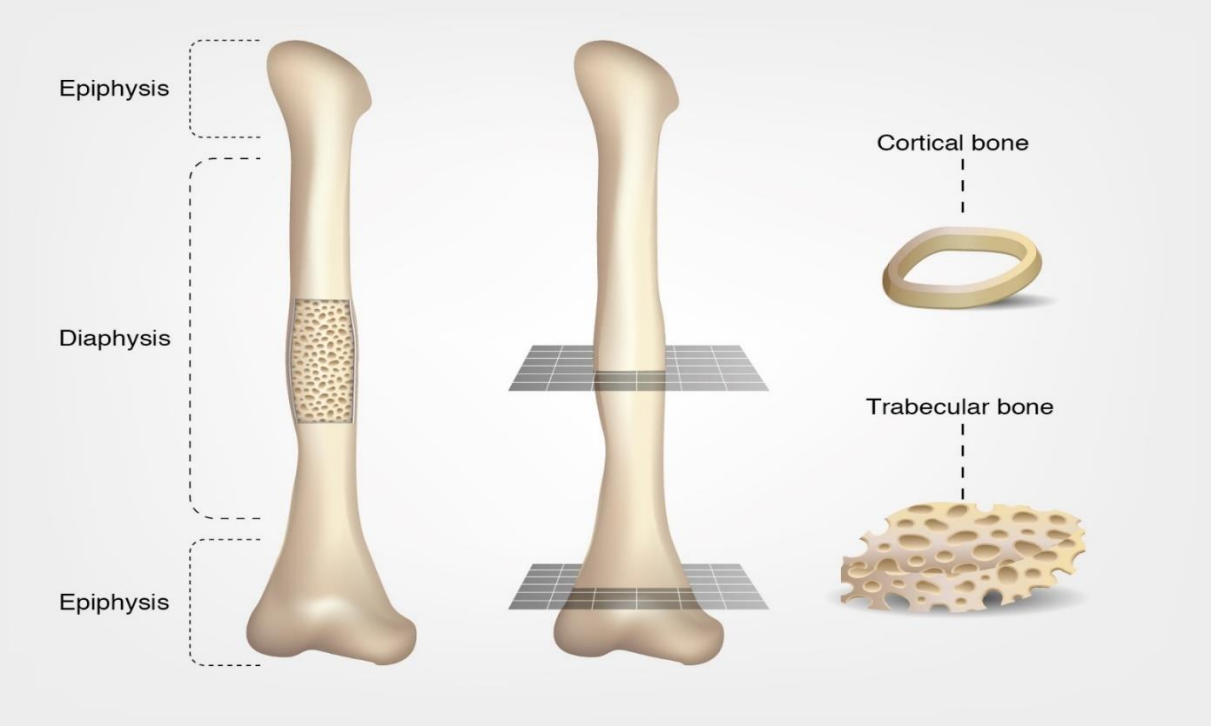

Figure 2.2. A long bone's macroscopic structure.

On the other hand, trabecular bone has a lower mass and high porosity when compared to cortical bone. Pores represent 50%-90% of total trabecular bone volume [19]. This makes it considered an open cell porous foam with a reduced compressive strength to about one-tenth of the cortical bone [20]. It does, however, provide a large surface area that is necessary for red bone marrow, blood vessels and bone-connected tissues and facilitates hematopoiesis and

homeostasis of minerals. The trabecular bone's physical and mechanical properties vary widely depending largely on the anatomical location, age and orientation of the cell structures [21,22]. Depending on the type and orientation of these basic cell structures, the mechanical properties can differ by a factor of 10. A comparison between the compressive properties of trabecular and cortical bones is shown in (Figure 2.3) [15]. As shown, the cortical bone acts as a typical brittle material at which the stress steeply increases at a low strain in the elastic region, and the fracture occurs without a noticeable change in the strain.

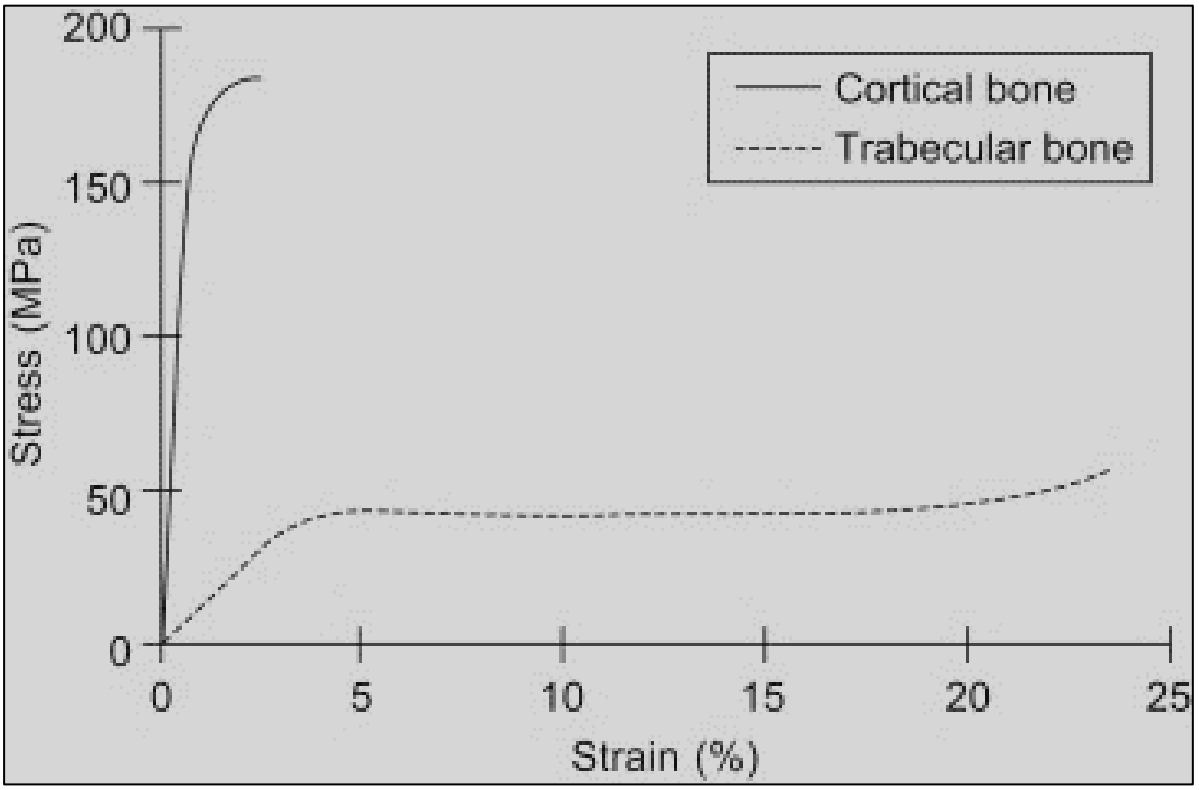

Figure 2.3. A comparison between the stress-strain properties of trabecular and cortical bones. Adapted from Damien Lacroix [15].

On the other hand, trabecular undergoes a ductile behaviour under compression loading with a substantial increase in the plastic deformation before fracture. Individual trabeculae bone damage and repair is a physiological process that occurs throughout life and increases with age [23].

Bone fracture healing process can be enhanced using several techniques, such as grafts, which replace defected bone with another bone from the patient's own body (autografts) or from a donor, or by using healing growth materials in fabricating bone implants or scaffolds [24]. Autografts are currently the bone regeneration golden standard [24]. However, Autografts techniques have several disadvantages, such as surgical complications and the limited supply of natural tissue. Tissue-engineered bone scaffolds are a suitable alternative to autografts as they improve fracture healing and enhance the incorporation of grafts [25,26]. Requirements of tissue-engineered scaffolds are to have properties close to those of autografts irrespective of their limitations [27].

Bone scaffolds need to have high porosity with sufficient sizes of pores around 100 μm across all sites of the scaffold in order to create an ideal environment for the formation of new tissue matrix and bone [17]. Moreover, growth factors like the basic growth factor of fibroblasts [28,29] can influence cell functions, proliferation, or differentiation. Promotive healing agents, for example, Human platelet-rich plasma (hPRP); [30-32] and also Tarantula cubensis extract, [33] could be incorporated into the scaffolds to improve the damaged connective tissue's ability to repair.

The scaffold's vascularity is important as if not present, ischemia will occur in the scaffold, and hence the cells would die. Therefore, it would be useful to incorporate growth factors such as FGF, PDGF, and VEGF to promote angiogenesis in scaffolds and grafts [34,35]. A combination of stem cells and scaffolds with growth factors can be one possible approach providing all the required characteristics to enhance bone repair and regeneration. Currently, none of the grafts provided all the desirable requirements such as biocompatibility, size limitation, cost, osteogenic, osteoconductive, osteoinductive, and angiogenic properties (Table 2.1), tissue engineering seeks to provide all or most of these characteristics [36,37]. Also, tissue engineering can cause bone defects to be repaired and reconstructed [27]. Incorporating the

basics of orthopaedic surgery with knowledge from various sciences such as biology, engineering, chemistry, materials science and physics could overcome current treatments' shortcomings [25]. Advances in biomaterials and tissue engineering can provide more appropriate tools to support the differentiation and proliferation of bone cells and improve bone fracture healing. While numerous studies in the literature examine the effects of various agents on bone healing, it is essential to also investigate the most effective manufacturing methods for fabricating the desired scaffolds [38-40].

Table 2.1. Terms, definitions and examples of bone repair [40].

Term's	Definitions	Examples
Osteogenesis	The process by which new bone is synthesised using donor cells taken either from the host or the graft donor.	Stem cell, autografts transplants
Osteoconduction	The passive ingrowth of host vasculature, tissue, and cells into an implanted scaffold.	Phosphate cements or calcium sulphate resorption
Osteoinduction	Exogenous growth factors enable host mesenchymal stem cells (MSCs) to differentiate into osteoblasts and chondroblasts capable of producing new bone.	Proteins involved in bone morphogenesis

2.4 Conventional manufacturing techniques

Conventional techniques used to prepare bone scaffolds are based on subtractive procedures to get the desired shape by removing sections of the material from an original block. The inability

to manage complex shapes and geometries, as well as to incorporate interior architecture, cavities or curved channels, is a major disadvantage of these techniques [41]. This is of special importance in the biomedical industry, where complex and organic shapes are usually needed for the implants to fit well. Additionally, cell viability and function can be affected by the use of organic solvents, even if only residues remain [42]. In order to obtain those geometries, until now, several conventional manufacturing methods, such as salt leaching, gas formation, phase separation, freeze drying, electrospinning, and self-assembly, have been employed in the fabrication of porous bone scaffolds despite their limitations (Figure 2.4). The principles of each procedure are covered in the following sections. The prevalence of research on each technique is summarised in (Figure 2.5), it is evident that more phase separation technique has attracted the attention of researchers over the last 10 years.

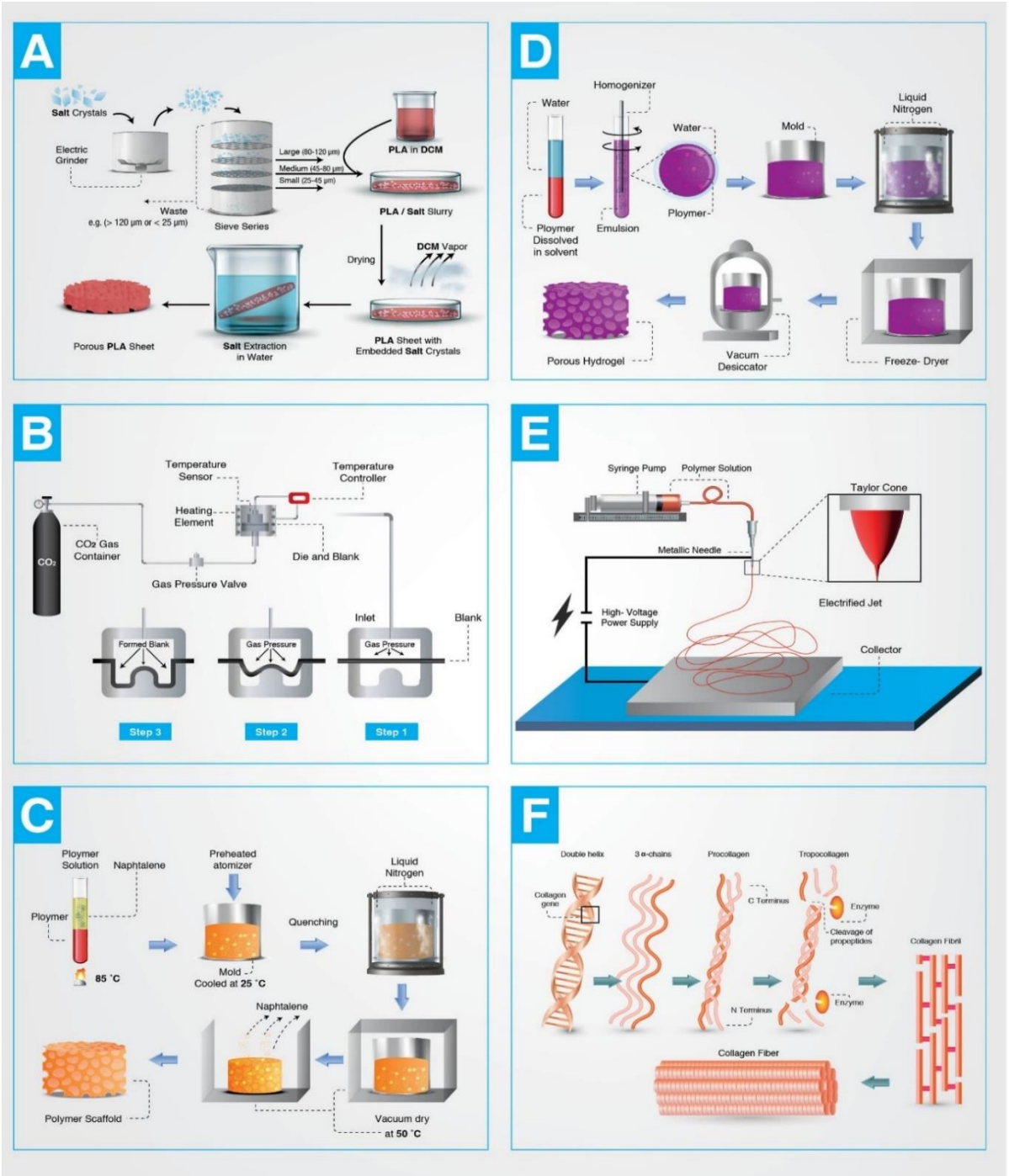

Figure 2.4. Conventional manufacturing techniques of bone scaffolds, (a) Salt leaching, (b) Gas forming, (c) Phase separation, (d) Freeze drying, (e) Electrospinning and (f) Self-assembly. . CO2, carbon dioxide; DCM, Dichloromethane; PLA, poly-L-lactide.

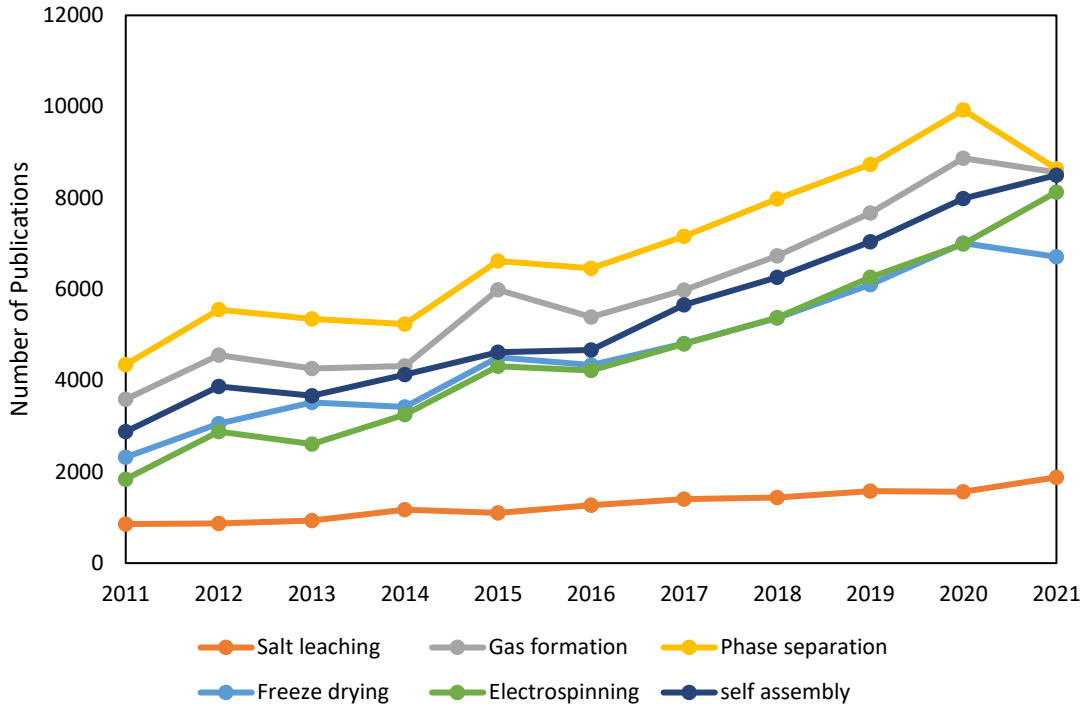

Figure 2.5. Number of papers published on bone scaffold fabricated by each conventional manufacturing technique over the last 10 years.

2.4.1 Salt leaching

This process was widely used in the manufacture of tissue-based scaffolds. In this technique, salt crystals or porogen (e.g. sodium chloride) are put in a mould, and the remaining gaps are filled with a polymer. The polymer is then solidified, and salt crystals are dissolved in a suitable solvent like alcohol or water by dissolution [43-45]. After all the salt leaches out, a solidified polymer with porosity is created, as illustrated in (Figure 2.4a) [46].

β-chitin and collagen have been successfully used to prepare membranes using salt leaching technique. The prepared membranes achieved a porosity of 77.81% and an average pore size of 260-330 μm. β-chitin membranes were prepared with NaCl salt-leaching, and then collagen solution crossed membranes by lyophilisation at −75 °C (Figure 2.6a-b) shows the scaffold's cross-sectional and surface morphologies. *In vitro* cell culture demonstrated that the human

fibroblasts attached to the collagen sites after 3 days, and proliferation took place within 14 days of cultivation [47].

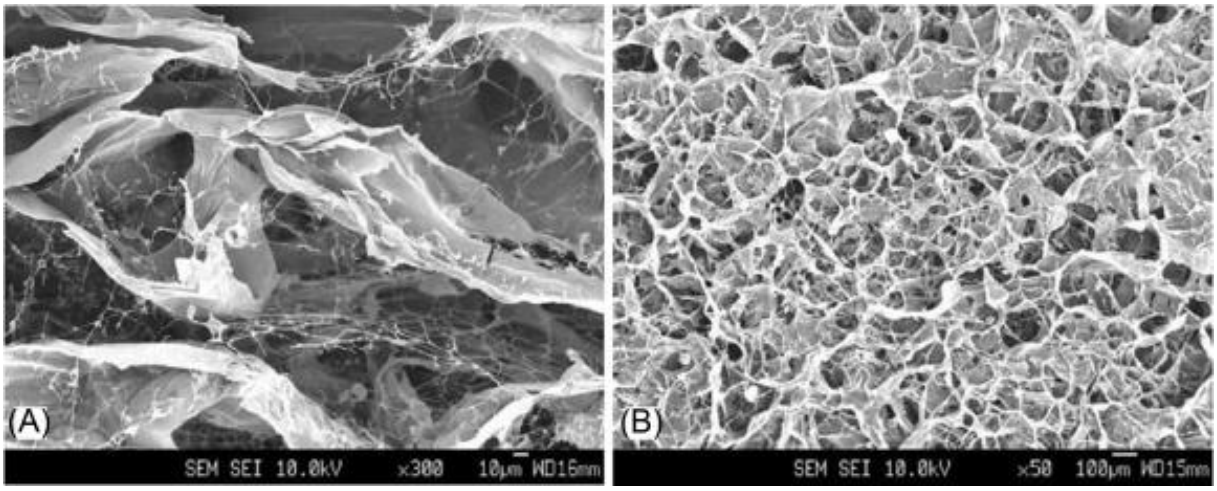

Figure 2.6. Collagen-coated chitin scaffold morphologies: (a) cross-section and (b) surface. Adopted from Sang Bong Lee [47].

The salt leaching technique enables the customisation of the pore size by adjusting the porogen size employed. It is also possible to control the porosity and pore size of the scaffold by manipulating the concentration and size of the salt particles used, respectively [43,48]. Despite the mentioned benefits of salt leaching for scaffold fabrication, this process has some limitations. For instance, it is not possible to control the pore distribution or the shape of scaffolds created [43]. Another drawback, this technique requires scaffolding to be manufactured only in the form of tubes and flat sheets, which means that it is ideal only for the manufacture of membrane scaffolds. Besides, the use of organic solvents can negatively impact the viability of cells and their biological functions [49]. Although the residues of any cytotoxic solvents could be detected [50], they pose limitations for general applications of salt leaching scaffolds.

2.4.2 Gas foaming

Gas foaming is a manufacturing approach in which a polymeric material is filled with a foaming agent such as carbon dioxide, water or nitrogen at high pressure [51-53]. Solid polymer disks like polyglycolide (PGA) and poly-L-lactide (PLA) are created at high temperatures before spreading high-pressure carbon dioxide gas through the disks for a few days before decreasing the pressure down to the ambient level (Figure 2.4b) [54].

Gas foaming was used by Kim et al. [55] to fabricate porous biphasic calcium phosphate (BCP) scaffold by using gas-foamed polyurethane as a model achieving a porosity of 75% to 85% and pore size around 300-800 μm. The BCP scaffold was biocompatible and successfully differentiated and regenerated bone according to both the *in vivo* and *in vitro* experiments conducted in this study [55]. In another study, a biodegradable poly (L-lactic acid) (PLLA) scaffold with high open porosity was fabricated using a gas-foaming technique along with salt leaching [56]. The scaffold had a porosity of around 90% with pore sizes around 300-400 μm, which is ideal for high-density seeding of cells (Figure 2.7). Upon seeding rat hepatocytes into the temporal tissue scaffold, 40% viability and around 95% seeding efficiency were achieved within 24 hours [56].

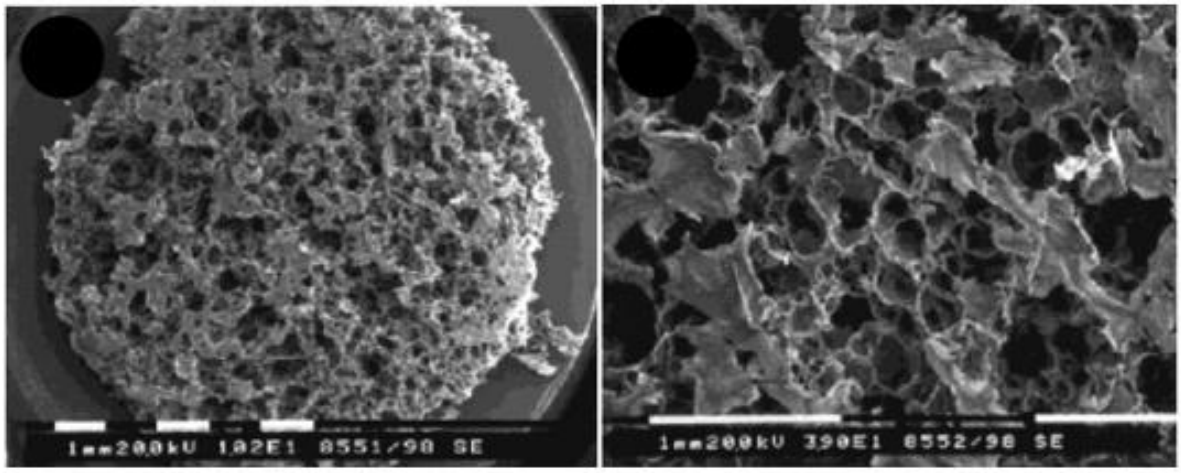

Figure 2.7. Scanning electron microscope (SEM) images of surface morphology of PLLA scaffolds. Adopted from Nam [56].

The key advantage of using the gas foaming technique is that it does not require the use of chemical solvents, thus reducing the overall manufacturing time. Nonetheless, it is challenging to control the internal structure of the scaffolds in terms of pore size and high connectivity using this technique [57,58]. In addition, high temperatures during the creation of disks often prevent the use of bioactive molecules in scaffolds [59]. Although this technique has the ability to fabricate scaffolds with 93 % porosity and pore sizes up to 100 μm [59], it has been noted that the scaffold interconnects only 10–30 % of the pores which may limit the proliferation of encapsulated scaffold cells [54].

2.4.3 Phase separation

In phase separation, a polymer is generally dissolved in an appropriate solvent and then deposited in a mould that is gradually cooled till the solution freezes. The solvent is then removed by freezing, leaving behind a porous matrix, as illustrated in (Figure 2.4c). Various types of phase separation methods are available, including thermal-induced, solid-liquid and liquid-liquid phase separation [60,61].

The study by Kim et al. employed thermally induced phase separation (TIPS) for the manufacture of polyethene-glycol (PEG) poly(l-lactic) acid (PLLA) scaffold to support MC3T3-E1 osteoblast-like cells [62]. It was shown in this study that ageing times and temperature have a significant effect on the pores morphology of the fabricated scaffold, quenching temperatures of 25°C, 30°C, and 35°C (Figure 2.8a-c). The TIPS technique allowed a simple control of the scaffold pore size between 100 – 300 μm. Authors noted that MC3T3-E1 cells could proliferate successfully within 4 weeks after being seeded on the microporous scaffold of PEG-PLLA [62].

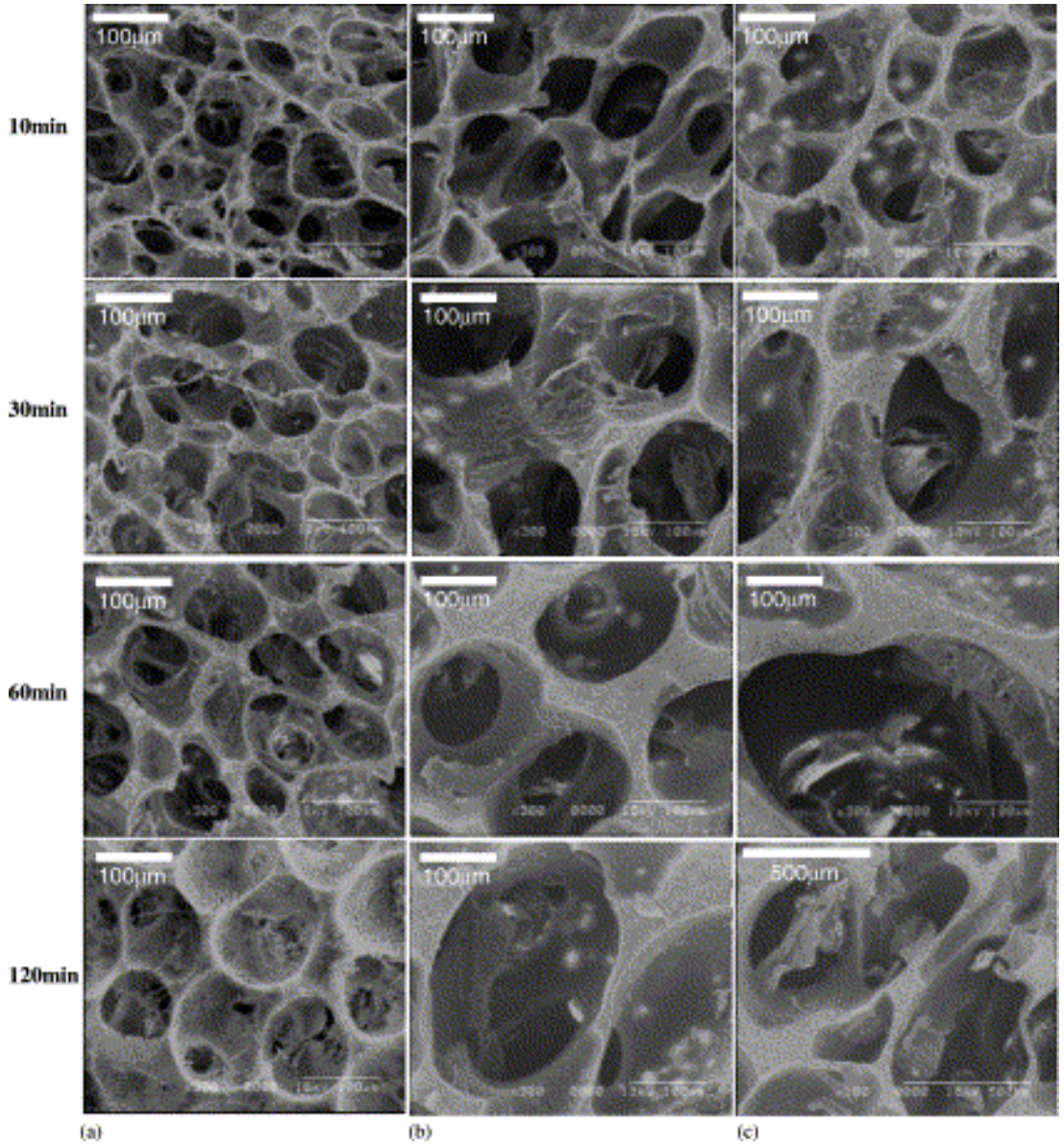

Figure 2.8. scanning electron micrograph of PLLA membranes as a function of aging time at quenching temperatures of 25°C (A), 30°C (B), and 35°C (C). Adopted from H Do Kim [62].

The main merit of using the phase separation technique is that it does not require extra leaching. However, the use of organic solutions like ethanol or methanol during the scaffold manufacturing process can prevent the integration of bioactive compounds or cells [59]. Furthermore, the generated small pore diameters around 13-35 μm are another constraint for phase-separation scaffolds. [43,59].

2.4.4 Freeze drying

Freeze drying technique is based on a frozen liquid that sublime directly into the gas phase leaving behind a porous hydrogel (Figure 2.4d) [63]. The manufacturing approach was first explored by Whang et al. to produce PLGA scaffolds [64]. The literature demonstrates that fabricated scaffolds' porosity and pore diameter are highly influenced by variables like the water-to-polymer mixture ratio and the viscosity of the emulsion [59]. Also, altering the cooling temperature can control the scaffold's internal pore structure [65].

In a study conducted by Park et al. [66], freeze drying was used to fabricate collagen and hyaluronic acid (HA) membranes and then crosslinked using 1-ethyl-3-(3-dimethylaminopropyl) carbodiimide (EDC). Porosity and pores' size were measured to assess the effect of freezing temperature and crosslinking on the internal structure of the scaffolds, freezes dried temperature used were at –20 ° C, −70 ° C, and −196 ° C (Figure 9a-c), (Table 2.2). The higher the freezing temperatures, the larger the pore size and the porosity percentage. Also, the use of EDC has significantly increased both the porosity and pore size. The prepared membranes were safe and did not exhibit significant toxicity to L929 fibroblast cells upon testing [66].

Table 2.2. Morphological properties of collagen-HA membranes. Adopted from SN Park [66].

Freezing temperature	**Porosity (%)**		**Pore size (µm)**	
	Before crosslinking	After crosslinking	Before crosslinking	After crosslinking
−196°C	58.1±3.4	61.95±3.8	40±7	84±20
−70°C	59.28±4.9	62.3±4.8	90±16	186±29
−20°C	66.46±2.6	64.93±2.3	230±52	190±42

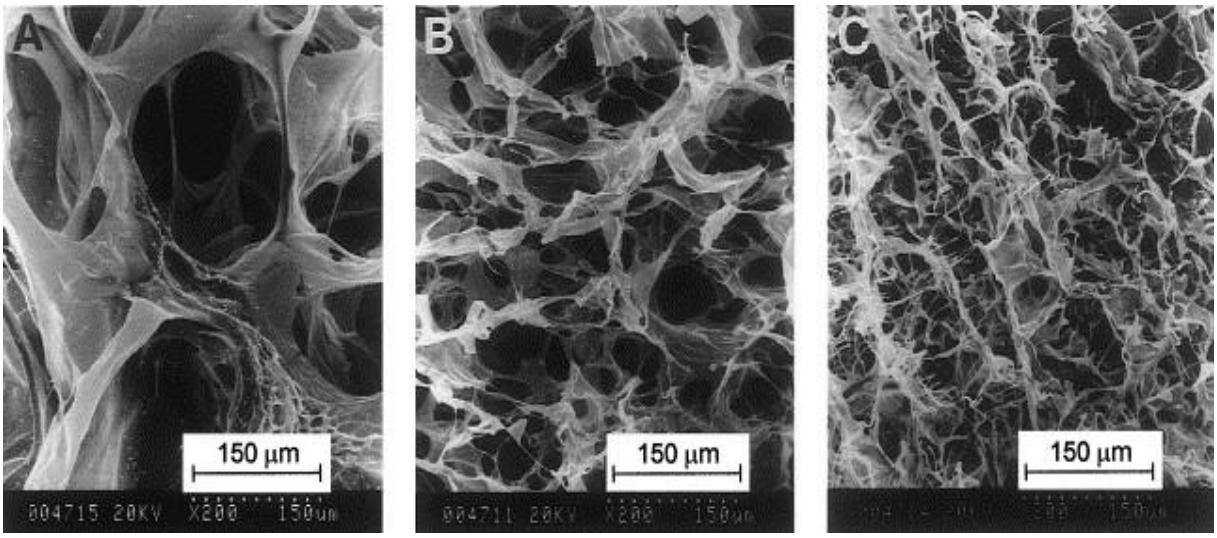

Figure 2.9. Effect of freezing temperature on morphology of the matrix. Collagen-hyaluronic acid scanning electron micrograph freezes dried at –20 ° C (A), −70 ° C (B) and −196 ° C (C) (magnification ×200). Adopted from SN Park [66].

The main benefit of the freeze drying technique is that it eliminates many rinsing processes by immediately removing scattered water and polymer solutions [64]. In addition, polymer liquids can be utilised directly instead of any monomer crosslinking. Nevertheless, in order to increase scaffold homogeneity, the freeze drying method must be managed to minimise heterogeneous freezing [65]. Moreover, this approach is associated with high energy consumption, long timescales, small irregular pores, and cytotoxic solvents [67,68].

2.4.5 Electrospinning

Electrospinning is an innovative electrochemical technology that utilises an electrical charge to create solid, nano-sized fibres from a liquid solution [69]. As illustrated in (Figure 2.4e), the electrospinning process begins with a syringe filled with a solution containing a precursor for the nanofiber material and a connecting polymer being loaded onto a regulated syringe pump.

A metallic needle is attached to the syringe and is connected to a high-voltage power source [70]. As the solution flows through the metallic tip, it becomes electrified, generating a deformed conical shape known as a Taylor cone. The Taylor cone's tip releases an electrified fibre jet. As the solution travels to a grounded collector, the solvent evaporates, and the fibres harden [70].

Wutticharoenmongkol et al. used electrospinning to create a 12% w/v PCL fibrous scaffold with HA nanoparticle concentrations ranging between 0.5 and 1.0%. The porosity of the constructed fibre scaffold increased by 82 and 90 %, and had pore sizes ranging from 4.3 to 5.6 μm. The prepared fibrous scaffolds had a tensile strength between 3.6 and 3.8 MPa [71]. Another study by He et al. reported the fabrication of a PCL/HA scaffold with different ratios of PCL/0.3 HA, PCL/0.4 HA, and PCL/0.5 HA (Figure 2.10a-c) and an average pore size of 167 μm which is suitable for osteoblasts, by stacking meshes using near-field electrospinning [72].

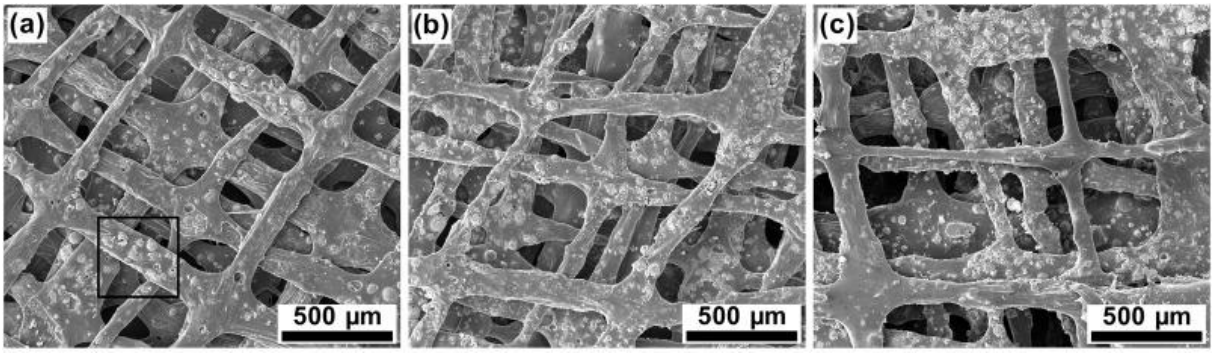

Figure 2.10. Morphological characterisation of the PCL/HA composite scaffolds. SEM image of (a) PCL/0.3 HA scaffold, (b) PCL/0.4 HA scaffold and (c) PCL/0.5 HA scaffold. Adopted from Feng-LiHe [72].

Electrospinning has the advantage of being able to manipulate both the mechanical properties and the porous structure of the fibre by regulating the voltages and distance between the syringe and the collectors [73,74]. Pores generated by this approach, however, are often fewer than a

few tens of micrometres in size, making them unsuitable for tissue growth and cell culturing [72]. Also, fabricating complex geometry can be challenging using this technique.

2.4.6 Self-assembly

Self-assembly is the process by which the components of a system, whether molecules, polymers, colloids, or macroscopic particles, arrange into ordered and/or functional structures or patterns without external direction as a result of specific, local interactions among the components [75]. Collagen should be examined to better understand the origins and significance of these structural features, as it is one of the most common proteins in the human body. Collagen is formed within the cell as a triple helix structure by the assembly of three distinct alpha strands (procollagen) (Figure 2.4f) [76]. Procollagen is enzymatically broken to generate tropocollagen, which combines and crosslinks with other tropocollagen molecules to create the characteristic 67 nm banded fibrils after vesicle transit to the exterior of the cell [76]. This fibrillar structure is retained in collagen types I (skin, tendon, and bone), II (cartilage), and III (skin, muscle) [76].

A recent study conducted by Nie W et al. [77]. Demonstrated the self-assembly of a 3D porous Reduced graphene oxide (RGO) composite scaffold that is composed of graphene oxide (GO) and nano-hydroxyapatite (nHA) with pore sizes ranging from 20–100 μm (Figure 2.11) [77]. The scaffold significantly improved the proliferation, alkaline phosphatase activity (ALP), and osteogenic gene expression of rat bone mesenchymal stem cells (rBMSCs) [77].

Another study used a combination of self-assembly and electrospinning techniques to create a hybrid scaffold with a honeycomb using Polyhydroxybutyrate/poly(-caprolactone)/58S sol-gel bioactive glass (PHB/PCL/58S) [78]. The scaffold was created by changing the solution composition and concentration during a single electrospinning process [78]. The nanofiber contained pores as small as a few micrometres in diameter, while the structure had pores

ranging from 200 μm to 1000 μm. This facilitated the cell ingrowth and infiltration of MG-63 osteoblast-like cells into the honeycomb-like scaffold [78].

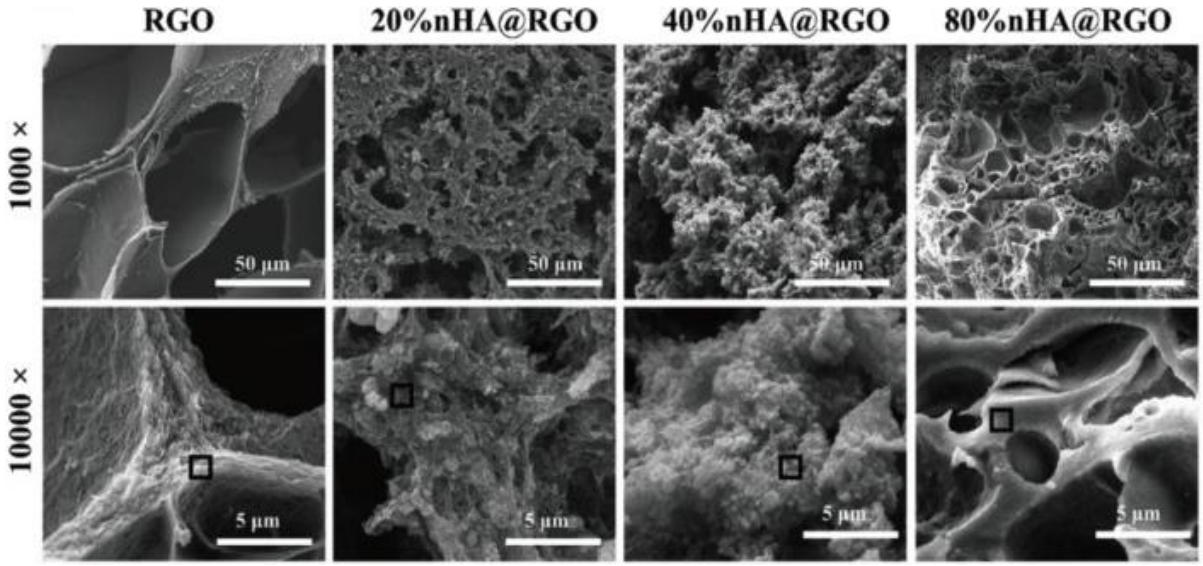

Figure 2.11. SEM of the nHA@RGO scaffold with the different nHA loading ratios. Reduced graphene oxide (RGO) and nano-hydroxyapatite (nHA). Adopted from WeiNie [77].

The self-assembly mechanisms are frequently triggered by the mixing of two elements or by an external stimulus (pH, ionic strength, or temperature), allowing these materials to be injected or even used directly to encapsulate cells, compared to the complex processing needed for other conventional manufacturing methods to fabricate a scaffold [76]. In comparison to other manufacturing processes, the mechanisms governing the development of self-assembled nanofibers are generally more complex, requiring more careful molecular design and more intricate synthesis. (Table 2.3) summarises the main applications, advantages and drawbacks of the manufacturing techniques presented in this section.

Table 2.3. Summary of conventional manufacturing.

Manufacturing technique	**Main applications**	**Advantages**	**Disadvantages**	**Ref.**
Salt leaching	Forming porosity in part by employing salt particles	• Controlled pore size • Suitable for manufacturing of membranes	• Lack of pores distribution control • Lack of scaffold structure control	[43,48,50]
Gas foaming	Forming porosity in part by applying high pressure	• It does not use chemical solvents • It is capable of fabricating parts with very high porosity	• Pore sizes are difficult to control • It employs a high temperature • Lack of scaffold structure control	[57-59]
Phase separation	Forming porosity in part by employing chemical solvents	• It does not require post-processing	• Pore sizes are very small • Lack of scaffold structure control	[43,59]
Freeze drying	Forming porosity in part by freezing the liquid mixture	• Pore sizes can be adjusted by controlling the temperatures	• Lack of scaffold structure control • high energy consumption • uses cytotoxic solvents	[66-68]

Electrospinning	Forming solid nano size fibres	• Mechanical and porosity properties of the fibre can be controlled by regulating the voltage and distance	• Lack of scaffold structure control	[72-74]
Self-assembly	Forming a pattern by the interactions of two components without external direction	• It does not require the use of cytotoxic solvents	• Pore sizes are very small • It necessitates greater attention to molecular design and intricate synthesis	[76,77]

From the literature review presented above, it can be concluded that conventional manufacturing methods such as gas formation, salt leaching, freeze drying, and phase separation do not allow for accurate regulation of the internal scaffolding design or the manufacture of complicated structures, which can be accomplished through AM modelled with computer-aided design (CAD) [79]. Besides, these conventional methods require good manufacturing skills to maintain a consistent architecture of scaffolds. In addition, special care must be taken to use toxic solvents that can lead to the death of cells if they are not removed completely [80]. Another limitation is that scaffolds manufactured in accordance with these conventional processing methods have poor mechanical properties [81]. Therefore, alternative techniques such as 3D printing offer a good opportunity to avoid these issues.

2.5 Three Dimensional Printers

Industry 4.0, commonly known as digital technology, is revolutionising industries by making factories smarter and assisting manufacturers in increasing quality, productivity, and profitability. 3D printing is a manufacturing tool that has advanced over the last three decades and is an essential component of digital technology. Charles Hull invented the technology in 1986, employing UV-sensitive polymers and ultraviolet light (UV) to generate three-dimensional structures [82]. Stereolithography (SLA) was the name given to the technology later on. Scientists and engineers have since developed a variety of unique 3D printing techniques. The main advantage of these new technologies is that they enable the fabrication of complex organic shapes and internal features and cavities in components that were difficult or even impossible to fabricate with conventional techniques [83].

Additional benefits of 3D printing can include; reduced lead time, elimination of extra processing required for mass customisation, develop supply chain expertise, printing systems and assemblies, fabricating complicated designs in functional components, lightweight production of cellular structures, material recycling and environmentally friendly production, scalable workflow, on-demand production and enhanced service quality [83,84]. (Figure 2.12) summarises the most employed 3D printing techniques. Binder Jetting, Fused Deposition Modelling, Selective Laser Sintering and Stereolithography are the most employed for the manufacturing of scaffolds and, therefore, will be discussed in detail in the following sections.

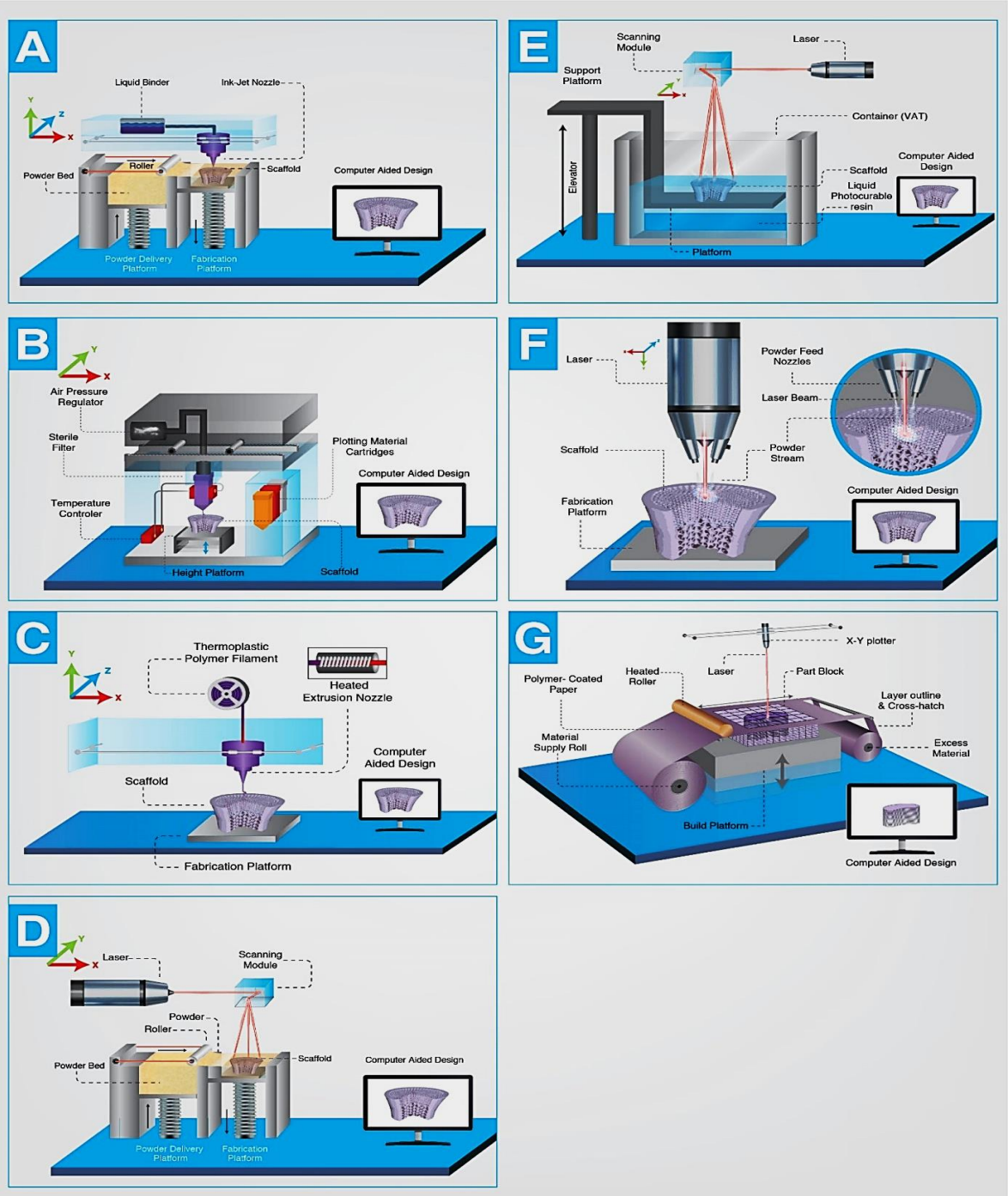

Figure 2.12. 3D printing techniques, (a) Binder jetting, (b) Materials jetting, (c) Materials extrusion, (d) Powder bed fusion, (e) Vat photopolymerisation, (f) Directed energy deposition, (g) Sheet lamination.

In regard to the bio-medical applications, the most significant benefit of 3D printing technologies is allowing the fabrication of completely customised components. In 3D printing, different materials such as polymers, metals, or ceramics can be created layer by layer to

produce the desired shape according to a computerised model, in contrast to typical manufacturing or foaming procedures that demand removing and/or adding, such as cutting, bending, and drilling [85]. 3D printing technologies have been used in many industries, such as biomedical, automotive, aerospace, defence, and many others. This is due to the capacity of AM technologies to rapidly build complicated structures with precision and accuracy, as well as the ability to recycle materials. Numerous researchers and industrial organisations have focused their efforts on enabling the widespread implementation of 3D printing and investigating its potential and limitations. [86-89]. Therefore, 3D printing can play a major role in the future of tissue engineering in general and bone scaffolds in particular. This is evident as the number of studies employing 3D printing technology for bone scaffolds has increased over the last decade (Figure 2.13).

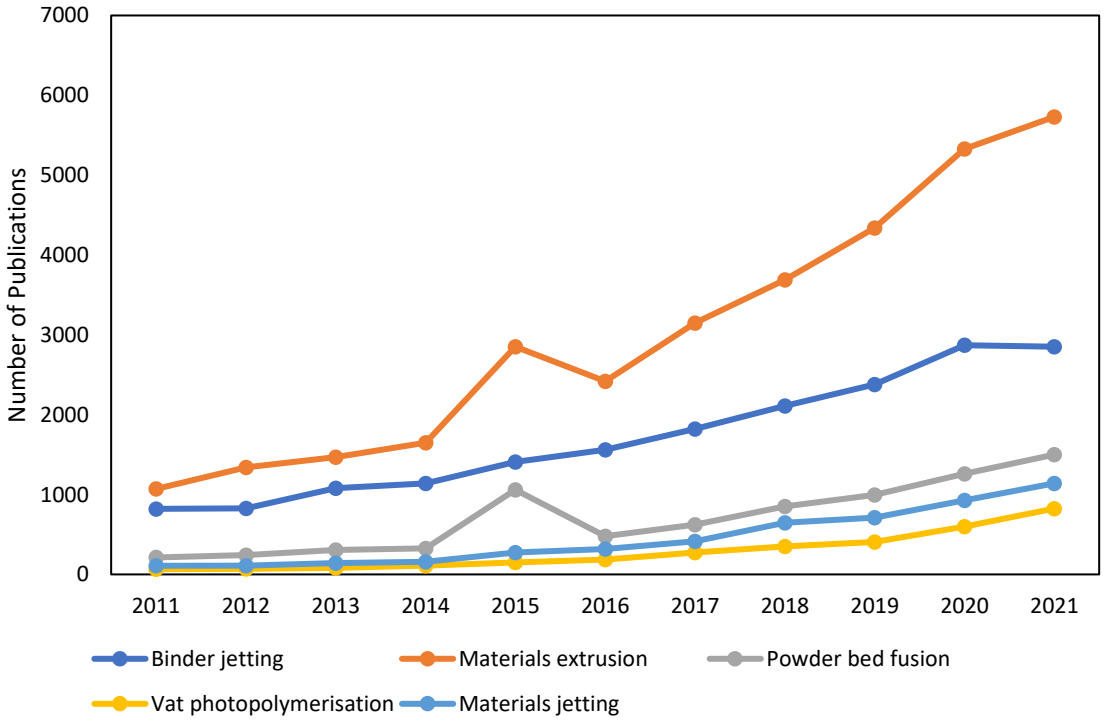

Figure 2.13. Number of papers published on bone scaffold fabricated by each 3D printing technique over the last 10 years.

2.5.1 Binder jetting

Binder jetting starts with a powder bed, the composition of which varies according to the materials employed, which is dispersed over the building platform and flattened with the aid of a roller system [90]. Following that, the printer nozzle spreads binder solution in the powdery regions indicated by the CAD. The excess powder is extracted (blown off) after the binder solvent and powder are mixed. The building platform is then lowered, allowing for the deposit and levelling of a new powder sheet [91]. Following that, the process will be repeated till the required design is fully fabricated (Figure 2.12a).

After the layer deposition, the part generated that is known as the green part usually has high porosity. In order to reduce the number of pores and to improve its integrity, the component is subjected to cleaning and post-processing operations: depowdering, debinding and finally, a sintering process in a furnace with densifying and strengthening purposes.

In a study conducted by Chavanne P et al.,[92] chitosan and hydroxyapatite biocomposite scaffolds were printed using a Z-Corp, Z-510 3D printer to create dense (solid, nonporous, 37.1% porosity) and cylindrical scaffolds [92]. These scaffolds were fabricated by applying a 40 wt% lactic acid binder solution to various chitosan/hydroxyapatite composites (20 wt%, 25 wt%, and 30 wt% chitosan) followed by a post-hardening process. The authors observed that the scaffolds printed with 25% chitosan had good mechanical properties, as evidenced by their compression strength of 16.32 MPa and 4.4 GPa Young's modulus [92]. Nevertheless, only the fabrication of nonporous scaffolds has achieved the desired mechanical strength. In another study, CALPHAD (Ca) and biodegradable Fe-Mn alloy were used to achieve higher decomposition rates (Figure 2.14a-b) [93]. The achieved ultimate tensile strength was 228.1 MPa for the Fe-Mn and 296.6 MPa for the Fe-Mn-1Ca [93]. During tensile testing, a brittle fracture occurred in a porous Fe-Mn-1Ca scaffold with 52.9 % open porosity. Fe-Mn scaffolds with an open porosity of 39.3 % had higher ductility than Fe-Mn-1Ca, demonstrating that

scaffold Fe-based alloys with less porosity have higher ductility (Figure 2.14c-d) [93]. This is a concern since porosity is a crucial feature as it promotes the diffusion of oxygen, nutrients, and cellular waste. The availability and diversity of the powder-binder solutions make the binder jetting attractive for manufacturing bone scaffold [90]. On the other hand, a drawback of this technique is that it needs post-processing, which may include heat treatment to assure durability [94].

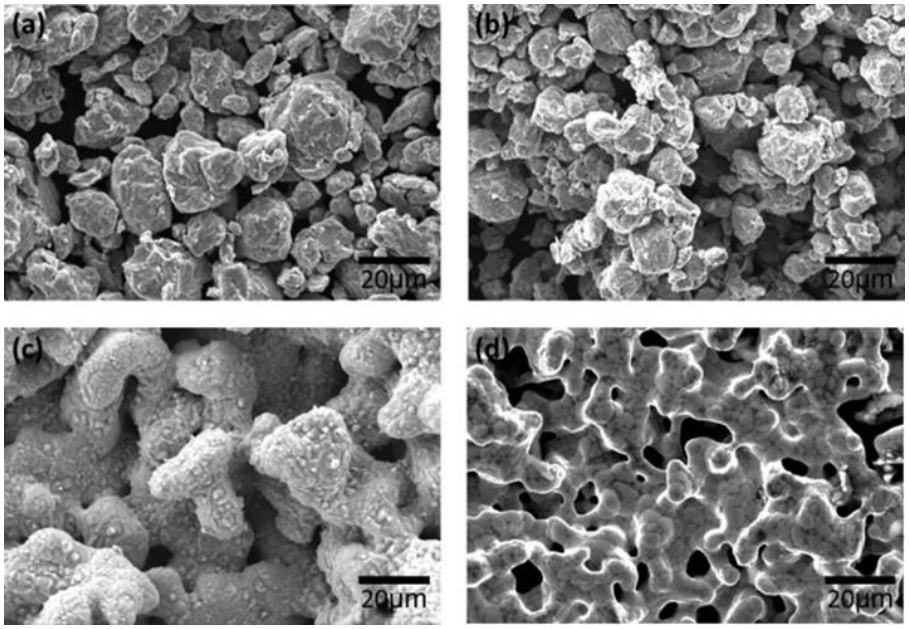

Figure 2.14. Morphology of (a) Fe-Mn powders (b) Fe-Mn-1Ca powders, (c) 3D printed Fe-Mn sample, and (d) 3D printed Fe-Mn-1Ca sample. Adopted from Hong D [93].

2.5.2 Materials jetting

Materials jetting printing (Bioplotter) is one of the most used 3D printing technologies for cellular research due to the low temperature it requires and the low volume it uses (between 3 and 5 mL) [95]. This technology is designed for high-precision printing of small objects using small nozzles with a minimum diameter of 250 μm and low volume [96]. The process starts by loading the printing material in a semi-liquid or liquid form into the syringe. Then, pneumatic pressure is applied to extrude the material through the printing nozzle (Figure 2.12b). The

materials are deposited in a layer-by-layer manner, and the process enables the combination of different materials in each layer.

In the study by Poldervaart et al. VEGF was incorporated into a 3D printed matrigel-alginate scaffold to promote vascularisation using BioScaffolder pneumatic dispensing system [97]. The incorporation of gelatin microparticles (GMPs) to sustainably regulate the release of VEGF led to higher vascularisation compared to scaffolds with no growth factors and rapidly released VEGF scaffolds when implemented in murine models (Figure 2.15). In another recent study, a biphasic scaffold model was fabricated with the BioScaffolder by combining the unmodified calcium phosphate cement (CPC) paste with a highly concentrated alginate-based hydrogel paste that was embedded with VEGF by two-channel plotting within a single scaffold [98]. The scaffold was designed and manufactured to be used for evaluating a femur defect of size in the range of 200 μm with a macro porosity of 57%. The scaffolds' size and high porosity made them suitable for enhancing bone regeneration [98].

A unique feature of materials jetting processes is that it allows the printing of cell-laden gels to deliver viable and usable scaffolds, often including other polymeric materials like PCL [99,100]. Another advantage of materials jetting is that it enables the growth factors such as platelet-derived growth factor (PDGF) or vascular endothelial growth factor (VEGF) to be added to the bio-ink to improve cell proliferation and differentiation which promotes angiogenesis [101]. Adding these growth factors will increase the tissue formation rate in scaffolds and generate robust tissue as a result of increased differentiation. On the other hand, the shear stress from the nozzles of various sizes can negatively impact cell viability [102].

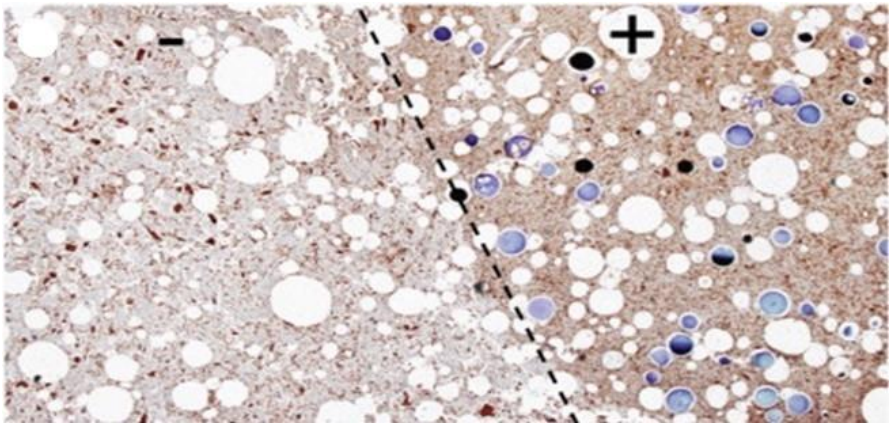

Figure 2.15. 3D printed matrigel-alginate scaffold the two regions (− without VEGF, + VEGF-laden GMPs). Adopted from M. T. Poldervaart [97].

2.5.3 Materials extrusion

In materials extrusion, thermoplastic polymers are heated above their glass transition temperature and then placed on a solid surface. It uses a winding thermoplastic polymer filament that is unwound and extruded through a heated nozzle on a fabrication platform. The polymer solidifies and sets after contact with the platform [103]. Upon depositing a layer, the process is repeated in a layer-by-layer process until the part is fully fabricated see (Figure 2.12c) [104].

Hong et al. employed a multi-head deposition method to combine PCL and PLGA to fabricate a multi-material scaffold with high compressive strength of 3.2 MPa and pore size of around 300 μm with 66.7% porosity (Figure 2.16). In combination with mussel adhesive proteins as a functional material, the fabricated scaffolds facilitated high cell attachment and proliferation of stem cells derived from human adipose tissue [105].

It also yielded positive outcomes *in vivo* tests, where increased bone regeneration was observed in a calvarial defect of a rat model [105]. Overall, Fused Deposition Modelling (FDM) was mainly used in combination with other techniques or in indirect 3D printing for tissue engineering purposes.

The primary drawbacks of FDM include its inability to support multi-material and multi-color fabrication processes in a single component and its limited accuracy, which can result in deviations of up to ±0.5 mm [90]. However, it prevents any possible toxicity caused mainly by organic solvents that are required for the solubilisation of certain polymers, like dichloromethane, used to solubilise PLGA. The thermoplastic criterion for this technique restricts it is application and adaptability in the production of scaffolds, as acrylonitrile butadiene styrene (ABS) is the most frequently used material. Other polymers have been used in FDM, like polycarbonate (PC), polyphenylsulfone (PPSF), and polyetherimide (PEI). However, these materials are not mainly used in tissue engineering applications [106]. Further investigation is needed to determine whether alternative thermoplastics, like polyesters, are suitable scaffolding materials for tissue engineering. Despite this drawback, FDM has been demonstrated to be a viable approach for manufacturing scaffolds for tissue engineering. Polyester, PLA, PCL, as well as PCL and PLA composites like PCL-TCP, HA - PCL and HA - PLA are the main option for FDM printed scaffolds [107-110].

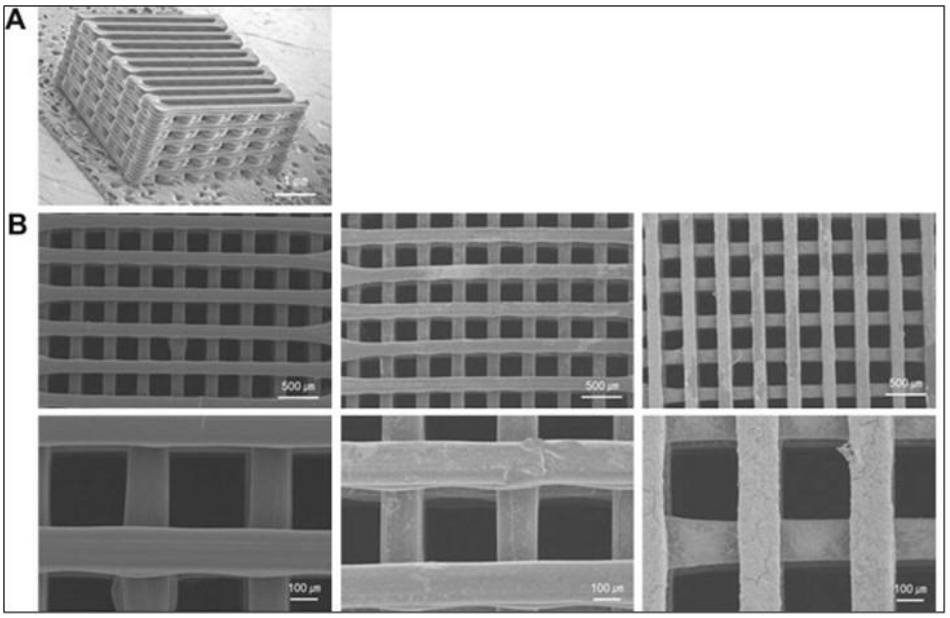

Figure 2.16. Solid Free-form Fabrication (SFF)-based 3-D PCL/PLGA Scaffold. Adopted from J. M. Hong [105].

2.5.4 Powder bed fusion

The laser powder bed fusion (L-PBF) technology begins with the powder layer being smeared on the surface of the base plate, followed by melting powdered particles together using a laser beam (normally a CO_2 laser) in the desired pattern [111]. The process is repeated after the first layer is deposited, and then another layer is added on top of the pre-existing one (Figure 2.12d) [112,113]. The L-PBF technique was used to make scaffolds from biocompatible and biodegradable polymers like poly(lactic acid), polyvinyl alcohol, polycaprolactone, and polyetheretherketone [114]. With the development of metal 3D printing, this technology is also employed for the fabrication of metallic scaffolds that can be created out of biocompatible metal alloys such as Ti6Al4V for the fabrication of implants [115]. The use of L-PBF for the manufacturing of scaffolds has been studied by many researchers in the literature. F.-H. Liu et al. utilised hydroxyapatite (HA), sodium tripolyphosphate and silica sol biocomposite slurry to manufacture scaffolds using L-PBF with different heat treatment temperatures at ambient temperature, 1200 °C, 1300 °C, and 1400 °C (Figure 2.17a-d). These scaffolds showed significant mechanical strength (up to 43.26 MPa) but had low porosity with a pores size of 5-25 μm. The *in vitro* research, however, suggested the possibility of using these scaffolds for osteoblast growth, such as cells [116]. In another study by I. Gibson, the authors optimised the laser beam power, scan spacing and laser thickness to fabricate a nanocomposite scaffold made of poly(hydroxybutyrate-co-hydroxyvalerate) and calcium phosphate [117]. The analysed parameters were found to have a substantial effect on the mechanical properties of the scaffold; compressive properties, precision, and durability [118]. Nevertheless, the scaffold's efficiency and utility must be evaluated *in vitro* and *in vivo*. Other scholars have fabricated a scaffold using bioresorbable polycaprolactone (PCL) at high precision and high compression moduli ranging from 52-67 MPa. The scaffold was loaded with bone morphogenetic protein-7 (BMP7), and has demonstrated bone generation *in vivo* [119].

When low porosity and high mechanical strength are needed, the use of L-PBF processes can be beneficial; nonetheless, the need for powdered material to be able to withstand laser heat and resistant shrinking throughout the melting process are some limitations of this technique. Another drawback of L-PBF is the pre-heating and post-heating treatments of the powdered material among the crystallisation glass transition or melting temperatures to lower the shrinking of the scaffolds induced by the laser [116,120].

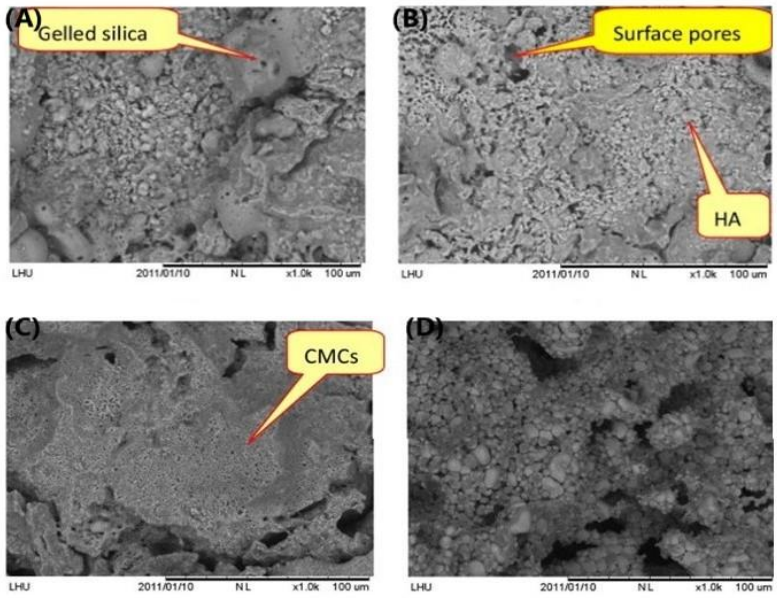

Figure 2.17. SEM images of the scaffold at (a) ambient temperature, (b) 1,200 °C, (c) 1,300 °C, and (d) 1,400 °C. hydroxyapatite (HA) and Ceramic-matrix composites (CMCs). Adopted from F.-H. Liu [116].

2.5.5 Vat photopolymerization

Vat photopolymerisation or stereolithography (SLA) technique is based on the fabrication of components from a liquid polymer via a chemical reaction mediated by light. A photocurable polymer is placed on a surface medium and then subjected to UV radiation in the 300–400 nm wavelength range, forming the first layer (Figure 2.12e) [121]. After the initial layer has been hardened, the process is repeated, overlaying the preceding layer until the part is completely

fabricated [122,123]. SLA biomaterials include polypropylene fumarate (PPF) with photoinitiators and polyethylene glycol acrylate.

A study conducted by Cooke et al. used the (SLA 250/40) stereolithography for Printing (PPF) scaffolds together with Irgacure 819 photoinitiator. The manufactured scaffolds had a porosity of 90% and a pore size range of 150–800 μm [125].

Their study demonstrated the possibility of fabricating scaffolds using (PPF) material (Figure 2.18). However, *in vitro* and *in vivo* studies must be carried out to determine the scaffold cytotoxicity and biocompatibility. Despite the magnificent results that SLA can achieve in terms of complex geometries fabrication, various novel biodegradable and biocompatible photocurable polymers must be further developed [124]. In addition, designing and improving visible light-based Spatial-Temporal Modulation STM systems is important in order to have a list of polymeric materials [124].

The advantage of the SLA technology is that it allows for precise control and fabrication of high-resolution detailed scaffold geometries that almost perfectly mimic the CAD model. Nonetheless, due to the use of an extra curing phase to enhance the properties of the prototype, the final resolution is affected by the shrinkage usually occurring in the post-processing phase [126,127]. However, the drawback of SLA techniques is that they are limited to only photopolymer materials [128]. In addition, the majority of photoinitiators include radical photopolymerisation by photocleavage, hydrogen extraction, and cationic photopolymerisation, with cationic photoinitiators being incompatible with biomedical applications because of the formation of toxic byproducts. Also, the widely used ultraviolet light source for the polymerisation process poses another risk as reports indicate that this light source is harmful to our DNA cells and might be a potential cause of skin cancer [129,130].

Figure 2.18. fabricated scaffold using stereolithography (SLA). Adopted from M. N. Cooke [125].

2.5.6 Directed energy deposition and Sheet lamination

The directed energy deposition (DED) technology fabricates the required object by melting materials using a laser beam while using a nozzle to deposit the material in specific locations, as demonstrated in (Figure 2.12f) [147]. It mostly uses metal types of materials, such as stainless steel, aluminium, or copper, in the form of powder or wire [148]. This technique usually require post-processing due to distortions in the fabricated part [149]. Due to the limited types of materials that can be processed and the poor quality of the fabrication, this technique has not been utilized much in biomedical applications.

In sheet lamination (SL), a sheet material is laminated in a layer-by-layer manner and cut using a laser beam to fabricate the required object as demonstrated in (Figure 2.12g). It uses different types of materials such as paper, metal, and plastic [150].

Similarly to directed energy deposition, sheet lamination has not been widely used in biomedical applications due to its poor fabrication quality, the need for post-processing, and the difficulty in fabricating complex shapes using this technique [151].

Table 2.4. summary of the 3D printing techniques.

AM technology	**Resolution (µm)**	**Material**	**Strength**	**Weakness**	**Refs**
Binder jetting	200-300	PLGA, PLLA, PEEK-HA, PCL, starch-based polymer	• No support structure is required • Fast processing • Uses a variety of materials	• Can require post-processing • Powdery surface finish • Trapped powder	[131, 132]
Materials jetting	10-1000	PCL, PLLA, TCP, Hydrogel, Organic ink	• Uses an enhanced range of materials • Can incorporate biomolecule	• Low mechanical strength • Smooth surface • Low accuracy • Slow processing • Complex design requires support structure	[133-138]
Materials extrusion	250	PCL, PP-TCP, PCL-HA, PCL-TCP, PETG-PBT, PLLA-TCP, PLA	• Good mechanical strength • Preparation time is reduced	• High temperature • Need to produce filament material • Narrow processing window • Complex design can require support structure	[107] [139-141]

Powder bed fusion	500	PEEK-HA, PCL, titanium, Stainless steel, cobalt-chromium alloys	• Microporosity induced in the scaffold • Uses an enhanced range of materials • No support structure needed • Fast processing	• Material must be in powder form • High temperature • Powdery surface finish • Trapped powder • Thermal damage can occur during processing	[142 - 144]
Vat photopolymerisation	366	Resin, PPF, polyethylene glycol acrylate, HA	• Control of both external and internal morphology • Uses an enhanced range of materials • High accuracy • Fast processing	• Multistep involved • Poor mechanical strength • Damages cell during photo curing • UV light can be toxic to cells	[145 ,146]

Poly(lactic-co-glycolic acid) (PLGA), Poly(L-lactide) (PLLA), (polyetheretherketone) (PEEK), Hydroxyapatite (HA), Polycaprolactone (PCL), Tricalcium phosphate (TCP), Polypropylene (PP), Polyethylene terephthalate glycol (PETG), Polybutylene terephthalate (PBT) and Paint protection film (PPF).

In general, both manufacturing technologies have different advantages and disadvantages, primarily depending on the application of the fabricated object. For example, when complex geometries and designs are required, additive manufacturing technology has proven to be a better option than conventional manufacturing as it allows for the creation of internal structures [152]. In contrast, conventional manufacturing is more precise, can handle a wider variety of materials, and is better suited for large-scale production than additive manufacturing [153]. Additive manufacturing is a relatively new technology that is still being developed and has

limitations regarding the types of materials it can process and the size of the components it can produce [153]. In fact, researchers have combined conventional and additive manufacturing technologies into a single machine for bone scaffold fabrication, effectively combining their respective advantages.

The research conducted by Jiankang He and his team, a new printing method was developed that combines FDM and electrospinning technologies to create 3D tissue-engineered scaffolds with intricate curved shapes and microscale fibrous structures (Figure 2.19a). The melting temperature was optimized to print PCL filaments of around 10 μm, which were stacked to create 3D walls with smooth surface [154]. By adjusting the stage movement speed and direction, they were able to print PCL scaffolds with curved outlines, predefined fiber spacing, and orientations at 90° and 45° (Figure 2.19b-g). Biological experiments demonstrated that the printed microscale scaffolds were biocompatible and promoted *in vitro* cellular proliferation and alignment [154].

In other research conducted by H. Hassanin et al., they successfully produced micro implantable components with the highest density of approximately 80 to 100 J/mm3 and the best possible surface roughness quality of Ra 0.6 μm and 0.8 μm. They achieved this by utilizing a hybrid microfabrication technology that combines the design flexibility of SLM with the surface quality of Micro-Electrical Discharge Machining (μ-EDM) [155]. Another group of researchers has developed a new approach to create three-dimensional graphene (3DG) composites scaffold by combining selective laser melting (SLM) and chemical vapor deposition (CVD) techniques [151]. They fabricated a 3D porous copper template using SLM and grew graphene in-situ via CVD on the template. This technique allowed for accurate control of the design and regulation of 3DG, resulting in enhanced electromagnetic interference (EMI) shielding and improved thermal diffusion [151].

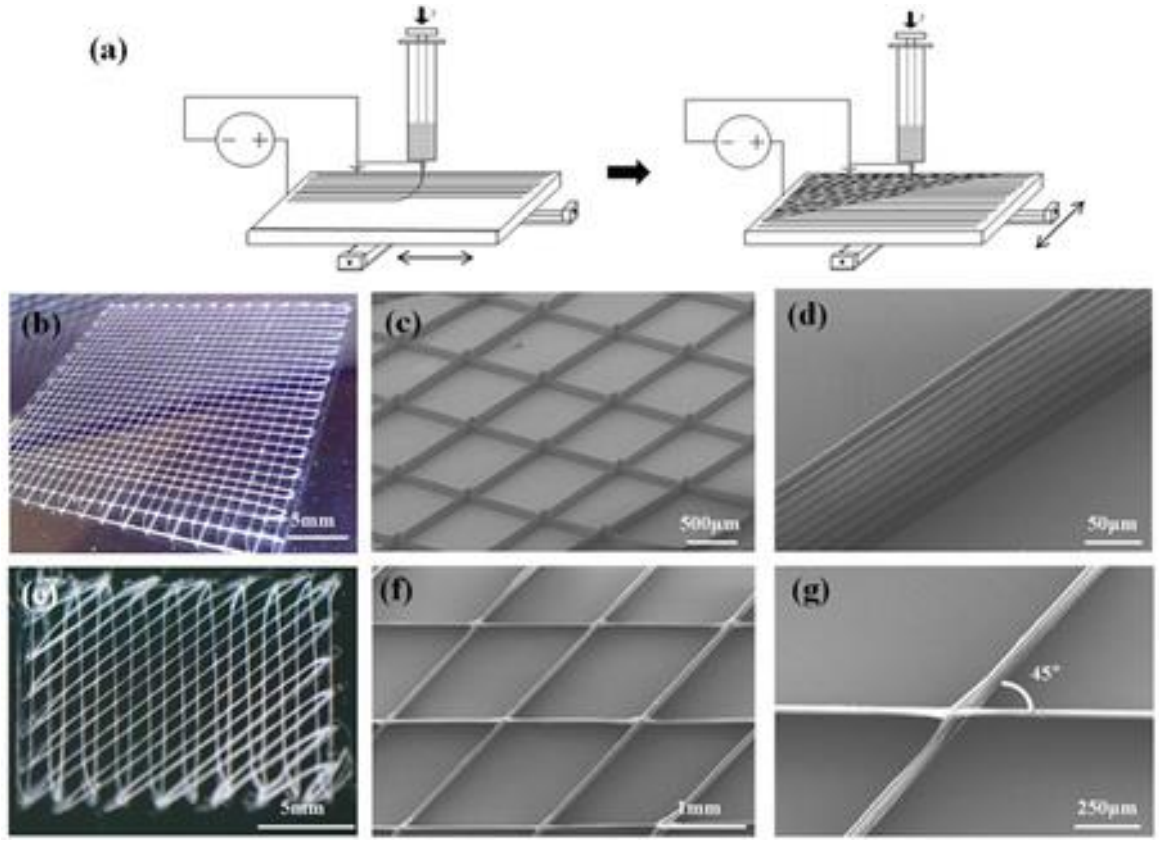

Figure 2.19. Fiber orientation manipulation during the melt electrohydrodynamic printing process. (a) Schematic illustration of manipulating fiber orientation through directing stage movement, (b-d) microscopic images of the printed scaffold, which have fibers spaced at 1 mm intervals and oriented at 90° and (e-g) oriented at 45°. Adopted from Jiankang He [154].

2.6 Conclusions

This paper presents a literature review of the most relevant works and recent advances concerning manufacturing bone scaffolds. Conventional manufacturing techniques have been reviewed, and their main benefits and shortcomings have been addressed. Additionally, 3D printing technologies that have emerged in the last years have proved to be a feasible alternative. In this context, the review demonstrated that 3D printing technologies enable the customisation of bone scaffolds to meet individual patients' unique needs and health situations. Progress in this area is facilitated by advancements in computer-aided design (CAD) and computer-aided manufacturing (CAM), which enable rapid and precise organ scanning and

design. The scaffold's structural properties, such as pore size and porosity, have a direct influence on their functionality *in vitro* and *in vivo*. In general, the impact of interconnected porous scaffolding networks that allow nutrient transport and waste disposal and promote cell migration and proliferation are significant. Pore size and porosity affect the behaviour of the cells and determine the overall mechanical properties of the scaffold. Presently, the concept of fabricating scaffolds is concentrated on generating materials with suitable pore size, structure, and porosity for specific uses. Typically, scaffolds are 3D printed, and cells are grown in/on these scaffolds. One of the challenges of 3D printing is using non-biocompatible materials in several 3D printing techniques, such as binders or photoinhibitors, even after the high-temperature debinding or sintering process. These components can not be removed entirely after heating or sintering processes and may compromise the biocompatibility of the constructs. Also, applying the temperature in some of the technologies restricts the applicability of materials. Incompatibility of the cellular application with the scaffold would gradually cause the entire scaffolding system to fail. In addition, 3D printing technology has altered the way bone fractures and has enabled the utilisation of drug-loaded implants and/or scaffolds of complicated geometries and high resolution to accelerate the healing procedure and recover bone structure and toughness. Bone scaffolds have been extensively manufactured using techniques like FDM and binder jetting. FDM has been demonstrated to be capable of processing a wide variety of scaffolds with complicated structures and a variety of polymeric materials. On the other hand, techniques like directed energy deposition and sheet lamination (Figure 2.12f-g) were not explored in this field due to their processing characteristics or the quality of their products or materials. Clinical trials conducted by academia or commerce on the developed systems demonstrate significant potential. However, challenges such as materials recycling, quality control, and the effect of inherited issues of 3D printing such as surface roughness, internal defects, and post-processing are still lacking.

2.7 References

[1] Nations U. Our world is growing older: UN DESA releases new report on ageing. 2019. [Last Accessed; 10/2023].

[2] Sözen T, Özışık L, Başaran N. An overview and management of osteoporosis. Eur J Rheumatol 2017;4(1):46-56, doi:10.5152/eurjrheum.2016.048

[3] Kumar A, Mandal S, Barui S, et al. Low temperature additive manufacturing of three dimensional scaffolds for bone-tissue engineering applications: Processing related challenges and property assessment. Mater Sci Eng R Rep 2016;103:1–39.

[4] Heuijerjans A, Wilson W, Ito K, et al. The critical size of focal articular cartilage defects is associated with strains in the collagen fibers. Clin Biomech (Bristol, Avon) 2017;50:40–46; doi: 10.1016/j.clinbiomech.2017.09.015.

[5] Yang Y, Wu P, Wang Q, et al. The enhancement of Mg corrosion resistance by alloying Mn and laser-melting. Materials (Basel) 2016;9(4):216; doi: 10.3390/ ma9040216.

[6] Wang Z, Wang C, Li C, et al. Analysis of factors influencing bone ingrowth into three-dimensional printed porous metal scaffolds: A review. J Alloys Compd 2017;717:271–285.

[7] Janik H, Marzec M. A review: Fabrication of porous polyurethane scaffolds. Mater Sci Eng C Mater Biol Appl 2015;48:586–591; doi: 10.1016/j.msec.2014.12.037.

[8] Bose S, Ke D, Sahasrabudhe H, et al. Additive manufacturing of biomaterials. Progr Mater Sci 2018;93:45–111.

[9] Gao C, Peng S, Feng P, et al. Bone biomaterials and interactions with stem cells. Bone Res 2017;5(1):17059; doi: 10.1038/boneres.2017.59

[10] Currey JD. The structure and mechanics of bone. J Mater Sci 2012;47(1):41–54.

[11] Lacroix D. 4 - Biomechanical aspects of bone repair. In: Bone Repair Biomaterials. (Planell JA, Best SM, Lacroix D, et al. eds.) Woodhead Publishing: Cambridge, UK; 2009; pp. 106–118.

[12] Hasegawa K, Turner CH, Burr DB. Contribution of collagen and mineral to the elastic anisotropy of bone. Calcif Tissue Int 1994;55(5):381–386; doi: 10.1007/BF00299319.

[13] Frost HM. Some ABC's of skeletal pathophysiology. 6. The growth/modeling/remodeling distinction. Calcif Tissue Int 1991;49(5):301–302; doi: 10.1007/BF02556248.

[14] Parfitt AM. Chapter 15 - Skeletal heterogeneity and the purposes of bone remodeling: Implications for the understanding of osteoporosis. In: Osteoporosis (Second Edition). (Marcus R, Feldman D, Kelsey J. eds.) Aca- demic Press: San Diego, CA, USA; 2001; pp. 433–447.

[15] Lacroix D. 3 - Biomechanical aspects of bone repair. In: Bone Repair Biomaterials (Second Edition). (Pawelec KM, Planell JA. eds.) Woodhead Publishing: Cambridge, UK; 2019; pp. 53–64.

[16] Mach DB, Rogers SD, Sabino MC, et al. Origins of skeletal pain: Sensory and sympathetic innervation of the mouse femur. Neuroscience 2002;113(1):155–166; doi: 10.1016/S0306-4522(02)00165-3.

[17] Bjørnerem A˚ . The clinical contribution of cortical porosity to fragility fractures. Bonekey Rep 2016;5:846–846; doi:10.1038/bonekey.2016.77.

[18] Schaffler MB, Radin EL, Burr DB. Mechanical and morphological effects of strain rate on fatigue of compact bone. Bone 1989;10(3):207–214; doi: 10.1016/8756-3282(89)90055-0.

[19] Fuchs RK, Thompson WR, Warden SJ. 2 - Bone biology. In: Bone Repair Biomaterials (Second Edition). (Pawelec KM, Planell JA. eds.) Woodhead Publishing: Cambridge, UK; 2019; pp. 15–52.

[20] Mow VC, Ratcliffe A, Woo SLY. Biomechanics of Diarthrodial Joints. Springer: New York, NY, USA; 2012.

[21] Gibson LJ. The mechanical behaviour of cancellous bone. J Biomech 1985;18(5):317–328; doi: 10.1016/0021- 9290(85)90287-8.

[22] Ding M, Dalstra M, Danielsen C, et al. Age variations in the properties of human tibial trabecular bone. J Bone Joint Surg Br 1997;79:995–1002; doi: 10.1302/0301-620X.79B6.7538.

[23] Melvin JW. Fracture mechanics of bone. J Biomech Eng 1993;115(4B):549–554; doi: 10.1115/1.2895538.

[24] Kumar P, Vinitha B, Fathima G. Bone grafts in dentistry. J Pharm Bioallied Sci 2013;5(Suppl. 1):S125–S127; doi: 10.4103/0975-7406.113312.

[25] Brydone AS, Meek D, Maclaine S. Bone grafting, orthopaedic biomaterials, and the clinical need for bone engineering. Proc Inst Mech Eng H 2010;224(12):1329–1343; doi: 10.1243/09544119JEIM770.

[26] Dimitriou R, Jones E, McGonagle D, et al. Bone regeneration: Current concepts and future directions. BMC Medicine 2011;9(1):66; doi: 10.1186/1741-7015-9-66.

[27] Moshiri A, Oryan A. Role of tissue engineering in tendon reconstructive surgery and regenerative medicine: Current concepts, approaches and concerns. Hard Tissue 2012;1(2):11.

[28] Oryan A, Moshiri A. Recombinant fibroblast growth protein enhances healing ability of experimentally induced tendon injury in vivo. J Tissue Eng Regen Med 2014;8(6):421–431; doi: 10.1002/term.1534.

[29] Oryan A, Moshiri A. A long term study on the role of exogenous human recombinant basic fibroblast growth factor on the superficial digital flexor tendon healing in rabbits. J Musculoskelet Neuronal Interact 2011;11(2):185–195.

[30] Parizi AM, Oryan A, Shafiei-Sarvestani Z, et al. Human platelet rich plasma plus Persian Gulf coral effects on experimental bone healing in rabbit model: Radiological, histological, macroscopical and biomechanical evaluation. J Mater Sci Mater Med 2012;23(2):473–483; doi: 10.1007/s10856-011-4478-1.

[31] Oryan A, Meimandi Parizi A, Shafiei-Sarvestani Z, et al. Effects of combined hydroxyapatite and human platelet rich plasma on bone healing in rabbit model: Radiological, macroscopical, hidtopathological and biomechanical evaluation. Cell Tissue Bank 2012;13(4):639–651; doi: 10.1007/s10561-011-9285-x.

[32] Shafiei-Sarvestani Z, Oryan A, Bigham AS, et al. The effect of hydroxyapatite-hPRP, and coral-hPRP on bone healing in rabbits: Radiological, biomechanical, macroscopic and histopathologic evaluation. Int J Surg 2012;10(2):96–101; doi: 10.1016/j.ijsu.2011.12.010.

[33] Oryan A, Moshiri A, Raayat AR. Novel Application of TheranekronÒ Enhanced the structural and functional performance of the tenotomized tendon in rabbits. Cells Tissues Organs 2012;196(5):442–455; doi: 10.1159/ 000337860.

[34] Zimmermann G, Moghaddam A. Allograft bone matrix versus synthetic bone graft substitutes. Injury 2011;42:S16–S21; doi: 10.1016/j.injury.2011.06.199.

[35] Janicki P, Schmidmaier G. What should be the characteristics of the ideal bone graft substitute? Combining scaffolds with growth factors and/or stem cells. Injury 2011;42:S77–S81; doi: 10.1016/j.injury.2011.06.014.

[36] Oryan A, Moshiri A, Sharifi P. Advances in injured tendon engineering with emphasis on the role of collagen im- plants. Hard Tissue 2012;1(2):12.

[37] Oryan A, Alidadi S, Moshiri A. Current concerns regarding healing of bone defects. Hard Tissue 2013;2(2):1–12.

[38] Athanasiou VT, Papachristou DJ, Panagopoulos A, et al. Histological comparison of autograft, allograft-DBM, xenograft, and synthetic grafts in a trabecular bone defect: An experimental study in rabbits. Med Sci Monitor 2009;16(1):BR24–BR31.

[39] Putzier M, Strube P, Funk JF, et al. Allogenic versus autologous cancellous bone in lumbar segmental spondylodesis: A randomized prospective study. Eur Spine J 2009;18(5):687–695; doi: 10.1007/s00586-008-0875-7.

[40] Roberts TT, Rosenbaum AJ. Bone grafts, bone substitutes and orthobiologics: The bridge between basic science and clinical advancements in fracture healing. Organogenesis 2012;8(4):114–124; doi: 10.4161/org.23306.

[41] Bajaj P, Schweller RM, Khademhosseini A, et al. 3D b AU15 biofabrication strategies for tissue engineering and re- generative medicine. Annu Rev Biomed Eng 2014;16: 247–276.

[42] Thavornyutikarn B, Chantarapanich N, Sitthiseripratip K, et al. Bone tissue engineering scaffolding: Computer-aided scaffolding techniques. Prog Biomater 2014;3(2–4):61–102.

[43] Ma PX. Scaffolds for tissue fabrication. Mater Today 2004;7(5):30–40; doi: 10.1016/S1369-7021(04)00233-0.

[44] Ma PX, Langer R. Fabrication of biodegradable polymer foams for cell transplantation and tissue engineering. In: Tissue Engineering Methods and Protocols. (Morgan JR, Yarmush ML. eds.) Humana Press: Totowa, NJ, USA; 1999; pp. 47–56.

[45] Lu L, Peter SJ, Lyman MD, et al. In vitro degradation of porous poly(l-lactic acid) foams. Biomaterials 2000;21(15): 1595–1605; doi: 10.1016/S0142-9612(00)00048-X.

[46] Lee SB, Kim YH, Chong MS, et al. Study of gelatin containing artificial skin V: Fabrication of gelatin scaffolds using a salt-leaching method. Biomaterials 2005;26(14): 1961–1968; doi: 10.1016/j.biomaterials.2004.06.032.

[47] Lee SB, Kim YH, Chong MS, et al. Preparation and characteristics of hybrid scaffolds composed of b-chitin and collagen. Biomaterials 2004;25(12):2309–2317; doi: 10.1016/j.biomaterials.2003.09.016.

[48] Tessmar J, Holland T, Mikos A. Salt Leaching for Polymer Scaffolds. In: (Ma PX, Elisseeff J. eds.) CRC press: New York, USA; 2005; pp. 111-124.

[49] Montanheiro TLdA, Schatkoski VM, de Menezes BRC, et al. Recent progress on polymer scaffolds production: Methods, main results, advantages and disadvantages. Express Polymer Letters 2022;16(2):197-219, doi: 10.3144/expresspolymlett.2022.16.

[50] Subia B, Kundu J, Kundu SC. Biomaterial scaffold fabrication techniques for potential tissue engineering applications. Tissue Eng 2010;141(13-18).

[51] Quirk RA, France RM, Shakesheff KM, et al. Super- critical fluid technologies and tissue engineering scaffolds. Curr Opin Solid State Mater Sci 2004;8(3):313–321; doi: 10.1016/j.cossms.2003.12.004.

[52] Zellander A, Gemeinhart R, Djalilian A, et al. Designing a gas foamed scaffold for keratoprosthesis. Mater Sci Eng C Mater Biol Appl 2013;33(6):3396–3403; doi: 10.1016/j.msec.2013.04.025.

[53] Haugen H, Ried V, Brunner M, et al. Water as foaming agent for open cell polyurethane structures. J Mater Sci Mater Med 2004;15(4):343–346; doi: 10.1023/B:JMSM.0000021099.33619.ac.

[54] Mooney DJ, Baldwin DF, Suh NP, et al. Novel approach to fabricate porous sponges of poly(d,l-lactic-co-glycolic acid) without the use of organic solvents. Biomaterials 1996; 17(14):1417–1422; doi: 10.1016/0142-9612(96)87284-X.

[55] Kim HJ, Park IK, Kim JH, et al. Gas foaming fabrication of porous biphasic calcium phosphate for bone regeneration. Tissue Eng Regen Med 2012;9(2):63–68; doi: 10.1007/s13770-012-0022-8.

[56] Nam YS, Yoon JJ, Park TG. A novel fabrication method of macroporous biodegradable polymer scaffolds using gas foaming salt as a porogen additive. J Biomed Mater Res 2000;53(1):1–7.

[57] Keskar V, Marion NW, Mao JJ, et al. In vitro evaluation of macroporous hydrogels to facilitate stem cell infiltration, growth, and mineralization. Tissue Eng Part A 2009;15(7):1695–1707; doi: 10.1089/ten.tea.2008.0238.

[58] Wachiralarpphaithoon C, Iwasaki Y, Akiyoshi K. Enzyme-degradable phosphorylcholine porous hydrogels cross-linked with polyphosphoesters for cell matrices. Biomaterials 2007;28(6):984–993; doi: 10.1016/j.biomaterials.2006.10.024.

[59] Mikos AG, Temenoff JS. Formation of highly porous biodegradable scaffolds for tissue engineering. Electr J Biotechnol 2000;3:23–24.

[60] Nam YS, Park TG. Porous biodegradable polymeric scaffolds prepared by thermally induced phase separation. J Biomed Mater Res 1999;47(1):8–17.

[61] Schugens C, Maquet V, Grandfils C, et al. Polylactide macroporous biodegradable implants for cell transplantation. II. Preparation of polylactide foams by liquid-liquid phase separation. J Biomed Mater Res 1996;30(4):449–461.

[62] Kim HD, Bae EH, Kwon IC, et al. Effect of PEG–PLLA diblock copolymer on macroporous PLLA scaffolds by thermally induced phase separation. Biomaterials 2004;25(12):2319–2329; doi: 10.1016/j.biomaterials.2003.09.011.

[63] Sachlos E, Czernuszka JT. Making tissue engineering scaffolds work. Review: The application of solid freeform fabrication technology to the production of tissue engineering scaffolds. Eur Cell Mater 2003;5:29–39.

[64] Whang K, Thomas CH, Healy KE, et al. A novel method to fabricate bioabsorbable scaffolds. Polymer 1995;36(4):837–842; doi: 10.1016/0032-3861(95)93115-3.

[65] O'Brien FJ, Harley BA, Yannas IV, et al. Influence of freezing rate on pore structure in freeze-dried collagen- GAG scaffolds. Biomaterials 2004;25(6):1077–1086; doi: 10.1016/S0142-9612(03)00630-6.

[66] Park S-N, Park J-C, Kim HO, et al. Characterization of porous collagen/hyaluronic acid scaffold modified by 1- ethyl-3-(3-dimethylaminopropyl)carbodiimide cross-linking. Biomaterials 2002;23(4):1205–1212; doi: 10.1016/S0142-9612(01)00235-6.

[67] Wu X, Liu Y, Li X, et al. Preparation of aligned porous gelatin scaffolds by unidirectional freeze-drying method. Acta biomaterialia 2010;6(3):1167-1177.

[68] Zhu N, Chen X. Biofabrication of tissue scaffolds. In: Advances in biomaterials science and biomedical applications. (Pignatello R. ed.) InTech Rijeka, Croatia; 2013; pp. 315-328.

[69] Ramakrishna S. An introduction to electrospinning and nanofibers. World scientific: Singapore; 2005.

[70] Nalbandian MJ-C. Development and Optimization of Chemically-Active Electrospun Nanofibers for Treatment of Impaired Water Sources. University of California, Riverside: Riverside, CA, USA; 2014.

[71] Wutticharoenmongkol P, Sanchavanakit N, Pavasant P, et al. Novel bone scaffolds of electrospun polycaprolactone fibers filled with nanoparticles. J Nanosci Nanotechnol 2006;6(2):514–522.

[72] He F-L, Li D-W, He J, et al. A novel layer-structured scaffold with large pore sizes suitable for 3D cell culture prepared by near-field electrospinning. Mater Sci Eng C Mater Biol Appl 2018;86:18–27; doi: 10.1016/j.msec.2017.12.016.

[73] Dhand C, Ong ST, Dwivedi N, et al. Bio-inspired in situ crosslinking and mineralization of electrospun collagen scaffolds for bone tissue engineering. Biomaterials 2016;104:323–338; doi: 10.1016/j.biomaterials.2016.07.007.

[74] Thavasi V, Singh G, Ramakrishna S. Electrospun nanofibers in energy and environmental applications. Energy Environ Sci 2008;1(2):205–221; doi: 10.1039/B809074M.

[75] Varga M. Chapter 3 - Self-assembly of nanobiomaterials. In: Fabrication and Self-Assembly of Nanobiomaterials. (Grumezescu AM. ed.) William Andrew Publishing: Norwich, NY, USA; 2016; pp. 57-90.

[76] Wade RJ, Burdick JA. Advances in nanofibrous scaffolds for biomedical applications: From electrospinning to self- assembly. Nano Today 2014;9(6):722–742; doi: 10.1016/j.nantod.2014.10.002.

[77] Nie W, Peng C, Zhou X, et al. Three-dimensional porous scaffold by self-assembly of reduced graphene oxide and nano-hydroxyapatite composites for bone tissue engineering. Carbon 2017;116:325–337; doi: 10.1016/j.carbon.2017.02.013.

[78] Ding Y, Li W, Schubert DW, et al. An organic-inorganic hybrid scaffold with honeycomb-like structures enabled by one-step self-assembly-driven electrospinning. Mater Sci Eng C Mater Biol Appl 2021;124:112079; doi: 10.1016/j.msec.2021.112079.

[79] Liu Tsang V, Bhatia SN. Three-dimensional tissue fabrication. Adv Drug Deliv Rev 2004;56(11):1635–1647; doi: 10.1016/j.addr.2004.05.001.

[80] Yeong W-Y, Chua C-K, Leong K-F, et al. Rapid proto- typing in tissue engineering: Challenges and potential. Trends Biotechnol 2004;22(12):643–652; doi: 10.1016/j.tibtech.2004.10.004.

[81] Hollister SJ. Porous scaffold design for tissue engineering. Nat Mater 2005;4(7):518–524; doi: 10.1038/nmat1421.

[82] Mohammed A, Elshaer A, Sareh P, et al. Additive manufacturing technologies for drug delivery applications. Int J Pharm 2020;580:119245.

[83] Pieterse FF, Nel AL. The advantages of 3D printing in undergraduate mechanical engineering research. In: 2016 IEEE Global Engineering Education Conference (EDU- CON), Abu Dhabi, United Arab Emirates. 2016; pp. 25–31.

[84] Berman B. 3-D printing: The new industrial revolution. Business Horizons 2012;55(2):155–162; doi: 10.1016/j.bushor.2011.11.003.

[85] Klippstein H, Diaz De Cerio Sanchez A, Hassanin H, et al. Fused deposition modeling for unmanned aerial vehicles (UAVs): A review. Adv Eng Mater 2018;20(2):1700552; doi: 10.1002/adem.201700552.

[86] Essa K, Hassanin H, Attallah MM, et al. Development and testing of an additively manufactured monolithic catalyst bed for HTP thruster applications. Appl Catal A Gen 2017;542:125–135; doi: 10.1016/j.apcata.2017.05.019.

[87] Qiu C, Adkins NJE, Hassanin H, et al. In-situ shelling via selective laser melting: Modelling and microstructural characterisation. Mater Des 2015;87:845–853; doi: 10.1016/j.matdes.2015.08.091.

[88] Sabouri A, Yetisen AK, Sadigzade R, et al. Three- dimensional microstructured lattices for oil sensing. En- ergy Fuels 2017;31(3):2524–2529; doi: 10.1021/acs.energyfuels.6b02850.

[89] Klippstein H, Hassanin H, Diaz De Cerio Sanchez A, et al. Additive manufacturing of porous structures for un- manned aerial vehicles applications. Adv Eng Mater 2018;20(9):1800290; doi: 10.1002/adem.201800290.

[90] Ferrari A, Frank D, Hennen L, et al. Additive bio-manufacturing: 3D printing for medical recovery and human enhancement. European Parliament's Science and Technology Options Assessment: France; 2018.

[91] Ziaee M, Crane NB. Binder jetting: A review of process, materials, and methods. Addit Manuf 2019;28:781–801; doi: 10.1016/j.addma.2019.05.031.

[92] Chavanne P, Stevanovic S, Wüthrich A, et al. 3D printed chitosan / hydroxyapatite scaffolds for potential use in regenerative medicine. Biomed Tech (Berl) 2013;58 Suppl 1(2, doi:10.1515/bmt-2013-4069.

[93] Hong D, Chou D-T, Velikokhatnyi OI, et al. Binder- jetting 3D printing and alloy development of new biodegradable Fe-Mn-Ca/Mg alloys. Acta Biomater 2016;45:375–386; doi: 10.1016/j.actbio.2016.08.032.

[94] Mostafaei A, Elliott AM, Barnes JE, et al. Binder jet 3D printing—Process parameters, materials, properties, modeling, and challenges. Progr Mater Sci 2021;119: 100707; doi: 10.1016/j.pmatsci.2020.100707.

[95] Lim SH, Kathuria H, Tan JJY, et al. 3D printed drug delivery and testing systems—A passing fad or the future? Adv Drug Deliv Rev 2018;132:139–168; doi: 10.1016/j.addr.2018.05.006.

[96] Pusch K, Hinton TJ, Feinberg AW. Large volume syringe pump extruder for desktop 3D printers. HardwareX 2018;3:49–61; doi: 10.1016/j.ohx.2018.02.001.

[97] Poldervaart MT, Gremmels H, van Deventer K, et al. Pro- longed presence of VEGF promotes vascularization in 3D bioprinted scaffolds with defined architecture. J Control Release 2014;184:58–66; doi: 10.1016/j.jconrel.2014.04.007.

[98] Ahlfeld T, Akkineni AR, Fo¨rster Y, et al. Design and fabrication of complex scaffolds for bone defect healing: Combined 3D plotting of a calcium phosphate cement and a growth factor-loaded hydrogel. Ann Biomed Eng 2017;45(1):224–236; doi: 10.1007/s10439-016-1685-4.

[99] Whulanza Y, Arsyan R, Saragih AS. Characterization of hydrogel printer for direct cell-laden scaffolds. AIP Con- fer Proceed 2018;1933(1):040002; doi: 10.1063/1.5023972.

[100] Negro A, Cherbuin T, Lutolf M. 3D inkjet printing of complex, cell-laden hydrogel structures. Sci Rep 2018;8:17099; doi: 10.1038/s41598-018-35504-2.

[101] Wei L, Wu S, Kuss M, et al. 3D printing of silk fibroin- based hybrid scaffold treated with platelet rich plasma for bone tissue engineering. Bioact Mater 2019;4:256–260; doi: 10.1016/j.bioactmat.2019.09.001.

[102] Ozbolat IT, Chen H, Yu Y. Development of 'Multi-arm Bioprinter' for hybrid biofabrication of tissue engineering constructs. Robot Comput Integr Manuf 2014;30(3):295– 304; doi: 10.1016/j.rcim.2013.10.005.

[103] Ngo TD, Kashani A, Imbalzano G, et al. Additive manufacturing (3D printing): A review of materials, methods, applications and challenges. Compos B Eng 2018;143: 172–196; doi: 10.1016/j.compositesb.2018.02.012.

[104] Langford T, Mohammed A, Essa K, et al. 4D printing of origami structures for minimally invasive surgeries using functional scaffold. Appl Sci 2021;11(1):332.

[105] Hong JM, Kim BJ, Shim J-H, et al. Enhancement of bone regeneration through facile surface functionalization of solid freeform fabrication-based three-dimensional scaffolds using mussel adhesive proteins. Acta Biomater 2012;8(7):2578–2586; doi: 10.1016/j.actbio.2012.03.041.

[106] Wong KV, Hernandez A. A review of additive manufacturing. ISRN Mech Eng 2012;2012:208760; doi: 10.5402/2012/208760.

[107] Zein I, Hutmacher DW, Tan KC, et al. Fused deposition modeling of novel scaffold architectures for tissue engineering applications. Biomaterials 2002;23(4):1169–1185; doi: 10.1016/S0142-9612(01)00232-0.

[108] Water JJ, Bohr A, Boetker J, et al. Three-dimensional printing of drug-eluting implants: Preparation of an anti- microbial polylactide feedstock material. J Pharmaceut Sci 2015;104(3):1099–1107; doi: 10.1002/jps.24305.

[109] Sandler N, Salmela I, Fallarero A, et al. Towards fabrication of 3D printed medical devices to prevent biofilm formation. Int J Pharm 2014;459(1):62–64; doi: 10.1016/j.ijpharm.2013.11.001.

[110] Melcˇova´ V, Svoradova´ K, Mencˇ´ık P, et al. FDM 3D printed composites for bone tissue engineering based on plasticized poly(3-hydroxybutyrate)/poly(d,l-

lactide) blends. Polymers (Basel) 2020;12(12):2806; doi: 10.3390/polym12122806.

[111] Bittredge O, Hassanin H, El-Sayed MA, et al. Fabrication and optimisation of Ti-6Al-4V lattice-structured total shoulder implants using laser additive manufacturing. Materials (Basel) 2022;15(9):3095.

[112] Elsayed M, Ghazy M, Youssef Y, et al. Optimization of SLM process parameters for Ti6Al4V medical implants. Rapid Prototyp J 2019;25(3):433–447; doi: 10.1108/RPJ- 05-2018-0112.

[113] El-Sayed MA, Essa K, Ghazy M, et al. Design optimization of additively manufactured titanium lattice structures for biomedical implants. Int J Adv Manuf Technol 2020;110(9):2257–2268; doi: 10.1007/s00170-020-05982-8.

[114] Kusoglu I, Don˜ate-Buend´ıa C, Barcikowski S, et al. Laser powder bed fusion of polymers: Quantitative research direction indices. Materials (Basel, Switzerland) 2021;14(5):1169; doi: 10.3390/ma14051169.

[115] Gaur B, Soman D, Ghyar R, et al. Ti6Al4V scaffolds fabricated by laser powder bed fusion with hybrid volumetric energy density. Rapid Prototyp J 2022;29(1):67–79; doi: 10.1108/RPJ-01-2022-0036.

[116] Liu F-H. Synthesis of biomedical composite scaffolds by laser sintering: Mechanical properties and in vitro bioactivity evaluation. Appl Surf Sci 2014;297:1–8; doi: 10.1016/j.apsusc.2013.12.130.

[117] Gibson I. Material properties and fabrication parameters in selective laser sintering process. Rapid Prototyp J 1997;3(4):129–136; doi: 10.1108/13552549710191836.

[118] Duan B, Cheung WL, Wang M. Optimized fabrication of Ca–P/PHBV nanocomposite scaffolds via selective laser sintering for bone tissue engineering. Biofabrication 2011;3(1):015001; doi: 10.1088/1758-5082/3/1/015001.

[119] Williams JM, Adewunmi A, Schek RM, et al. Bone tissue engineering using polycaprolactone scaffolds fabricated via selective laser sintering. Biomaterials 2005;26(23):4817– 4827; doi: 10.1016/j.biomaterials.2004.11.057.

[120] Kruth JP, Levy G, Klocke F, et al. Consolidation phenomena in laser and powder-bed based layered manufacturing. CIRP Ann Manuf Technol 2007;56(2):730–759; doi: 10.1016/j.cirp.2007.10.004.

[121] Park HK, Shin M, Kim B, et al. A visible light-curable yet visible wavelength-transparent resin for stereolithography 3D printing. NPG Asia Mater 2018;10(4):82–89; doi: 10.1038/s41427-018-0021-x.

[122] Huang J, Qin Q, Wang J. A review of stereolithography: Processes and systems. Processes 2020;8(9):1138.

[123] Schmidleithner C, Kalaskar DM. Stereolithography. In: 3D Printing. (Cvetković D. ed.) IntechOpen: London, UK; 2018; pp. 196.

[124] Nguyen KT, West JL. Photopolymerizable hydrogels for tissue engineering applications. Biomaterials 2002;23(22): 4307–4314; doi: 10.1016/S0142-9612(02)00175-8.

[125] Cooke MN, Fisher JP, Dean D, et al. Use of stereo- lithography to manufacture critical-sized 3D biodegradable scaffolds for bone ingrowth. J Biomed Mater Res B Appl Biomater 2003;64B(2):65–69; doi: 10.1002/jbm.b.10485.

[126] Harris RA, Newlyn HA, Hague RJM, et al. Part shrinkage anomilies from stereolithography injection mould tooling. Int J Mach Tools Manuf 2003;43(9):879–887; doi: 10.1016/S0890-6955(03)00080-4.

[127] Wang WL, Cheah CM, Fuh JYH, et al. Influence of process parameters on stereolithography part shrinkage. Mater Des 1996;17(4):205–213; doi: 10.1016/S0261-3069(97)00008-3.

[128] Kim K, Yeatts A, Dean D, et al. Stereolithographic bone scaffold design parameters: Osteogenic differentiation and signal expression. Tissue Eng Part B Rev 2010;16(5):523– 539; doi: 10.1089/ten.teb.2010.0171.

[129] Sinha RP, Ha¨der D-P. UV-induced DNA damage and repair: A review. Photochem Photobiol Sci 2002;1(4): 225–236; doi: 10.1039/B201230H.

[130] de Gruijl FR, van Kranen HJ, Mullenders LHF. UV- induced DNA damage, repair, mutations and oncogenic pathways in skin cancer. J Photochem Photobiol B Biol 2001;63(1):19–27; doi: 10.1016/S1011-1344(01)00199-3.

[131] Lam CXF, Mo XM, Teoh SH, et al. Scaffold development using 3D printing with a starch-based polymer. Mater Sci Eng C Mater Biol Appl 2002;20(1):49-56, doi: https://doi.org/10.1016/S0928-4931(02)00012-7.

[132] Zeltinger J, Sherwood JK, Graham DA, et al. Effect of Pore Size and Void Fraction on Cellular Adhesion, Proliferation, and Matrix Deposition. Tissue Engineering 2001;7(5):557-572, doi:10.1089/107632701753213183.

[133] Therriault D, White SR, Lewis JA. Chaotic mixing in three-dimensional microvascular networks fabricated by direct-write assembly. Nat Mater 2003;2(4):265-271, doi:10.1038/nmat863.

[134] Do A-V, Smith R, Acri TM, et al. 9 - 3D printing technologies for 3D scaffold engineering. In: Functional 3D Tissue Engineering Scaffolds. (Deng Y, Kuiper J. eds.) Woodhead Publishing: 2018; pp. 203-234.

[135] Xiong Z, Yan Y, Wang S, et al. Fabrication of porous scaffolds for bone tissue engineering via low-temperature deposition. Scripta Materialia 2002;46(11):771-776, doi: https://doi.org/10.1016/S1359-6462(02)00071-4.

[136] Yan Y, Xiong Z, Hu Y, et al. Layered manufacturing of tissue engineering scaffolds via multi-nozzle deposition. Materials Letters 2003;57(18):2623-2628, doi: https://doi.org/10.1016/S0167-577X(02)01339-3.

[137] Vozzi G, Previti A, De Rossi D, et al. Microsyringe-Based Deposition of Two-Dimensional and Three-Dimensional Polymer Scaffolds with a Well-Defined Geometry for Application to Tissue Engineering. Tissue Engineering 2002;8(6):1089-1098, doi:10.1089/107632702320934182.

[138] Landers R, Mülhaupt R. Desktop manufacturing of complex objects, prototypes and biomedical scaffolds by means of computer-assisted design combined with computer-guided 3D plotting of polymers and reactive oligomers. Macromol Mater Eng 2000;282(1):17-21.

[139] An J, Teoh JEM, Suntornnond R, et al. Design and 3D Printing of Scaffolds and Tissues. Engineering 2015;1(2):261-268, doi: https://doi.org/10.15302/J-ENG-2015061.

[140] Woodfield TBF, Malda J, de Wijn J, et al. Design of porous scaffolds for cartilage tissue engineering using a three-dimensional fiber-deposition technique. Biomaterials 2004;25(18):4149-4161, doi: https://doi.org/10.1016/j.biomaterials.2003.10.056.

[141] Wang F, Shor L, Darling A, et al. Precision Extruding Deposition and Characterization of Cellular Poly-e-Caprolactone Tissue Scaffolds 573. 2003.

[142] Tan KH, Chua CK, Leong KF, et al. Scaffold development using selective laser sintering of polyetheretherketone–hydroxyapatite biocomposite blends. Biomaterials 2003;24(18):3115-3123, doi: https://doi.org/10.1016/S0142-9612(03)00131-5.

[143] Wang D, Wang Y, Wu S, et al. Customized a Ti6Al4V bone plate for complex pelvic fracture by selective laser melting. Materials 2017;10(1):35.

[144] Turnbull G, Clarke J, Picard F, et al. 3D bioactive composite scaffolds for bone tissue engineering. Bioact Mater 2018;3(3):278-314, doi: https://doi.org/10.1016/j.bioactmat.2017.10.001.

[145] Chu TMG, Halloran JW, Hollister SJ, et al. Hydroxyapatite implants with designed internal architecture. Journal of Materials Science: Materials in Medicine 2001;12(6):471-478, doi:10.1023/A:1011203226053.

[146] Bittner SM, Guo JL, Melchiorri A, et al. Three-dimensional printing of multilayered tissue engineering scaffolds. Materials Today 2018;21(8):861-874, doi: https://doi.org/10.1016/j.mattod.2018.02.006.

[147] Palmero EM, Bollero A. 3D and 4D printing of functional and smart composite materials. In: Encyclopedia of Materials: Composites. (Brabazon D. ed.) Elsevier: Oxford; 2021; pp. 402–419.

[148] Ashish, Ahmad N, Gopinath P, et al. Chapter 1 - 3D Printing in Medicine: Current Challenges and Potential Applications. In: 3D Printing Technology in Nanomedicine. (Ahmad N, Gopinath P, Dutta R. eds.) Elsevier: Amsterdam 2019; pp. 1-22.b AU23.

[149] Da´vila J, Neto P, Noritomi P, et al. Hybrid manufacturing: A review of the synergy between directed energy deposition and subtractive processes. Int J Adv Manuf Technol 2020;110:3377–3390; doi: 10.1007/s00170-020-06062-7.

[150] Ashish, Ahmad N, Gopinath P, et al. Chapter 1 - 3D printing in medicine: Current challenges and potential applications. In: 3D Printing Technology in Nanomedicine. (Ahmad N, Gopinath P, Dutta R. eds.) Elsevier: New York, NY, USA; 2019; pp. 1–22.

[151] Rouf S, Malik A, Singh N, et al. Additive manufacturing technologies: Industrial and medical applications. Sustainable Operations and Computers 2022;3:258–274; doi: 10.1016/j.susoc.2022.05.001.

[152] Nadagouda MN, Ginn M, Rastogi V. A review of 3D printing techniques for environmental applications. Curr Opin Chem Eng 2020;28:173–178; doi: 10.1016/j.coche.2020.08.002.

[153] Gibson I, Rosen D, Stucker B. Additive Manufacturing Technologies: 3D Printing, Rapid Prototyping, and Direct Digital Manufacturing. Springer: New York, NY, USA; 2014.

[154] He J, Xia P, Li D. Development of melt electro- hydrodynamic 3D printing for complex microscale poly (e-caprolactone) scaffolds. Biofabrication 2016;8(3): 035008; doi: 10.1088/1758-5090/8/3/035008.

[155] Hassanin H, Modica F, El-Sayed MA, et al. Manufacturing of Ti–6Al–4V micro-implantable parts using hybrid selective laser melting and micro-electrical discharge machining. Adv Eng Mater 2016;18(9):1544–1549; doi: 10.1002/adem.201600172.

[156] Cheng K, Xiong W, Li Y, et al. In-situ deposition of three- dimensional graphene on selective laser melted copper scaffolds for high performance applications. Comp Part A Appl Sci Manuf 2020;135:105904; doi: 10.1016/j.compositesa.2020.10590

3 Chapter Three: Preparation of Polylactic Acid/Calcium Peroxide Composite Filaments for Fused Deposition Modelling

Abdullah H. Mohammed [1] , Nikolina Kovacev [1] , Amr Elshaer [3] , Ammar A. Melaibari [2,4] , Javed Iqbal [2] , Hany Hassanin [5] , Khamis Essa [1] and Adnan Memic´ [2,*]

1. School of Engineering, University of Birmingham, Birmingham B15 2TT, UK
2. Center of Nanotechnology, King Abdulaziz University, Jeddah 21589, Saudi Arabia
3. Drug Discovery, Delivery and Patient Care, School of Life Sciences, Pharmacy and Chemistry, Kingston University London, Kingston upon Thames KT1 2EE, UK
4. School of Engineering, King Abdulaziz University, Jeddah, Saudi Arabia
5. School of Engineering, Canterbury Christ Church University, Canterbury CT1 1QU, UK

Authorship contribution statement

Conceptualization, **A.H.M**., H.H. and K.E.; Methodology, **A.H.M**., A.M., H.H. and K.E.; Formal analysis, **A.H.M**., A.E., H.H., A.M. and K.E.; Investigation (Operating SEM and Tensile Test machines), **A.H.M**., N.K. and J.I.; Resources A.M., A.A.M. and K.E. Writing—original draft, **A.H.M**. and H.H.; Writing—review & editing, A.M., H.H., A.A.M., A.E. and K.E.; Visualization, **A.H.M**., J.I.; Supervision, A.M., H.H., A.E. and K.E.; Project administration, A.M., A.A.M., H.H. and K.E.

3.1 Abstract

Fused Deposition Modelling (FDM) 3D printers have gained significant popularity in the pharmaceutical and biomedical industries. In this study, a new biomaterial filament was developed by preparing a polylactic acid (PLA)/calcium peroxide (CPO) composite using wet solution mixing and extrusion. The content of CPO varied from 3% to 24% wt/wt., and hot-melt extruder parameters were optimised to fabricate 3D printable composite filaments. The filaments were characterised using X-ray diffraction analysis, surface morphology assessment, evaluation of filament extrudability, microstructural analysis, and examination of their rheological and mechanical properties. Our findings indicate that increasing the CPO content resulted in increased viscosity at 200 ˚C, while the PLA/CPO samples showed microstructural changes from crystalline to amorphous. The mechanical strength and ductility of the composite filaments decreased except for in the 6% CPO filament. Due to its acceptable surface morphology and strength, the PLA/CPO filament with 6% CPO was selected for printability testing. The 3D-printed sample of a bone scaffold exhibited good printing quality, demonstrating the potential of the PLA/CPO filament as an improved biocompatible filament for FDM 3D printing.

3.2 Introduction

Today, 3D printing, also known as additive manufacturing (AM), is a revolutionary technology that utilises computer-aided design to print three-dimensional objects layer by layer based on a digital model [1]. This technology has gained widespread use across various industries owing to its numerous advantages over conventional techniques, such as rapid production, the elimination of tooling requirements, high geometrical freedom, and the efficient use of materials [2–4]. According to the ISO/ASTM 52,900 standard, 3D

printing technologies are classified into seven distinct groups, which include VAT polymerisation, powder bed fusion, binder jetting, material extrusion, direct energy deposition, material jetting, and sheet lamination [5]. Material extrusion is a vital category of additive manufacturing that is commonly employed by researchers, hobbyists, and numerous industries, including pharmaceuticals and biomedical engineering. The technology, originally developed by Stratasys in 1989, is known as Fused Deposition Modelling (FDM) and is used for 3D printing thermoplastic materials [6,7]. Fused Deposition Modelling (FDM) is a popular 3D printing technology because of its versatility and ability to produce functional parts and prototypes from a wide variety of materials [8,9]. It can be utilised to fabricate objects using thermoplastics, metals, ceramics, and composite materials, which has contributed to its widespread adoption [10,11]. In FDM, filaments are heated, softened, and extruded through a hot nozzle and deposited on a building bed layer by layer according to a computer-aided design (CAD) model.

Since filament materials are the backbone of any FDM process, industry and academia have expressed much interest in the production and development of new materials, particularly biocompatible and biodegradable materials that are high quality [11–13]. Currently, polylactic acid (PLA), polycaprolactone (PCL), and acrylonitrile butadiene styrene (ABS) have been the most often utilised polymers for filament production [14]. Compared to ABS and PCL, there is a growing demand and promising future for PLA filaments due to their excellent mechanical properties, processability, biodegradability, and biocompatibility, all of which are highly influenced by their molecular structure and molecular weight [5,15]. Furthermore, PLA's unique properties make it a viable material with a wide range of industrial uses, including for use in biomedical devices [16,17]. In addition, the US Food and Drug Administration (FDA) has approved it for a number of biomedical and clinical applications [18]. In particular, PLA has been extensively used in bone scaffolds [16]. This is a result

of its excellent bioresorption properties, which facilitate its integration with host tissues. PLA has also been combined with other materials to produce FDM filaments for biomedical applications, such as hydroxyapatite (HA), polyethene glycol (PEG), and ferromagnetic materials (Fe_3O_4), due to their excellent healing properties [19–22].

Despite the promising results of using PLA and their composites, an insufficient oxygen supply is a barrier to widely adopting their application in tissue engineering. Several approaches have been used to promote oxygen delivery to bone implants. Growth factors have been added to the implant in order to promote bone neovascularisation. However, it can only be effective with implant sizes of a few millimetres. Other approaches have been adopted to include oxygen-generating materials with the implanted device.

Hydrogen peroxide (H_2O_2) has been found to be highly effective in tissue engineering at low concentrations due to its low toxicity, which can be well controlled for tissue engineering applications [23,24]. H_2O_2 is generated as an intermediate product during the oxygenation process of oxygen-generating particles, such as calcium peroxide [25,26]. Studies have demonstrated that having an oxygen supply within the scaffold holds great promise for the success of the scaffold's functionality, as it encourages vascularisation [27]. One study by Hilde et al. [28] fabricated a PLA/CaO_2 (i.e., calcium peroxide (CPO)) composite bone scaffold via wet solution mixing. They conducted an XTT assay to assess the scaffold cytotoxicity after adding a catalase to the culture medium. The study showed that the incorporation of CaO_2 particles into biodegradable composite materials made with PLA or PLGA polymers has been found to increase the release of oxygen and to reduce cytotoxicity [28]. Studies found in the biomedical literature have shown that incorporating oxygenation particles into biomedical materials can have a positive impact on bone tissue by promoting vascularisation and regeneration, and by improving the overall healing process. In addition, they also demonstrated that PLA/CPO has potential for use in bone tissue engineering.

However, there has been no research on the preparation of PLA/CPO composite filaments for 3D printing using Fused Deposition Modelling (FDM) technology, despite its potential as a promising biomaterial. To address this gap, we developed a novel FDM filament, which was composed of PLA and CPO, which was produced using a wet solution mixing and hot-melt extruder approach. CPO powder was selected as an oxygen generator due to its proven effectiveness in biomedical applications while remaining non-harmful to the human body. The content of CPO varied from 3% to 24% wt/wt., allowing us to examine filament printability and determine the maximum CPO load that can be added. The prepared filaments were characterised in terms of their rheological properties, X-ray diffraction, surface morphology, extrudability, microstructural analysis, mechanical properties, and printability.

3.3 Materials and Methods

3.3.1 Materials

The materials used include: 1.75 mm polylactic acid (PLA) natural filament, which was purchased from Shenzhen eSUN Industrial Co. Ltd., Shenzhen, China; calcium peroxide (CPO) CaO_2 (−200 mesh size, 74 μm particles size, 75% purity), which was purchased from Sigma-Aldrich (St. Louis, MO, USA); dichloromethane (DCM), which was purchased from Sigma-Aldrich (St. Louis, MO, USA); and deionised water.

3.3.2 Preparation of Composite Filament

To prepare the PLA/CPO composite filaments, 20 g of PLA filaments were cut into small pieces and dissolved in 100 mL of DCM for approximately 30 min at room temperature using a magnetic stirrer set to a speed of 700 rpm. Once the PLA was completely dissolved, CPO powder was added to the solution at different ratios (Table 3.1) under vigorous magnetic stirring for 90 min before it was poured into a large plate to dry at room

temperature of 22 °C for 24 h. After the prepared composite materials were dried, they were cut into small pieces around 2x2 cm to be loaded into a hot-melt extruder. Figure 3.1 illustrates the schematic diagram of this process. The extrusion of the composite materials was carried out using a customised single-screw extruder with a nozzle diameter of approximately 2 mm. Our objective was to achieve an optimal filament diameter of 1.75 mm and a smooth surface suitable for commercial Fused Deposition Modelling (FDM) 3D printers. To accomplish this, the composite materials were extruded at various temperatures and feed rates. Experiments were conducted at four different extrusion temperatures, specifically 130 °C, 140 °C, 150 °C, and 155 °C, while maintaining a constant screw speed of 1.5 rpm. The composite was introduced into the extruder at two different feed rates, which are referred to as F1, the feed rate of approximately 1.5 g, and F2, the feed rate of approximately 6.5 g. The extrusion speed was dependent on the feed rates, while the screw speed remained constant at all times.

Table 3.1. PLA/CPO composite ratios.

Sample Name	**PLA (%wt.)**	**CPO (%wt.)**
3% CPO	97	3
6% CPO	94	6
12% CPO	88	12
24% CPO	76	24

3.3.3 Filament Characterisation

The JSM-7600F field-emission scanning electron microscope (JEOL, Tokyo, Japan) was employed to examine the surface morphology of samples with different ratios and extrusion conditions. Additionally, optical images of the 3D-printed scaffolds using the composite filament were captured using a Canon 1000D digital camera. Prior to SEM analysis, all samples were sputter-coated with a thin layer of gold using a JFC-1600 auto fine coater (JEOL, Tokyo, Japan). The samples' elemental compositions were assessed using energy-dispersive X-ray spectroscopy (EDX), which was linked to the SEM. Additionally, an Ultima IV X-ray diffractometer (XRD) (Rigaku, Japan), ICDD (PDF-2/release 2011 RDB), attached with Cu Ka radiations and DB card No. 01-071-4107 were used to observe the material microstructure and phase changes of the samples before and after extruding at a goniometer speed of 1.00 sec and a step of 0.100°.

The samples' filaments were preheated in a 40 mm cylindrical mould at approximately 230 °C by Bosch heat gun model EasyHeat 500, were compressed manually, and then were allowed to cool at room temperature of 22 °C for 24 h to prepare test specimens for rheology testing. Temperatures were measured using Etekcity non-contact digital laser infrared thermometer model Lasergrip 774. The rheological analysis was conducted at room temperature around 22°C using a discovery HR-3 hybrid rheometer (TA Instruments, New Castle, DE, USA) in a parallel plate configuration (diameter = 40 mm) with a constant gap of 0.5 mm. A flow ramp was performed at 200 °C with a shear rate ranging from 0.1 to 1000 s^{-1}.

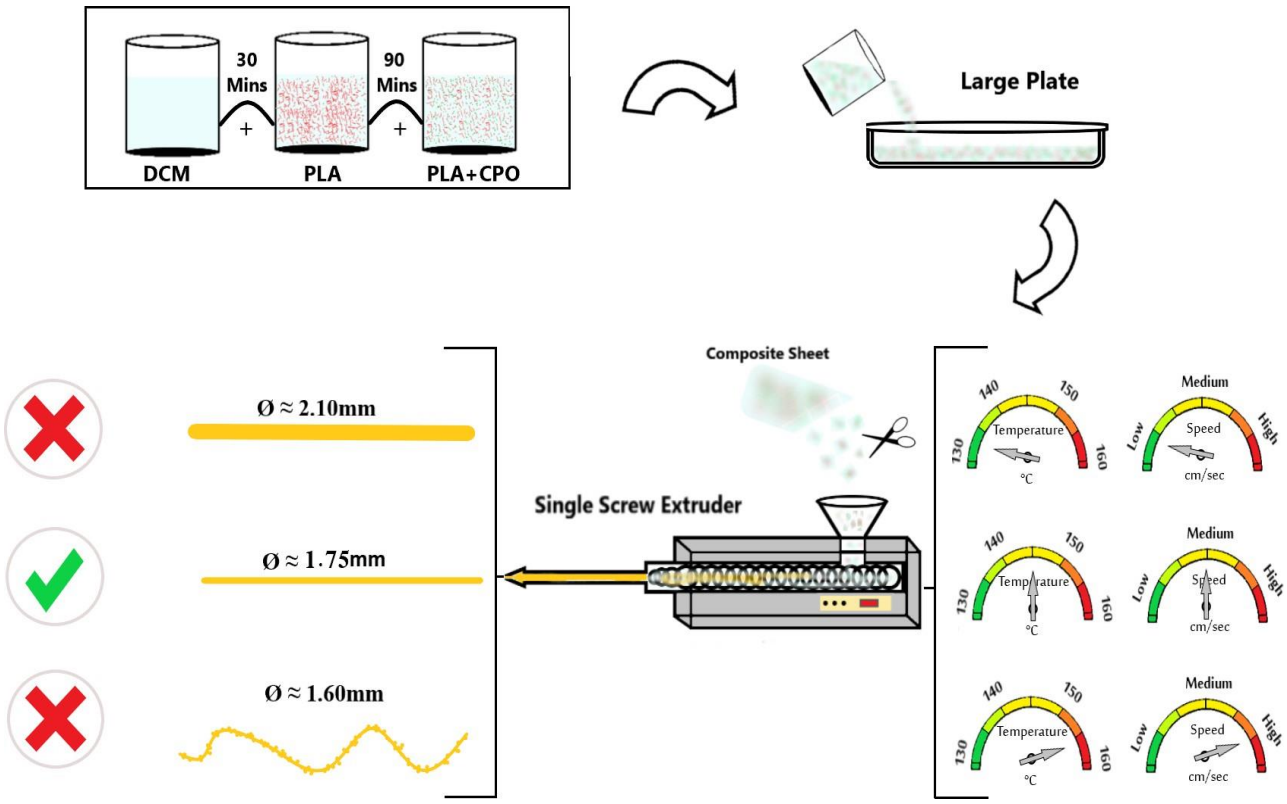

Figure 3.1. Schematic illustration of composite filament preparation.

The mechanical properties of the samples were determined using a universal Instron 3367 testing machine (Norwood, MA, USA) equipped with a 30 kN load cell according to ASTM D4603. Tensile testing was conducted on filament samples ranging in diameter from 1.75 mm to 1.95 mm and with a length of 90 mm using manual grips. The machine was set at a constant crosshead speed of 5 mm/min. The engineering stress–strain curves were used to calculate Young's modulus (E), yield or ultimate tensile strength (σy), strain at the maximum stress (εm), and strain at break (εb). To ensure accuracy, each experiment was performed three times, and the average was calculated. The information is presented as the mean ± standard deviation (SD). Origin software (OriginPro 8.0, Origin Lab Inc., Northampton, MA, USA) was used to analyse and display the data in the form of graphs.

3.4 Results and Discussion

3.4.1 Optimisation of Extrusion Parameters

To obtain high-quality filaments with a consistent diameter and smooth surface morphology, the extrusion of the PLA/CPO raw material was systematically investigated. The extrusion temperature and feed rate are crucial parameters for achieving optimal results, as shown in Figure 3.2. The diameter and speed of the extruded filaments were evaluated under different nozzle temperatures (130 °C, 140 °C, 150 °C, and 155 °C) and two sets of feed rates (F1 ≈ 1.5 g and F2 ≈ 6.5 g), as shown in Figure 3.1. The PLA feedstock was chopped into small pieces to fit the extruder feeder and was loaded simultaneously. The extruder screw speed was maintained at a constant 1.5 rpm throughout the extrusion process. Figure 3.2 summarises the results for filament diameter and speed at different extrusion conditions.

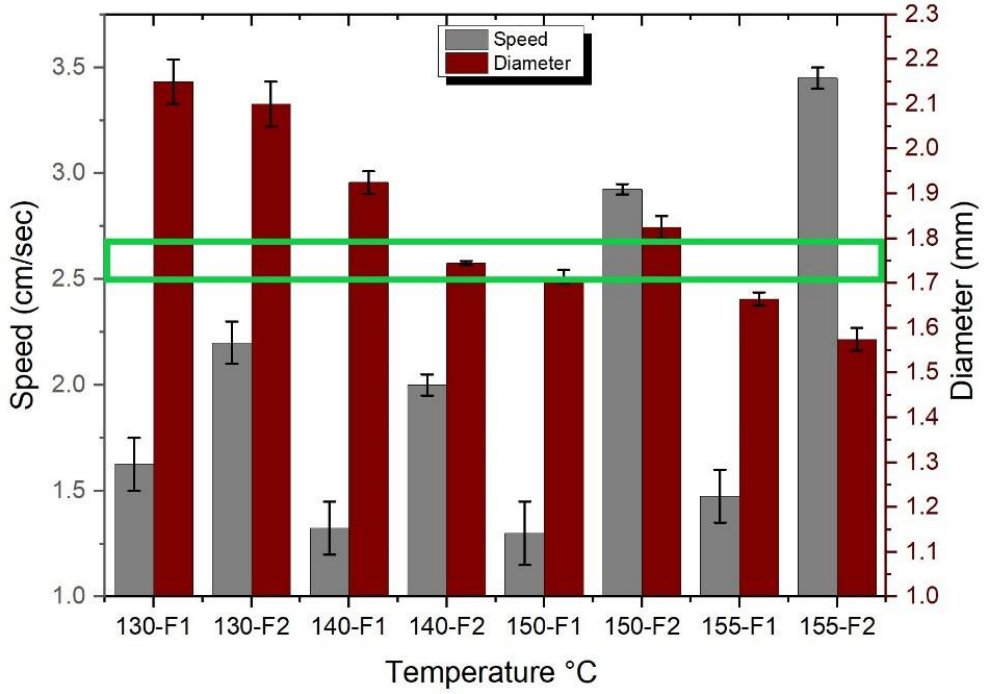

Figure 3.2. Extrudability window of PLA material (i.e., green square) (n=3)

Figure 3.2 shows that, irrespective of the feed rate, a decrease in extrusion temperature (Except for condition 150-F2) leads to an increase in filament diameters. The deviation in the trend associated with condition 150-F2 could be attributed to the size of the composite pieces, where the cutting into small pieces was done manually and may have not being consistent. The largest diameter occurred when using a nozzle temperature of 130 °C. The average diameter was 2.10 mm and 2.15 mm when using the feed rates of F1 and F2, respectively. On the other hand, the smallest diameter was found when extruding the filament at a temperature of 155 °C. Filaments with diameters of 1.58 mm and 1.65 mm were obtained when using the feed rates of F1 and F2, respectively. The speed of extrusion is often increased by increasing either the temperature or the feed rates; for example, by increasing the temperature, the viscosity decreases, causing a faster extrusion flow and resulting in a smaller diameter filament. Similarly, with a higher feeding rate, the flow speed increases. However, the results show that the feed rates only affect the filament diameter by ±0.15 mm. This means that the diameter is greatly affected by the extrusion temperature. An optimal diameter of 1.75 mm was achieved using 140-F2, as illustrated in Figure 3.2 where the extrudability window is highlighted in green with an error of ±0.005, by determining the right temperature range for the desired diameter and then regulating the feed rate for precise results. The findings discussed in the given analysis are consistent with those from previous research on the extrusion of PLA filaments. For instance, a study by Suhaili et al. [29] investigated the effect of extrusion temperature and feed rate on the diameter of 3D-printed filaments. The study found that the extrusion temperature had a significant effect on the filament diameter, while the effect of feed rate was relatively small. Moreover, the study found that decreasing the extrusion temperature resulted in an increase in the filament diameter.

Figure 3.3 shows SEM images of the produced filaments at different magnifications. Figure 3.3a shows that at a low temperature of 130 °C, the filament had a large diameter of

around 2.15 mm and demonstrated peeling on its surface, as depicted by the red circles. On the other hand, at a high temperature of 155 ◦C, the filament had an asymmetrical surface morphology and inconstant diameters (Figure 3.3c). In comparison to other filaments, the ideal filament diameter of 1.75 mm achieved at 140 ◦C had a very smooth surface morphology, and an extruding speed of 1.97 cm/sec allowed for greater control over the extruding process (Figure 3.3b). At high temperatures, PLA becomes less viscous and the extruding speed is accelerated, resulting in an unsymmetrical filament morphology.

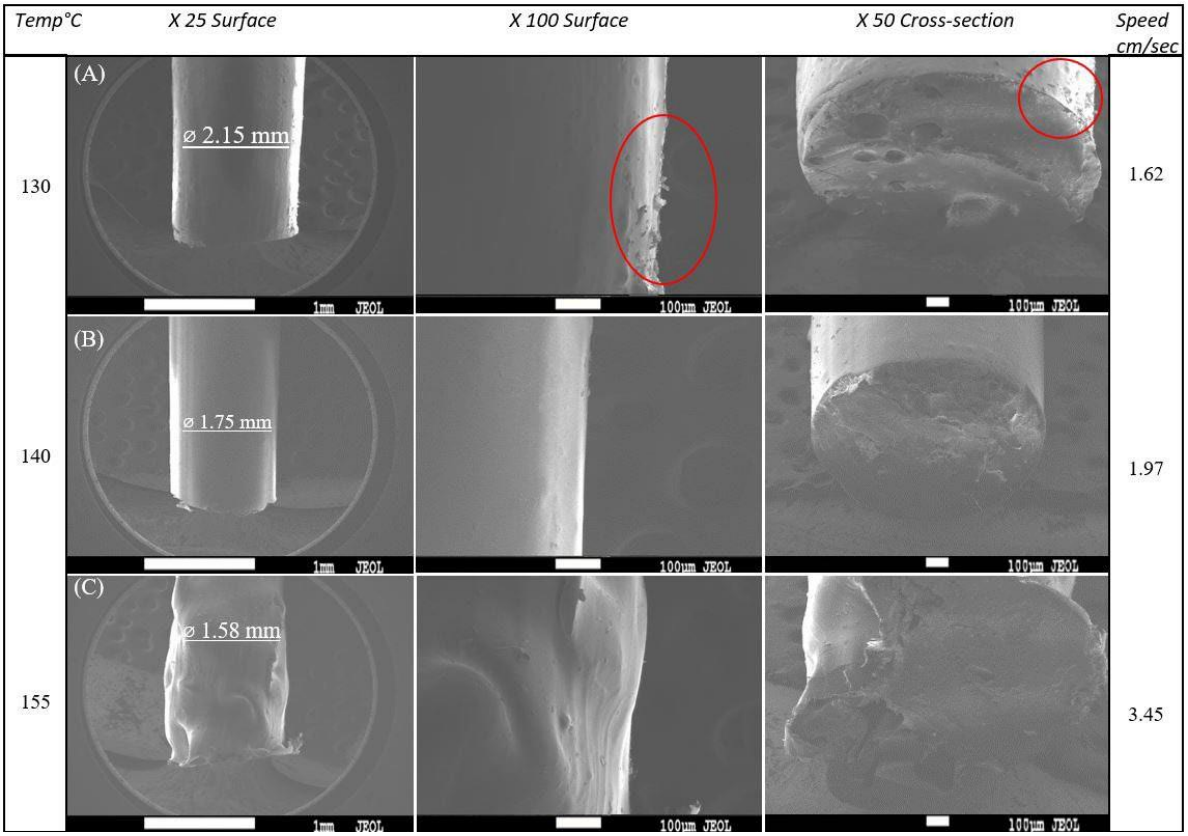

Figure 3.3. SEM images of extruded filaments at (A) 130 ◦C, (B) 140 ◦C, and (C) 155 ◦C. Surface peeling is depicted by red circles.

When keeping the temperature and feed rate constant, the extruding speed of the filament decreased as the CPO ratio increased (Table 3.2). Moreover, a high CPO content resulted in filament accumulation and nozzle clogging, which is a common issue reported in the 3D printing of ABS and graphene composites. For example, in a study involving a ratio of 7.4

wt% of graphene, the 3D printer nozzle became clogged due to the increased graphene content [30]. To ensure a consistent filament diameter, all subsequent samples were extruded at a constant temperature of 140 °C with a feed rate of F2, which had been optimised to achieve the desired diameter of 1.75 mm.

Table 3.2. Speed of extrusion for different CPO ratios.

CPO Ratio (%)	Speed (cm/Sec)
3% CPO	9.5
6% CPO	6
12% CPO	4.25
24% CPO	2.75

3.4.2 Rheological Properties

The rheological properties of the PLA/CPO composites were analysed and are presented in (Figure 3.4) in order to assess the viscosity and its suitability for extrusion and 3D printing. As a general rule, materials with a lower viscosity are more suitable for flowing and extrusion, which can improve the quality of 3D printing. Therefore, minimising the viscosity of the material is often desirable to achieve better printing performance. The viscosity-shear rate of the PLA/CPO composite filament samples was measured at 200 °C. All samples exhibited shear-thinning behaviour, which is a typical characteristic of linear polymers and is known as pseudo-plastic fluid behaviour. Moreover, the PLA samples with varying CPO ratios displayed similar shear rates with minor variations in viscosity, most notably for the high and low CPO ratios.

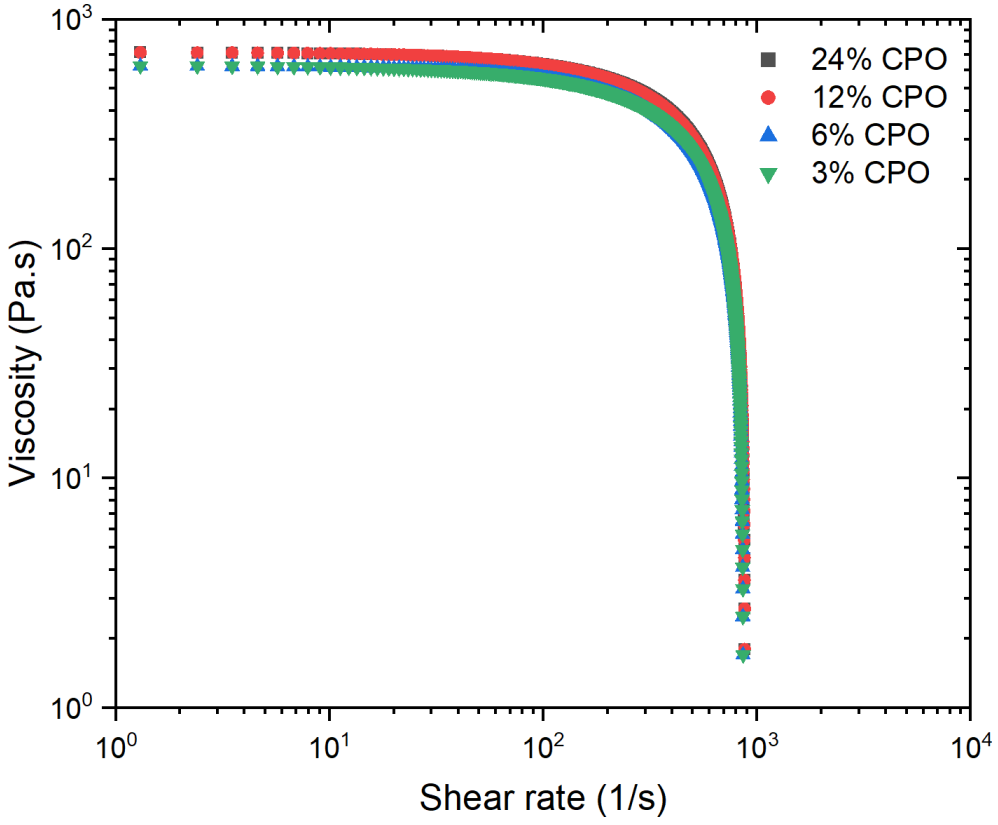

Figure 3.4. Viscosity-shear rate for the PLA/CPO composite filament samples (n=3).

The results demonstrate that all PLA/CPO composite samples exhibit shear-thinning behaviour, which is a typical pseudo-plastic fluid behaviour observed in linear polymers. Interestingly, the viscosity of samples containing a low CPO content (3% and 6%) is quite similar to that of pure PLA [31]. However, samples with higher CPO concentrations (12% and 24%) showed a slightly higher viscosity compared to those with lower concentrations. This suggests that the concentration of CPO in the composite is directly proportional to its viscosity. The increase in viscosity is dependent on various factors, including the concentration, size, distribution, and shape of the filler particles [32]. This suggests that CPO particles disrupt the normal polymer flow, hindering chain segment mobility and making it difficult for the minor phase to disperse evenly in the melt. As a result, higher CPO concentrations can result in poorer dispersion and increased viscosity of the filled

polymer. This can be especially problematic during the 3D printing of complex geometries, as it can restrict the deformation of the composite.

3.4.3 Microstructure

Figure 3.5 illustrates the X-ray diffraction (XRD) patterns of the PLA/CPO composites before and after the extrusion process. These patterns were analysed to confirm the microstructure of the composite material, which can significantly influence its properties. As shown in the figure, the diffraction peak centred at around 16° that corresponds to the PLA indicates its crystalline structure. Additionally, four crystalline peaks were found at 2 θ° of 30°, 35°, 47°, and 53°, corresponding to the CPO particles present in the composites. It was observed that the intensity of CPO peaks increased significantly with the increase in the amount of CPO in the polymeric matrix. The broadening of the XRD peaks of CPO (3%, 6%, 12%, and 24%) was mostly due to the presence of particles in the composites. This broadening became more evident in the XRD pattern after extrusion.

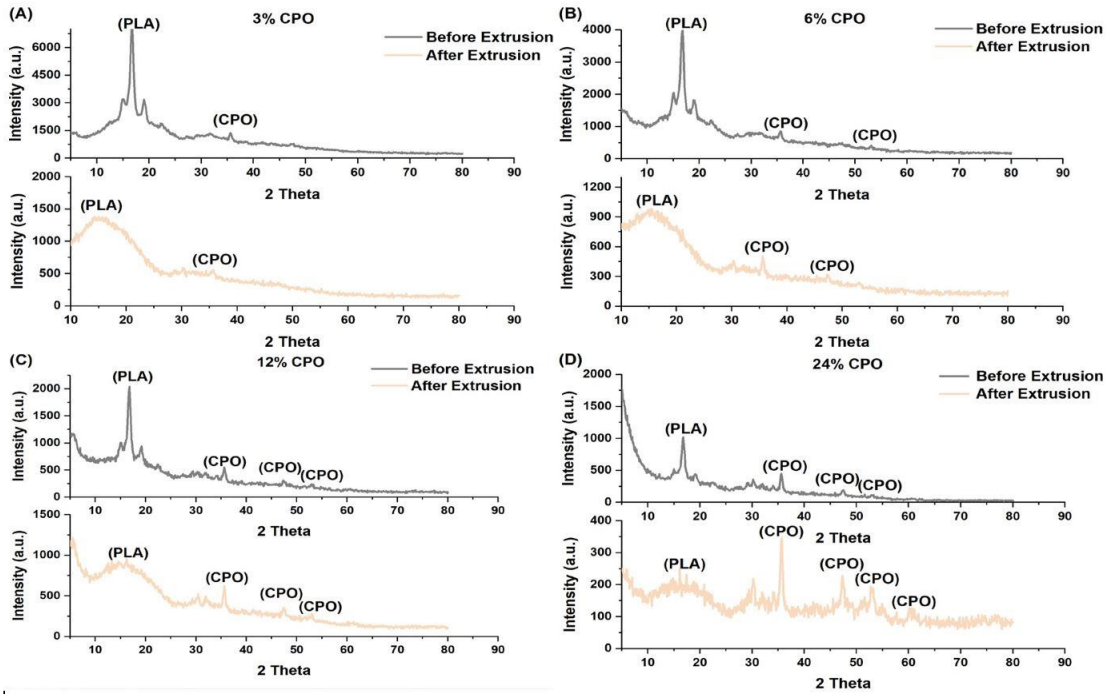

Figure 3.5. X-ray diffraction (XRD) patterns of PLA/CPO composites before and after hot-melt extrusion: (A) 3% CPO, (B) 6% CPO, (C) 12% CPO, and (D) 24% CPO.

Interestingly, the PLA peak disappeared after extrusion, indicating a transformation from a crystalline to amorphous structure. The XRD patterns for all samples, regardless of the CPO ratios, showed a completely amorphous PLA peak after extrusion. This transformation in the material structure can have significant implications for the mechanical properties of the material. Crystalline polymers have stronger intermolecular bonds, leading to increased strength [33]. However, an amorphous structure can improve bioavailability by increasing the solubility of CPO [33,34]. The transition from a crystalline to amorphous structure observed in the XRD patterns can be attributed to the heating temperature during the extrusion process of the filament [35]. The PLA/CPO composite was melted and extruded, leading to the formation of a new material with a different structure. This transformation can have implications for the mechanical properties of

the material, and the next section studies the mechanical properties of the extruded filaments in more detail.

3.4.4 Mechanical Properties

The tensile properties of the PLA/CPO composites were evaluated to investigate the impact of CPO on the mechanical behaviour of the PLA matrix. Moreover, it was examined whether the transformation to an amorphous structure significantly deteriorated the mechanical strength of the composites. Figure 3.6 and Table 3.3 show an example of the stress–strain curves and the mechanical properties of PLA/CPO composites with varying CPO contents. Samples prepared using 12% and 24% CPO had linear curves at a low strain followed by plastic deformation in the region of about a 2% strain, while samples prepared using 3% CPO yielded a breaking strain of around 2.8%, which is similar to that for pure PLA. In addition, the tensile strength of the composites varied significantly with increasing CPO concentration.

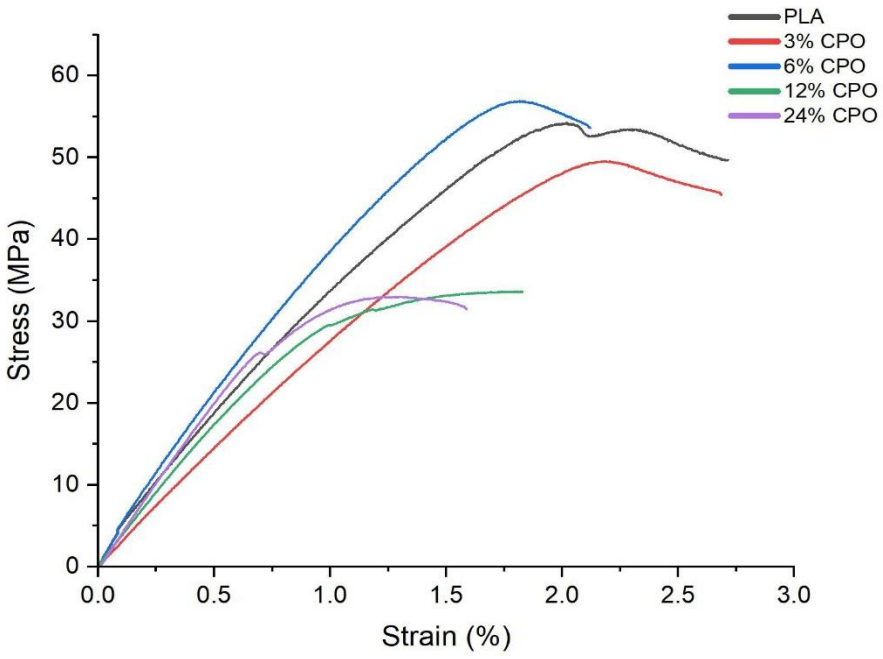

Figure 3.6. Stress–strain curves of PLA/CPO composites (n=3).

Table 3.3. Mechanical properties of PLA/CPO composites with standard deviation.

CPO Ratios	Tensile Strength σ_m, MPa	Strain at Break ε_b, %	Young's Modulus E, GPa
0%	52.2 ± 2.1	2.7 ± 0.25	3.5 ± 0.32
3%	49.5 ± 2.0	2.7 ± 0.25	2.9 ± 0.31
6%	55.8 ± 1.8	2.0 ± 0.22	4.1 ± 0.36
12%	33.6 ± 1.4	2.0 ± 0.26	3.3 ± 0.38
24%	32.9 ± 1.5	1.6 ± 0.28	4.1 ± 0.45

Samples prepared using 3% and 6% CPO had the highest ultimate strength, whereas samples prepared using 12% and 24% had the lowest ultimate strength. On the other hand, the strain at break decreased as the CPO concentration increased for all CPO concentrations, especially for those with high concentrations. The figure also shows a significant reduction in ultimate strength by approximately 65% for samples with a CPO concentration greater than 6%. The significant decrease in tensile strength and strain seen for samples with a CPO ratio greater than 6% can be attributed to the agglomeration of CPO particles in the polymer matrix, which act as stress concentrators and weaken the composite structure. These results are consistent with those from other studies that have investigated the effect of filler content on the mechanical properties of polymer composites [36]. The study also reported that the experimental error in the strength and Young's modulus values for 6% CPO overlaps with the range of variations observed in pure PLA. This suggests that the strength and Young's modulus of 6% CPO is comparable to 0% CPO. This finding suggests that 6% CPO can be more suitable for biomedical applications, such as bone scaffolds, where high strength is required [37,38].

3.4.5 Surface Morphology

To ensure the quality of the produced filaments, the surface morphology was carefully examined to confirm that they were consistent and smooth. The findings of this investigation demonstrate that increasing the CPO ratio results in a rough and irregular surface morphology of the filaments, which is clearly demonstrated in Figure 3.7. Further analysis of SEM images and surface texture indicates that filaments with higher CPO ratios of 24% and 12% exhibit rougher surfaces compared to those with lower CPO ratios of 6% and 3%. Moreover, the study highlights that an increase in CPO concentration, especially above 6%, leads to a reduction in filament ductility, as depicted in Figure 3.6. This reduction in ductility causes the filaments to become brittle, rendering them unsuitable for FDM 3D printing. The inflexible filaments cannot be fed through the feeder/tubing for extrusion and CPO particles can block the nozzle head, as observed in previous studies [39]. Additionally, the reduced strength in samples with a CPO concentration higher than 6% resulted in fragile filaments that may crack while being fed through the nozzle head, leading to further issues in the printing process [40].

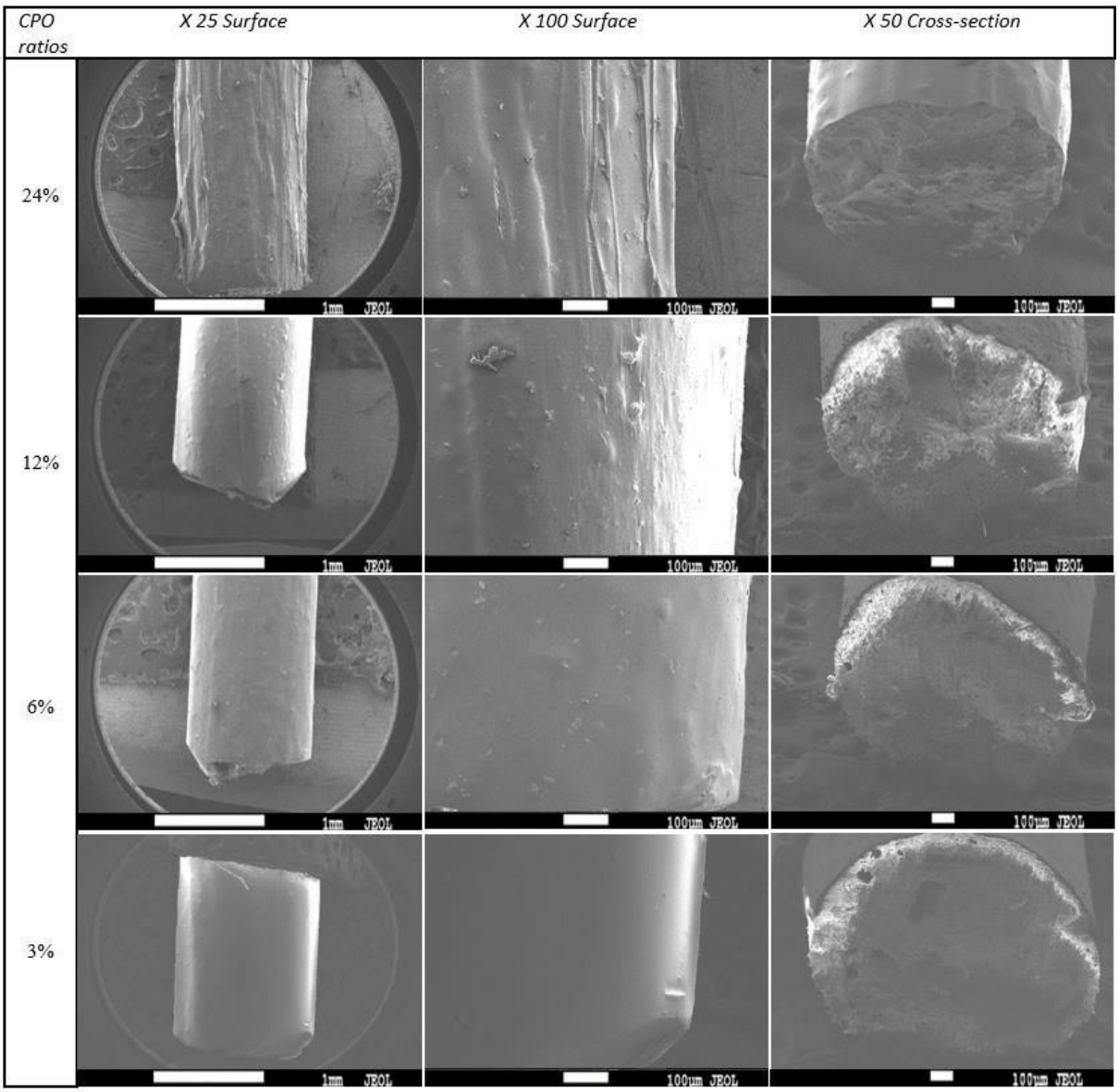

Figure 3.7. SEM images of PLA and CPO composite filaments at different ratios.

Previous studies have suggested that reducing the distance between the filament feed inlet and the extruder nozzle can be helpful in overcoming the issue of feeding the filament through the pipes/tubing [36]. However, this solution does not address the low strength issue associated with using filaments with high CPO ratios. Based on the results obtained in the previous sections, it can be concluded that using a PLA filament with a CPO concentration of 6% is a favourable choice. This is because, at this concentration, the composite exhibited not only a

smooth surface morphology but also better viscosity and improved mechanical properties such as strength and ductility.

To demonstrate the printability of filaments with a CPO concentration of 6%, a proof- of-concept scaffold object was fabricated using a commercial Fused Deposition Modelling (FDM) 3D printer; specifically, the Creality Ender 3 Pro (manufactured by Shenzhen Creality 3D Technology Co., LTD., Shenzhen, China) was used. The scaffold was designed to have a square shape with dimensions of 8 × 8 mm and a height of 1.5 mm, and with a porosity of 25% and a pore size of 0.60 mm. The printer bed was maintained at 60 ◦C, and the nozzle temperature was set at 200 ◦C. Figure 3.8 presents an optical image of the 3D-printed scaffold using a CPO concentration of 6%. The image demonstrates the successful printing of the scaffold and the good quality of the optimised CPO content. The optimised CPO concentration allowed for the production of a scaffold with smooth and uniform surfaces, indicating good printability. The geometry shows a well-structured scaffold with a strong and robust structure. Overall, the results suggest that PLA filaments with a 6% CPO concentration could be utilised to produce high-quality and functional bone scaffolds for biomedical applications. This concentration ensures good printing quality, strength, and roughness while avoiding issues such as blockages, nozzle head clogs, and filament breakage, making it an ideal choice for FDM 3D printing applications.

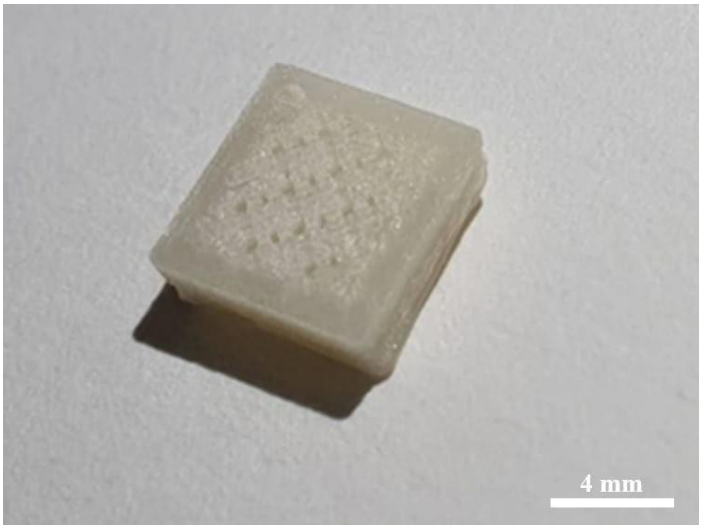

Figure 3.8. Optical image of the 3D-printed scaffold using CPO of 6% at a magnification of ×10.

3.5 Conclusions

The study aimed to develop PLA/CPO composite filaments through wet solution mixing and extrusion for biomedical applications. The extrusion process was optimised to achieve filament quality and a diameter of 1.75 mm. Viscosity analysis showed similar results for all samples, with slightly higher viscosities for those with a higher CPO content. Samples with a CPO content over 6% showed a significant reduction in ultimate strength of around 33.6 MPa, while those with 6% CPO had the highest ultimate strength of 56.9 MPa. SEM analysis of the samples revealed that filaments with a lower CPO content had a visually smoother surface and were more ductile of around 2.7%, making them suitable for FDM. All samples exhibited a change in microstructure from crystalline to amorphous after extrusion while still retaining CPO viability. The composite material filaments with a 6% CPO concentration had comparable mechanical strength of around 55.8 MPa to pure PLA of around 52.2 MPa and consistent visual surface roughness. These filaments were used to print samples using a commercial FDM 3D printer and showed good printability. These findings suggest that PLA/CPO composite material filaments with a CPO content of 6% can be used to fabricate bone scaffolds with suitable mechanical properties and an acceptable surface morphology for

biomedical applications. Further research is required to determine the maximum CPO content that can be loaded into the composite filament without compromising its flexibility. Additionally, the research highlights the importance of conducting biological studies to evaluate the potential biocompatibility and safety of the composite filament for medical applications.

3.6 References

[1] Fouly, A.; Alnaser, I.A.; Assaifan, A.K.; Abdo, H.S. Evaluating the Performance of 3D-Printed PLA Reinforced with Date Pit Particles for Its Suitability as an Acetabular Liner in Artificial Hip Joints. *Polymers* 2022, *14*, 3321. [CrossRef] [PubMed]

[2] Cox, S.C.; Jamshidi, P.; Eisenstein, N.M.; Webber, M.A.; Hassanin, H.; Attallah, M.M.; Shepherd, D.E.; Addison, O.; Grover, L.M. Adding functionality with additive manufacturing: Fabrication of titanium-based antibiotic eluting implants. *Mater. Sci. Eng. C* 2016, *64*, 407–415. [CrossRef] [PubMed]

[3] Hassanin, H.; Abena, A.; Elsayed, M.A.; Essa, K. 4D Printing of NiTi Auxetic Structure with Improved Ballistic Performance. *Micromachines* 2020, *11*, 745. [CrossRef] [PubMed]

[4] Srivastava, M.; Rathee, S. Additive manufacturing: Recent trends, applications and future outlooks. *Prog. Addit. Manuf.* 2022, *7*, 261–287. [CrossRef]

[5] Sodeifian, G.; Ghaseminejad, S.; Yousefi, A.A. Preparation of polypropylene/short glass fiber composite as Fused Deposition Modeling (FDM) filament. *Results Phys.* 2018, *12*, 205–222. [CrossRef]

[6] Liu, W.; Zhou, J.; Ma, Y.; Wang, J.; Xu, J. Fabrication of PLA filaments and its printable performance. In Proceedings of the 5th Annual International Conference on Material Science and Engineering (ICMSE2017), Xiamen, China, 20–22 October 2017; Volume 275, p. 012033. Available online: https://iopscience.iop.org/article/10.1088/1757-899X/275/1/012033 (accessed on 25 March 2023).

[7] Zarei, M.; Dargah, M.S.; Azar, M.H.; Alizadeh, R.; Mahdavi, F.S.; Sayedain, S.S.; Kaviani, A.; Asadollahi, M.; Azami, M.; Beheshtizadeh, N. Enhanced bone tissue

regeneration using a 3D-printed poly(lactic acid)/Ti6Al4V composite scaffold with plasma treatment modification. *Sci. Rep.* 2023, *13*, 3139. [CrossRef] [PubMed]

[8] Klippstein, H.; Diaz De Cerio Sanchez, A.; Hassanin, H.; Zweiri, Y.; Seneviratne, L. Fused Deposition Modeling for Unmanned Aerial Vehicles (UAVs): A Review. *Adv. Eng. Mater.* 2018, *20*, 1700552. [CrossRef]

[9] Crespo-Miguel, J.; Garcia-Gonzalez, D.; Robles, G.; Hossain, M.; Martinez-Tarifa, J.; Arias, A. Thermo-electro-mechanical aging and degradation of conductive 3D printed PLA/CB composite. *Compos. Struct.* 2023, *316*, 116992. [CrossRef]

[10] Bikas, H.; Stavropoulos, P.; Chryssolouris, G. Additive manufacturing methods and modelling approaches: A critical review. *Int. J. Adv. Manuf. Technol.* 2016, *83*, 389–405. [CrossRef]

[11] Ferrari, A.; Baumann, M.; Coenen, C.; Frank, D.; Hennen, L.; Moniz, A.; Torgersen, H.; Torgersen, J.; Van Bodegom, L.; Van Duijne, F.; et al. *Additive Bio-Manufacturing: 3D Printing for Medical Recovery and Human Enhancement*; European Parliament: Strasbourg, France, 2018.

[12] Felfel, R.M.; Poocza, L.; Gimeno-Fabra, M.; Milde, T.; Hildebrand, G.; Ahmed, I.; Scotchford, C.; Sottile, V.; Grant, D.M.; Liefeith, K. In vitro degradation and mechanical properties of PLA-PCL copolymer unit cell scaffolds generated by two-photon polymerization. *Biomed. Mater.* 2016, *11*, 015011. [CrossRef]

[13] Chen, Y.; Lu, T.; Li, L.; Zhang, H.; Wang, H.; Ke, F. Fully biodegradable PLA composite with improved mechanical properties via 3D printing. *Mater. Lett.* 2023, *331*, 133543. [CrossRef]

[14] Dudek, P. FDM 3D Printing Technology in Manufacturing Composite Elements. *Arch. Met. Mater.* 2013, *58*, 1415–1418. [CrossRef]

[15] Armentano, I.; Bitinis, N.; Fortunati, E.; Mattioli, S.; Rescignano, N.; Verdejo, R.; Lopez-Manchado, M.; Kenny, J. Multifunctional nanostructured PLA materials for packaging and tissue engineering. *Prog. Polym. Sci.* 2013, *38*, 1720–1747. [CrossRef]

[16] Lasprilla, A.J.R.; Martinez, G.A.R.; Lunelli, B.H.; Jardini, A.L.; Filho, R.M. Poly-lactic acid synthesis for application in biomedical devices A review. *Biotechnol. Adv.* 2012, *30*, 321–328. [CrossRef] [PubMed]

[17] Fouly, A.; Assaifan, A.K.; Alnaser, I.A.; Hussein, O.A.; Abdo, H.S. Evaluating the Mechanical and Tribological Properties of 3D Printed Polylactic-Acid (PLA) Green-Composite for Artificial Implant: Hip Joint Case Study. *Polymers* 2022, *14*, 5299. [CrossRef]

[18] Tyler, B.; Gullotti, D.; Mangraviti, A.; Utsuki, T.; Brem, H. Polylactic acid (PLA) controlled delivery carriers for biomedical applications. *Adv. Drug Deliv. Rev.* 2016, *107*, 163–175. [CrossRef]

[19] Zhao, W.; Huang, Z.; Liu, L.; Wang, W.; Leng, J.; Liu, Y. Porous bone tissue scaffold concept based on shape memory PLA/Fe_3O_4. *Compos. Sci. Technol.* 2021, *203*, 108563. [CrossRef]

[20] Zhang, B.; Wang, L.; Song, P.; Pei, X.; Sun, H.; Wu, L.; Zhou, C.; Wang, K.; Fan, Y.; Zhang, X. 3D printed bone tissue regenerative PLA/HA scaffolds with comprehensive performance optimizations. *Mater. Des.* 2021, *201*, 109490. [CrossRef]

[21] Xu, H.; Han, D.; Dong, J.-S.; Shen, G.-X.; Chai, G.; Yu, Z.-Y.; Lang, W.-J.; Ai, S.-T. Rapid prototyped PGA/PLA scaffolds in the reconstruction of mandibular condyle bone defects. *Int. J. Med. Robot. Comput. Assist. Surg.* 2010, *6*, 66–72. [CrossRef]

[22] Zia, A.A.; Tian, X.; Liu, T.; Zhou, J.; Ghouri, M.A.; Yun, J.; Li, W.; Zhang, M.; Li, D.; Malakhov, A.V. Mechanical and energy absorption behaviors of 3D printed continuous carbon/Kevlar hybrid thread reinforced PLA composites. *Compos. Struct.* 2023, *303*, 116386. [CrossRef]

[23] Mallepally, R.R.; Parrish, C.C.; Mc Hugh, M.A.; Ward, K.R. Hydrogen peroxide filled poly(methyl methacrylate) microcapsules: Potential oxygen delivery materials. *Int. J. Pharm.* 2014, *475*, 130–137. [CrossRef] [PubMed]

[24] Colombani, T.; Eggermont, L.J.; Hatfield, S.M.; Rogers, Z.J.; Rezaeeyazdi, M.; Memic, A.; Sitkovsky, M.V.; Bencherif, S.A. Oxygen-Generating Cryogels Restore T Cell Mediated Cytotoxicity in Hypoxic Tumors. *Adv. Funct. Mater.* 2021, *31*, 2102234. [CrossRef]

[25] Abdullah, T.; Gauthaman, K.; Hammad, A.H.; Navare, K.J.; Alshahrie, A.A.; Bencherif, S.A.; Tamayol, A.; Memic, A. Oxygen- Releasing Antibacterial Nanofibrous Scaffolds for Tissue Engineering Applications. *Polymers* 2020, *12*, 1233. [CrossRef]

[26] Mohammed, A.; Saeed, A.; Elshaer, A.; Melaibari, A.A.; Memic´, A.; Hassanin, H.; Essa, K. Fabrication and Characteriza- tion of Oxygen-Generating Polylactic Acid/Calcium Peroxide Composite Filaments for Bone Scaffolds. *Pharmaceuticals* 2023, *16*, 627. [CrossRef] [PubMed]

[27] Oh, S.H.; Ward, C.L.; Atala, A.; Yoo, J.J.; Harrison, B.S. Oxygen generating scaffolds for enhancing engineered tissue survival. *Biomaterials* 2009, *30*, 757–762. [CrossRef]

[28] Steg, H.; Buizer, A.T.; Woudstra, W.; Veldhuizen, A.G.; Bulstra, S.K.; Grijpma, D.W.; Kuijer, R. Control of oxygen release from peroxides using polymers. *J. Mater. Sci. Mater. Med.* 2015, *26*, 207. [CrossRef]

[29] Kuo, C.-C.; Chen, J.-Y.; Chang, Y.-H. Optimization of Process Parameters for Fabricating Polylactic Acid Filaments Using Design of Experiments Approach. *Polymers* 2021, *13*, 1222. [CrossRef]

[30] Kalsoom, U.; Nesterenko, P.N.; Paull, B. Recent developments in 3D printable composite materials. *RSC Adv.* 2016, *6*, 60355–60371. [CrossRef]

[31] Duhduh, A.; Noor, H.; Kundu, A.; Coulter, J. Advanced Additive Manufacturing of Functionally Gradient Multi Material Polymer Components with Single Extrusion Head: Melt Rheology Analysis. 2019. Available online: https://www.researchgate.net/publication/339585944_Advanced_Additive_Manufacturing_of_Functionally_Gradient_Multi_Material_Polymer_Components_with_Single_Extrusion_Head_Melt_Rheology_Analysis (accessed on 25 March 2023).

[32] Shumigin, D.; Tarasova, E.; Krumme, A.; Meier, P. Rheological and mechanical properties of poly (lactic) acid/cellulose and LDPE/cellulose composites. *Mater. Sci.* 2011, *17*, 32–37. [CrossRef]

[33] Frank, D.S.; Matzger, A.J. Effect of Polymer Hydrophobicity on the Stability of Amorphous Solid Dispersions and Supersaturated Solutions of a Hydrophobic Pharmaceutical. *Mol. Pharm.* 2019, *16*, 682–688. [CrossRef]

[34] Wang, X.; Schröder, H.C.; Müller, W.E.G. Amorphous polyphosphate, a smart bioinspired nano-/bio-material for bone and cartilage regeneration: Towards a new paradigm in tissue engineering. *J. Mater. Chem. B* 2018, *6*, 2385–2412. [CrossRef] [PubMed]

[35] Kobayashi, Y.; Ueda, T.; Ishigami, A.; Ito, H. Changes in Crystal Structure and Accelerated Hydrolytic Degradation of Polylactic Acid in High Humidity. *Polymers* 2021, *13*, 4324. [CrossRef] [PubMed]

[36] Dong, C.; Davies, I.J.; Junior, C.C.M.F.; Scaffaro, R. Mechanical properties of Macadamia nutshell powder and PLA bio-composites. *Aust. J. Mech. Eng.* 2017, *15*, 150–156. [CrossRef]

[37] Eddy, G.; Poinern, E.; Brundavanam, R.; Fawcett, D. Nanometre Scale Hydroxyapatite Ceramics for Bone Tissue Engineering. *Am. J. Biomed. Eng.* 2013, *2013*, 148–168.

[38] Pakkanen, J.; Manfredi, D.; Minetola, P.; Iuliano, L. About the Use of Recycled or Biodegradable Filaments for Sustainability of 3D Printing. In *Sustainable Design and Manufacturing 2017*; Springer: Cham, Switzerland, 2017; pp. 776–785. Available online: https://link.springer.com/chapter/10.1007/978-3-319-57078-5_73 (accessed on 25 March 2023).

[39] Beran, T.; Mulholland, T.; Henning, F.; Rudolph, N.; Osswald, T.A. Nozzle clogging factors during fused filament fabrication of spherical particle filled polymers. *Addit. Manuf.* 2018, *23*, 206–214. [CrossRef]

[40] Bahraminasab, M. Challenges on optimization of 3D-printed bone scaffolds. *BioMed. Eng. OnLine* 2020, *19*, 69. [CrossRef]

4 Chapter Four: Fabrication and Characterization of Oxygen-Generating Polylactic Acid/Calcium Peroxide Composite Filaments for Bone Scaffolds

Abdullah Mohammed [1,2], Abdu Saeed [2], Amr Elshaer [3], Ammar A. Melaibari [2,4], Adnan Memic´ [2], Hany Hassanin [5] and Khamis Essa [1]

1. School of Engineering, University of Birmingham, Birmingham B15 2TT, UK
2. Center of Nanotechnology, King Abdulaziz University, Jeddah 21589, Saudi Arabia
3. Drug Discovery, Delivery and Patient Care, School of Life Sciences, Kingston University London, Kingston Upon Thames KT1 2EE, UK
4. Department of Mechanical Engineering, King Abdulaziz University, Jeddah, Saudi Arabia
5. School of Engineering, Canterbury Christ Church University, Canterbury CT1 1QU, UK

Authorship contribution statement

Conceptualization, A.M., H.H., A.E. and K.E.; Methodology, **A.M. (Abdullah Mohammed)**, A.S., A.M., H.H. and K.E.; Formal analysis, **A.M. (Abdullah Mohammed)**, A.E., H.H., A.M., H.H. and K.E.; Investigation (Conducting the Antibacterial Activity Test) **A.M. (Abdullah Mohammed)** and A.S.; Resources A.M., A.A.M. and K.E. Writing—original draft, **A.M. (Abdullah Mohammed)** and H.H.; Writing—review & editing, A.M., H.H., A.E. and K.E.; Visualization, **A.M. (Abdullah Mohammed)**; Supervision, A.M., H.H., A.E. and K.E.; Project administration, A.M., A.A.M., H.H. and K.E.

4.1 Abstracts

The latest advancements in bone scaffold technology have introduced novel biomaterials that have the ability to generate oxygen when implanted, improving cell viability and tissue maturation. In this paper, we present a new oxygen-generating polylactic acid (PLA)/calcium peroxide (CPO) composite filament that can be used in 3D printing scaffolds. The composite material was prepared using a wet solution mixing method, followed by drying and hot melt extrusion. The concentration of calcium peroxide in the composite varied from 0% to 9%. The prepared filaments were characterized in terms of the presence of calcium peroxide, the generated oxygen release, porosity, and antibacterial activities. Data obtained from scanning electron microscopy and X-ray diffraction showed that the calcium peroxide remained stable in the composite. The maximum calcium and oxygen release was observed in filaments with a 6% calcium peroxide content. In addition, bacterial inhibition was achieved in samples with a calcium peroxide content of 6% or higher. These results indicate that an optimized PLA filament with a 6% calcium peroxide content holds great promise for improving bone generation through bone cell oxygenation and resistance to bacterial infections.

4.2 Introduction

The shortage of organ donors is a significant challenge for global healthcare systems. The growing need for tissue and organ transplants has led to a significant gap between the availability of donors and the demand for transplants. This issue is particularly pronounced in the United States, where, as of March 2022, 106,097 people were waiting for organ transplants [1]. Unfortunately, the shortage of donors results in a tragic loss of life. Current statistics indicate that, as of March 2022, an average of 17 deaths per day in the United States were attributed to delays in transplant surgery due to a lack of available organs [1]. Bone is an essential component

of our skeletal system that provides structural support, protects vital organs, and enables movement. However, the human body's ability to repair bone injuries is limited, making bone grafting a crucial procedure for bone fracture healing and regeneration. A bone graft is a surgical procedure in which bone tissue is transferred from one location in the body to another location where bone loss has occurred [2]. The use of autografts, which involves using the patient's own tissue, is the current standard for bone fracture healing and regeneration. However, this method may not be practical in situations where the fractured bone is too large or precise shaping is needed, such as in facial bones [3]. Tissue engineering presents a potential solution to these challenges by creating a bone scaffold using stem cells, biocompatible materials, growth factors, and biodegradable materials to improve bone fracture healing [4]. These bone scaffolds are designed to supply the required physical support and foster tissue regrowth, leading to the recovery of functionality [5–7].

Recently, there has been a growing interest in fabricating bone scaffolds using 3D printing technologies [8]. This approach allows the design of porous scaffolds with a specific exterior design and porous interior structure to achieve scaffolds with tailored functionality. This enables the scaffold to mimic the natural bone structure and support bone growth. Furthermore, 3D printing technology also allows for the customised production of scaffolds, making it more cost-effective and efficient [8]. Fused Deposition Modelling (FDM), a technique that utilizes filament polymers, is commonly adopted in tissue engineering due to its cost-effectiveness, accessibility, and availability [9]. Additionally, it offers a printing accuracy of +/−0.5 mm and can incorporate a wide range of biocompatible and biodegradable polymeric materials suitable for tissue engineering [9,10]. Materials such as polylactic acid (PLA, $(C_3H_4O_2)_n$), polycaprolactone (PCL, $(C_6H_{10}O_2)_n$), and poly(glycolic acid) (PGA, $(C_2H_2O_2)_n$) are commonly used in bone repairs, tendons, and skin, as they possess favorable characteristics [11,12]. PLA is particularly attractive due to its physical and mechanical properties, biocompatibility, and

biodegradability, which can be affected by its molecular weight [13]. Its excellent properties make it useful in a wide range of biomedical applications [14]. Furthermore, PLA has been used in 3D printing and has been approved by the US Food and Drug Administration (FDA) for use in healthcare applications, such as biomedical scaffolding [15]. PLA composites have been explored by researchers to enhance the properties of pure PLA by incorporating micro- or nano-sized bioactive materials, such as hydroxyapatite (HA), to improve its mechanical strength and ability to integrate with surrounding bone tissue [16]. Chitosan is another material mixed with PLA to enhance its properties. PLA-chitosan-HA scaffolds with large pores were used to create a composite hydrogel that facilitated high levels of human stem cell osteogenesis. A composite of PLA, polycaprolactone, and titanium oxide has also been 3D printed to create a bone replacement with improved tensile strength and fracture strain [17].

Despite the promising results of tissue engineering research, it has had limited success in clinically treating small tissue defects of less than a few millimetres. The main reason for this is the lack of vascularization, which results in an insufficient oxygen supply [18]. Poor oxygen supply in engineered tissues is a major constraint in scaffold applications, as it is essential for the survival and growth of cells attached to the scaffold [19]. Researchers have developed scaffolds that generate oxygen from solid particles such as sodium percarbonate, magnesium peroxide, and calcium peroxide [19]. These particles typically decompose and generate oxygen through hydrolysis, as shown in Equations (1) and (2) [20].

$$\text{(Calcium peroxide) } C_aO_2(s) + 2H_2O \rightarrow Ca(OH)_2(s) + H_2O_2 \quad (1)$$

$$2H_2O_2 \rightarrow O_2 + 2H_2O \text{ (Catalase)} \quad (2)$$

Hydrogen peroxide, an intermediate product of the reaction, is thought to be a cytotoxic agent. Mammalian cells in the human body have mechanisms in place to decompose hydrogen peroxide into water and oxygen with the help of catalase enzyme and are generally able to

tolerate low levels of hydrogen peroxide [21]. Due to their low toxicity, they can be used for tissue-engineering applications at concentrations that are well-controlled [22]. Zhang et al. [23] prepared polycaprolactone (PCL) mixed with CPO composite micro spheres using three different methods. The resulting microspheres were found to support the ability of MIN6 cells, a pancreatic beta-cell line, to survive for a period of one week. Recent literature suggests that 3D-printed oxygenation filaments in bone scaffolds can significantly improve bone tissue regeneration and healing. The filaments generate and release oxygen within the scaffold, providing an optimal environment for the scaffold- attached cells and promote their survival, proliferation, and differentiation. Additionally, the oxygen supply within the scaffold enhances the success of the scaffolding functionality by promoting vascularization, which is the formation of blood vessels within the scaffold and is crucial for the transport of oxygen, nutrients, and other substances to the cells. Three- dimensional printing technology is a powerful tool for the fabrication of these filaments and allows for precise control of the filament's structure, composition, and size. This enables the creation of scaffolds that mimic the properties of natural bone, promoting better cell attachment and tissue regeneration. Overall, the use of 3D-printed oxygenation filaments in bone scaffolds shows great promise as a method for improving bone tissue regeneration and healing [19]. PLA/CPO is considered a promising composite material, yet research in this area is limited. A novel PLA/CPO composite filament was developed by utilizing wet solution mixing and hot melt extrusion in this research. The wet solution mixing method allows for the homogenous distribution of the CPO particles in the PLA matrix, while the hot melt extrusion process ensures that the filament has a consistent and uniform diameter. The prepared filaments were tested for 3D printing and analyzed using techniques including X-ray diffraction and scanning electron microscopy. Additionally, we also evaluated the oxygen release, porosity generation, and antibacterial activity of the filaments.

4.3 Materials and Methods

4.3.1 Materials

For the study, 1.75 mm-diameter polylactic acid (PLA) filaments, molecular weight Mw 60,000, were obtained from (Shenzhen eSUN Industrial Co., Hubei, China). Calcium peroxide (CPO) with a particle size of −200 mesh and a purity level of 75% was purchased from (Sigma-Aldrich, Saint Louis, MO, USA). Additionally, pure natural bulk enzyme catalase powder (50,000 μ/g) was purchased from (Enzymes. Bio, Wellington, New Zealand). Lastly, dichloromethane (DCM) was obtained from (Sigma Aldrich, Saint Louis, MO, USA).

4.3.2 Preparation of PLA/CPO Filaments

The process of preparing the PLA/CPO composite filament starts by cutting PLA into 20 g pieces and dissolving it in 100 mL of DCM for 30 min at room temperature with a magnetic stirrer at 700 rpm, see Figure 4.1. Once the PLA samples were fully dissolved, various ratios of CPO were added to the mix while magnetic stirring vigorously for 90 min. The mixture was then poured onto a large plate and left to dry at room temperature around 22 °C for 24 h. After drying, the composite was cut and loaded into a hot melt extruder. A composite material was extruded using a customised single screw extruder with a nozzle diameter of 2 mm from (King Abdelaziz University, Saudi Arabia). The extrusion process was carried out at a nozzle temperature of 140 °C and an extruding speed of 2.5 cm/s. This resulted in a filament diameter of 1.75 mm, which is suitable for use in a commercial 3D printer. A diagram showing the process is depicted in Figure 4.1 and the prepared samples list is provided in Table 4.1.

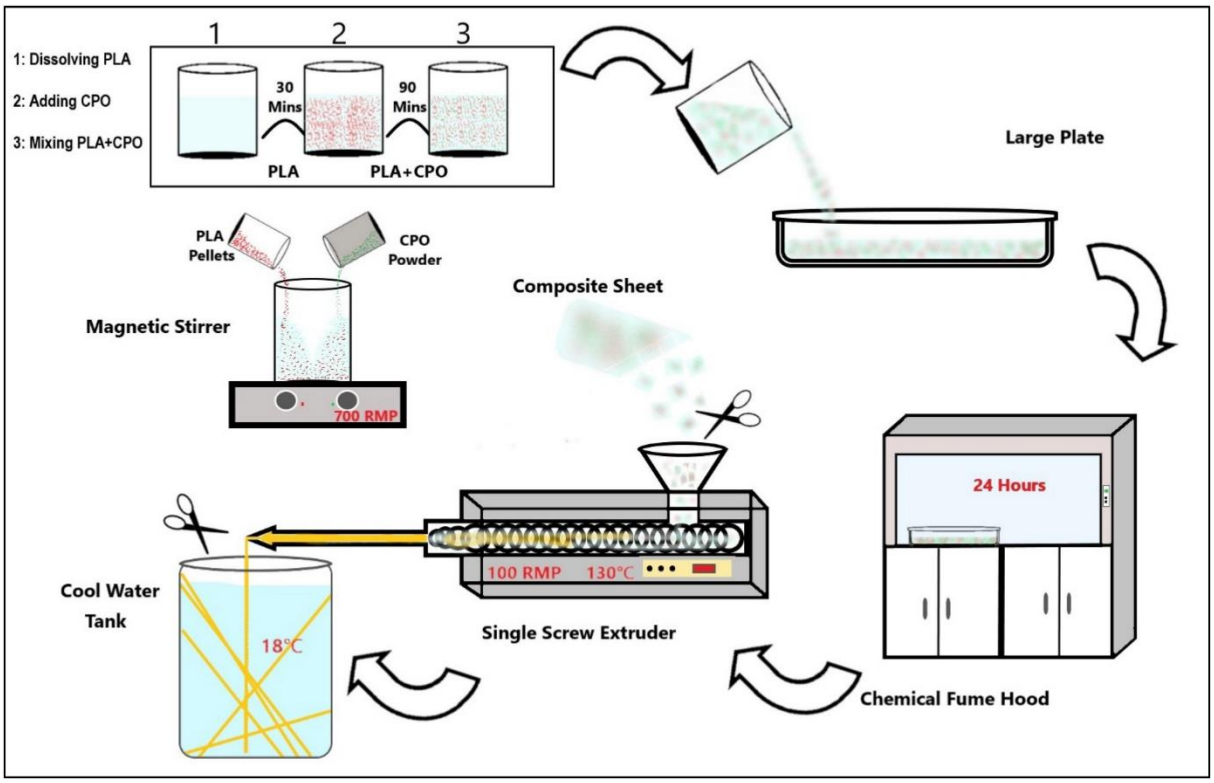

Figure 4.1. Schematic illustration of composite filament production.

Table 4.1. PLA/CPO ratios.

Sample No.	Samples Name	PLA (%wt)	CPO (%wt)
1	0% CPO	100	0
2	1.5% CPO	98.5	1.5
3	3% CPO	97	3
4	6% CPO	94	6
5	9% CPO	91	9

4.3.3 3D Printing of Bone Scaffolds

To examine the generated filaments, a scaffold was printed using a commercial Fused Deposition Modelling (FDM) 3D printer—the Creality Ender 3 Pro model manufactured by (Shenzhen Creality 3D Technology Co., Ltd., Shenzhen, China). The printing process was carried out with the highest CPO ratio (9%) at a temperature of 200 °C and a speed of 75 mm/s. The scaffold was printed successfully in a box shape with dimensions of 8 × 8 × 8 mm for length, width, and height. The scaffold had a porosity of 25% with a pore size of 0.60 mm.

4.3.4 Characterisation

The composite filament's surface and cross-sectional micrographs were captured using field emission scanning electron microscopy (FESEM) (JEOL JSM 7600F, Tokyo, Japan). The imaging was performed at an acceleration voltage of 5 keV, and gold sputter coated prior to imaging to enhance the conductivity and provide better resolution. The images were used to study the morphology of the filament and to confirm the dispersion of the CPO particles in the PLA matrix. Additionally, optical images of composite filaments surface were captured using a Canon 1000D camera. This provided a visual representation of the filament's surface and helped in identifying any morphological changes. Additionally, the XRD was carried out using Cu Ka radiations ULTIMA IV XRD systems from (Rigaku, Japan). The analysis of material elements was conducted using ICDD, DB card No. 01-071-4107. Additionally, Alizarin Red Staining purchased from (Sigma-Aldrich, Saint Louis, MO, USA), was used to detect CPO particles within the fabricated filament.

To prepare the solution, 0.40 g of the Alizarin Red Staining powder was dissolved in 20 mL of distilled water with the aid of a stirrer. The samples were first soaked in an alkaline solution for 20 min and then left to soak in the same solution for 20 h in a dark environment.

4.3.5 Degradation and Oxygen Release

The degradation of the filament was examined by measuring the mass loss over time. A solution with a pH of 13.2 was made by dissolving 2 g of sodium hydroxide purchased from (VWR Prolabo Chemicals, Leuven, Belgium) in 50 mL of distilled water to accelerate the degradation process. Each filament weighing 10 g was immersed in an alkaline solution at a room temperature of 18 °C, and the weight loss and calcium ion release were measured every 24 h during the degradation process for three days. The weight loss of the samples was measured using (Mettler Toledo analytical balance model NewClassic MS, Singapore) and calculated using Equation (3). The calcium ion release was observed using an ICP optical emission spectrometer (ULTIMA 2, HORIBA SCIENTIFIC Ltd., Kyoto, Japan).

$$\text{Weight} = (\text{Wt}/\text{Wo}) \times 100\% \quad (3)$$

where Wt represents the sample weight after degradation, and Wo represents the initial sample weight.

To measure the oxygen released by the filament, the samples were placed in a phosphate-buffered saline (PBS) solution with a pH of 7.4 purchased from (Fisher Scientific, Loughborough,UK) and their oxygen levels were measured using an customised dissolved oxygen meter. In addition, 10 mg of catalase were added in the solution. The acidity level (pH) of the samples were measured every 24 h using a Adwa digital pH meter (model AD31, Szeged, Hungary).

4.3.6 Porosity Measurements

The porosity was characterized using field emission scanning electron microscopy (FESEM) (FESEM, JEOL JSM 7600F, Tokyo, Japan) with an accelerating voltage of 5 keV. For each sample, three SEM images were captured from random spots. From the obtained SEM images, the porosity percentage of the total area was calculated, after converting the images into a

grayscale using ImageJ (version 1.53f51). The SEM images were converted to 8-bit binary (white and black) images for ImageJ analysis, where the white spots indicate the solid surface and the black spots represent the pores.

4.3.7 Antibacterial Activity

The antimicrobial performance of the composite filaments was examined using disk diffusion tests. We utilized the following prevalent bacteria strains in the study: gram-negative *Escherichia coli* ATCC 11,775 (*E. coli*) and Pseudomonas aeruginosa ATCC 9027 (PA). And gram-positive *Staphylococcus aureus* ATCC 12,600 (SA) and Methicillin-resistant *Staphylococcus aureus* ATCC 33,591 (MRSA). We cultivated these bacteria strains on blood agar and stored them on Mueller Hinton agar (MHA) (Condalab, Madrid, Spain) plates in the refrigerator at 4 °C for later use. When the experiments were performed, the bacteria strains were activated in Mueller Hinton broth (MHB) (Scharlau, Barcelona, Spain); after measuring their turbidity (0.1 ± 0.02), they were spread on the MHA plates via swab cotton. The composite filaments were prepared in a disk shape and then fixed on the surface of the MHA plates containing the bacteria strain beside a standard 30 μg cefoxitin antibiotic disc (FOX) from Mast (Mast Group Ltd., Bootle, UK). Then, all MHA plates were placed in incubator model ST180 PLUS CO2 from (Benchmark Scientific, Darmstadt, Germany) at 37 °C for 24 h. Finally, we measured the diameters of the bacteria growth inhibition zone; the antibacterial performances of the prepared composites were compared with the standard antibiotic FOX disks.

4.3.8 Statistics Analysis

Each test was conducted in triplicate, and a mean value was calculated. The data are calculated as the mean with a ± standard deviation (SD). OriginPro 8.0 software (OriginLab, Northampton, MA, USA) was employed to analyze the data.

4.4 Results and Discussion

4.4.1 Presence of CPO and Printability of Filament

CPO particles within the fabricated filament were detected using XRD and Alizarin Red Staining solution. XRD was used to identify the crystalline phases in the composite filament and confirm the presence of CPO. Furthermore, the XRD was also used to investigate the effect of CPO solid loading on the crystal structure of the composite filament. The results demonstrate the presence of the CPO in each sample. The XRD pattern shown in Figure 4.2a for PLA highlights two characteristic peaks at 2θ 16.8° and 19.5°. For the pure CPO, several characteristic peaks appeared at 2θ 30.3°, 35.8°, 47.5°, 53.3°, and 60.7°. In all of the prepared samples, the PLA and CPO peaks were observed in the prepared composite. The intensity of the CPO peaks, which indicate the presence of CPO in the composite, varied depending on the concentration of the CPO in the composite filament. Samples with smaller CPO contents had smaller peaks than those with higher contents, indicating that increasing the CPO concentration in the composite filament also increases the presence of CPO.

Additionally, Alizarin red staining, which is a common method for detecting calcium ions qualitatively, was applied to detect the presence of CPO in the samples by its ability to interact with calcium. This staining powder, Alizarin Red S, binds with calcium through its sulfonic acid and/or OH groups, making the calcium visible to a naked eye as a red stain. The composite filaments were stained red, and the intensity of the stain reflected the concentration of CPO embedded in the composite. The stain intensified from CPO-free to 9% CPO, further confirming the presence of CPO and the concentration in the composite filament, see Figure 4.2b. As CPO-PLA concentrations increased, the staining intensity also increased, indicating that CPO was successfully embedded into the PLA composite [24].

The filaments were tested for printability, and a 3D cubed-shaped scaffold was successfully printed using the sample with the highest CPO ratio of 9%. The printing quality of this scaffold appears to be comparable to those printed with pure PLA, as shown in Figure 4.3. However, for scaffold applications, higher resolution is needed as significant differences in the mesh accuracy were observed when comparing the 3D model to the 3D-printed scaffold for both pure PLA and composite filaments. This suggests that further optimization of printing conditions is necessary to improve scaffold printing quality. Optimization can be achieved by varying the nozzle diameter, printing speed, and bed and nozzle temperature. Overall, these findings highlight the potential of using composite filaments for the 3D printing of scaffolds, but further improvements are necessary to achieve higher accuracy and resolution.

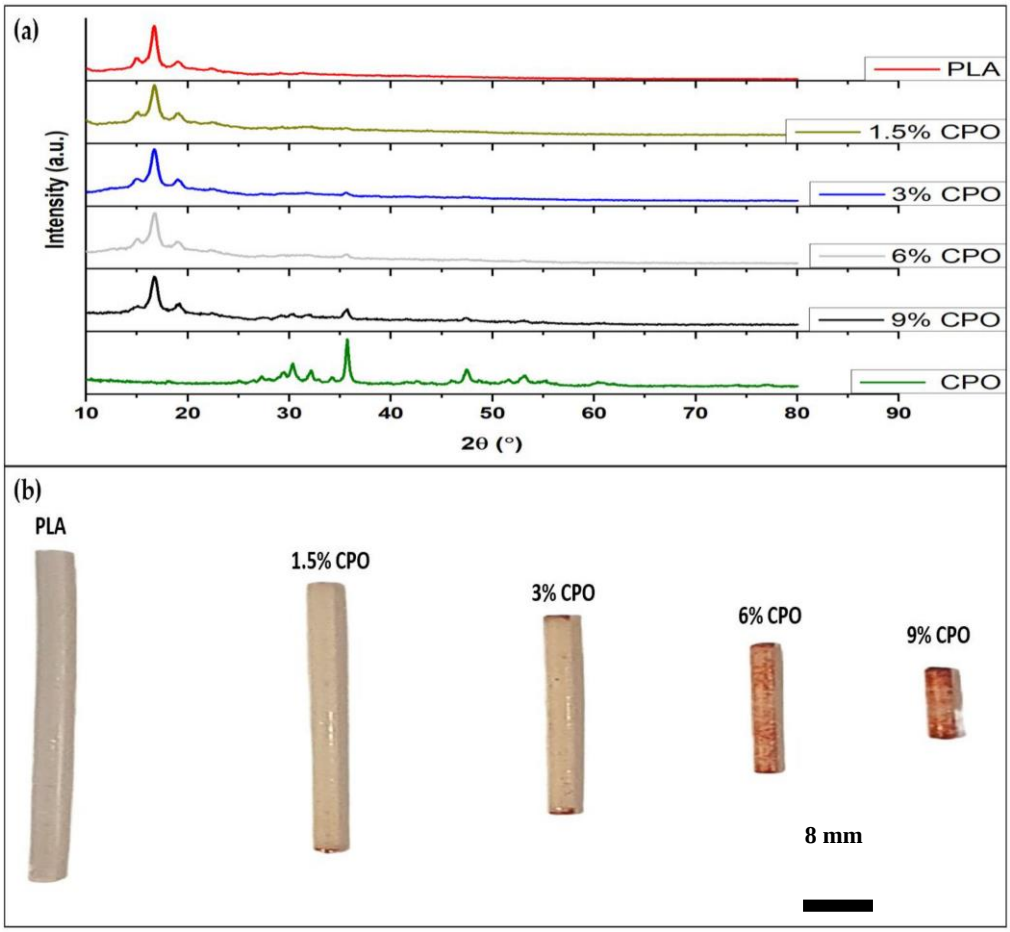

Figure 4.2. Calcium peroxide detection using (a) XRD and (b) Alizarin Red staining.

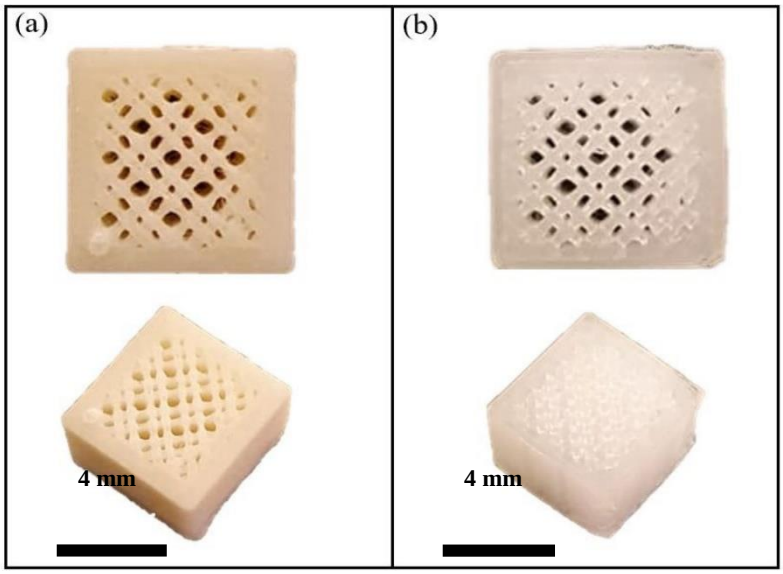

Figure 4.3. 3D-printed scaffold by (a) 9% CPO composite filament (b) pure natural colour PLA.

4.4.2 Filament Degradation, Oxygen and Calcium Ion Release

The aim of the degradation study was to investigate the degradation characteristics of a filament produced from a specific material. To expedite the degradation process, the samples were immersed in an alkaline solution and measured the percentage of weight loss over a specific period [25]. Previous studies have also used alkaline solutions to accelerate the degradation of polymer scaffolds. This approach was chosen to facilitate the degradation of both PLA and composite scaffolds as PBS, another degradation medium, can take more than six months to achieve significant weight loss [26]. By using an alkaline solution, we were able to compare the different CPO content in the filaments more effectively [26]. Figure 4.4 shows the degradation of the filaments with different CPO content over three days. It can be noted that the weight loss of 1.5% CPO samples was lower than 3%, 6%, and 9% CPO samples on days 1, 2, and 3 respectively. In general, there is a correlation between the degradation rate and CPO content in the composite filament. Increasing the CPO content increased the degradation percentage of the samples. It is worth noting that the 9% CPO sample completely degraded after 24 h. This was because the sample broke into smaller pieces and fell apart, unlike the other samples that

retained their shape as a single solid piece while their weight decreased. The reason for the degrading behavior of the 9% CPO ratio can be understood when looking at the porosity section. Therefore, it appears that 9% CPO composites may not be an ideal ratio for the application of bone scaffolds.

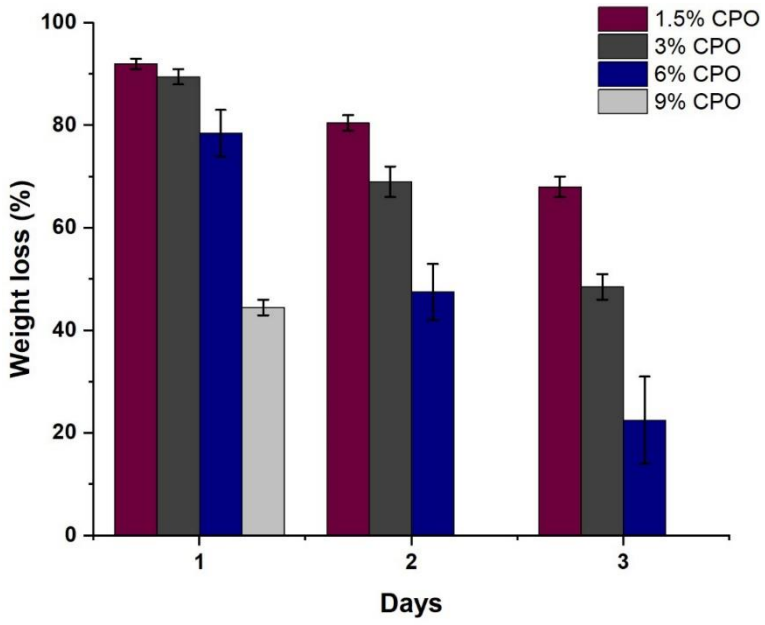

Figure 4.4. The weight loss percentage of samples over a three-day period (n = 3).

Figure 4.5 shows the cumulative percentages of calcium release for the samples from day one to day three. Percentages are calculated based on the total amount of CPO loaded for each sample. From the graph, we can note that the 1.5% sample released 1.3% of its total amount of CPO by day three, making it the fastest sample to release CPO compared to the other ratios. It is observable that there is an inverse relationship between the samples' ratio and the release of CPO on the third day. The higher the CPO ratio, the slower the CPO content is released. Additionally, similar to the weight loss, the 9% CPO sample had a substantial decrease in the release of both CPO content and oxygen, as illustrated in Figure 4.6a.

The cumulative release of oxygen for all samples as a percentage of the loaded CPO is shown in Figure 4.6. Apart from the 9% CPO sample, all samples showed a linear positive correlation

relation with respect to the CPO ratios. The oxygen release was greatest in 6% CPO at 0.00007mg/L from day one, followed by 3% CPO and 1.5% CPO. That can be due to the distribution and small sizes of CPO particles embedded in the PLA matrix, which accelerate the chemical reactions. On the other hand, although 9% CPO has the highest CPO content, we observed minimal oxygen release on day one (0.000005 mg/L) and no oxygen release on days two and three compared to the other CPO ratios. The acidity level of the samples remained the same but there was a decline of about 0.3.

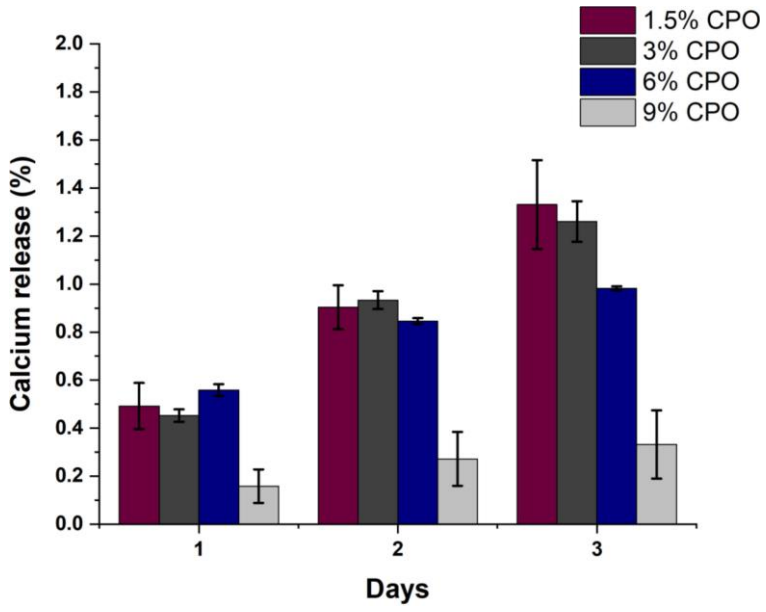

Figure 4.5. Calcium release percentage of samples over a three-day period (n = 3).

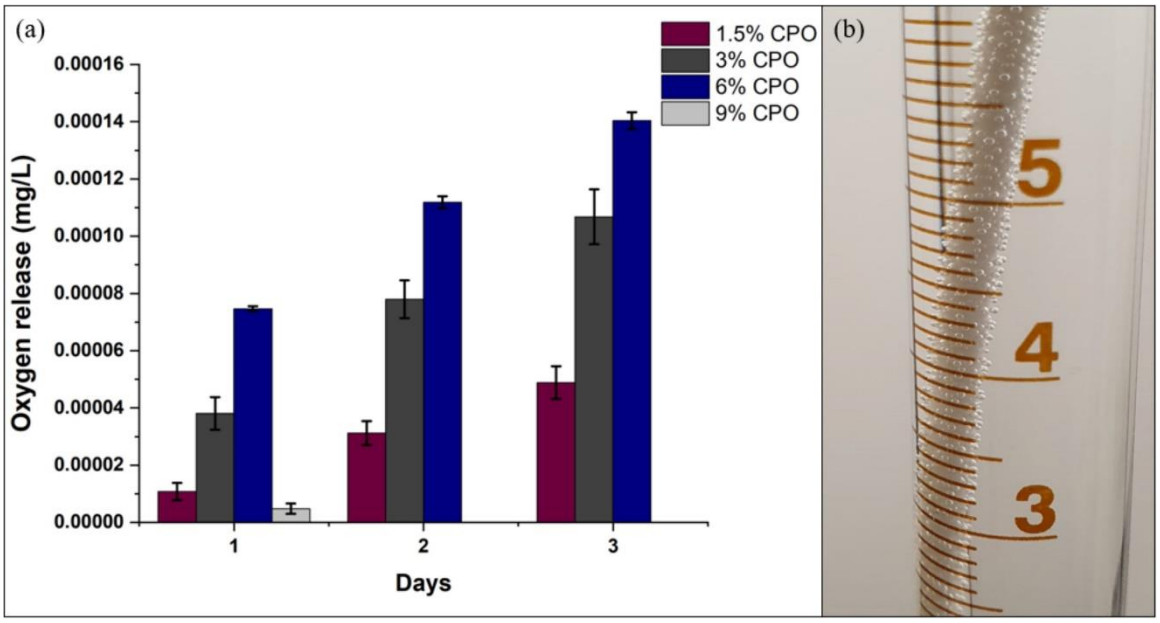

Figure 4.6. Oxygen release: (a) chart of oxygen release of samples over a three-day period (n = 3); (b) oxygen released during the degradation process evidenced in the release of gas bubbles from the filaments.

Scaffolds for bone tissue that are made using materials that produce oxygen, such as PLA/CPO, can increase the oxygen concentration and result in enhanced cell survivability of the 3D-printed scaffolds. A biphasic calcium phosphate (BCP) scaffold, made up of 40% beta-tricalcium phosphate and 60% hydroxyapatite, was fabricated using the robocasting technique [27]. Touri et al. fabricated biphasic calcium phosphate (BCP) scaffold composed of 60% hydroxyapatite and 40% beta-tricalcium phosphate using the robocasting technique. Although an alternative composite filament was investigated, the findings mirror that of our study, with the oxygen release behaviour dependent on the concentration of CPO encapsulated in the PLA filaments. It was found that a 3% concentration of CPO was sufficient to produce desirable results in terms of promoting bone ingrowth, increasing the survival of osteoblast cells, and stimulating proliferation in low oxygen conditions [27].

Oversaturation remains a challenge in the preparation of composite filaments, with Zhang et al. observing that an environment with significantly oversaturated oxygen tension was created in the first 48 h in single-walled microspheres. In turn, this may result in the creation of a hyperoxia

environment in cases where the oxygen demand by cells is not as high. Double-walled microspheres may better support the oxygen tension, but further research is warranted to determine their efficacy [28]. The available evidence suggests that oxygen-releasing materials are limited by their short release periods of 24 to 48 h [29–31]. However, the findings of our study indicate a more sustainable oxygen release over a three-day period, as seen in Figure 4.6. Similar oxygen release patterns were observed by Montazeri et al. and Lee et al. [32,33]. Future investigations should focus on the release periods of these materials and determine if they are of sufficient sustainability.

4.4.3 Antibacterial Activities

None of the samples displayed any inhibition zone when tested against *P. aeruginosa* bacteria and Gram-negative *E. coli* Figure 4.7a,b. However, when samples were tested against the Gram-positive bacterium *S. aureus* and MRSA, which has a higher antibacterial resistance [32], some samples exhibited a clear inhibition zone [33,34].

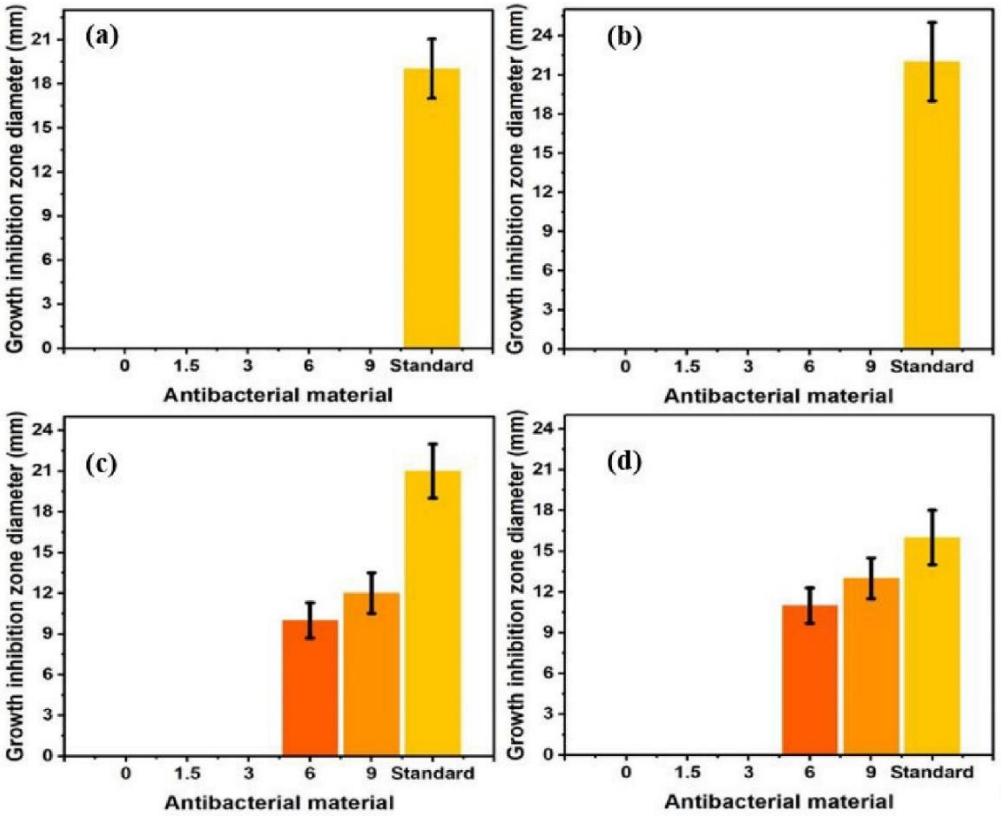

Figure 4.7. Antibacterial activity of composite scaffolds against (a) Escherichia coli, (b) Pseudomonas aeruginosa, (c) Staphylococcus aureus, and (d) Methicillin-resistant Staphylococcus aureus (n = 4). Note: The used standard is Cefoxitin (FOX).

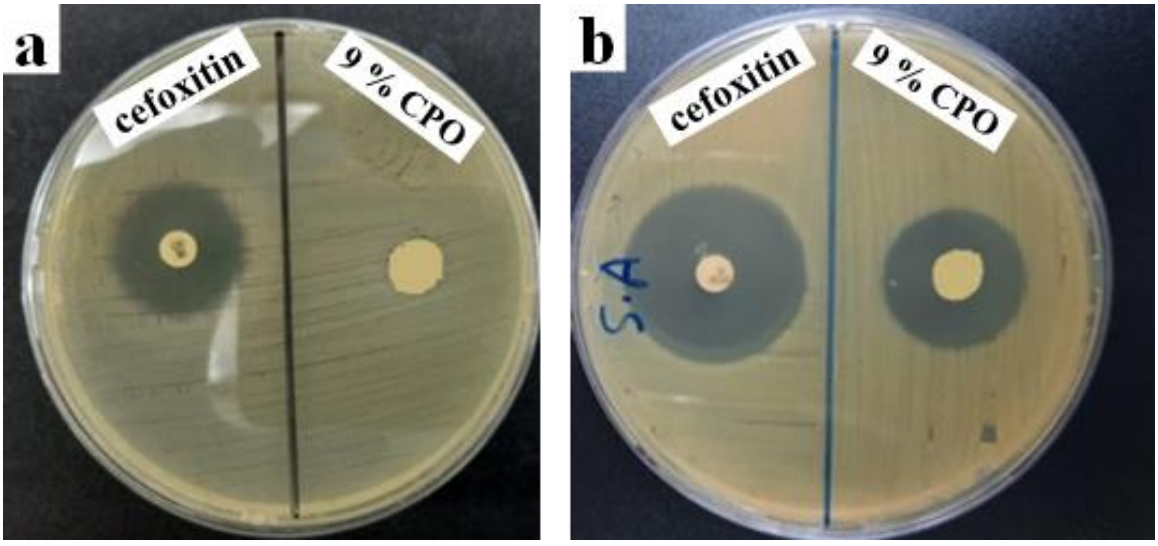

Figure 4.8 Disk diffusion tests using composite at 9% CPO and cefoxitin as standard; optical images of growth inhibition zones in agars for the bacteria of (a) E. coli and (b) S. aureus.

As shown in the graphs in Figure 4.7c,d, the CPO-free, 1.5% CPO, and 3% CPO scaffolds did not produce any inhibition zone against *S. aureus* and MRSA, indicating that these PLA scaffolds with low CPO content had no effect on the bacteria. A significant inhibition zone was seen at 6% CPO and 9% CPO, indicating that increasing the CPO content to 6% or higher resulted in an antibacterial activity against Gram-positive bacteria, which is consistent with previous research [35], indicating that the antibacterial activity may be attributed to the residual hydrogen peroxide, which is a by-product of CPO decomposition [36].

4.4.4 Porosity

Porosity is among the most critical properties of biomaterials, particularly in tissue engineering applications, as it is correlated to the biomaterials' swelling capability. Figure 4.9a,b shows the SEM observation of the samples after 20 min of degradation. The scanning was carried out to show the porosity size and distribution on the surface of the material, as after a few hours of degradation, the sample will have inner and merged porosities, see the red circles in Figure 4.9a,b. In all of the samples, there were many pores of different sizes all over the surface. This is because the dissolved calcium ions in the PLA/CPO composite left pores behind. In addition, the SEM image shows that several large particles around 0.3 mm of CPO did not sufficiently disperse in the composite with a high CPO concentration Figure 4.9a. Conversely, at CPO concentrations lower than 6%, small sized pores around 1 µm were found (Figure 4.8b) with a porosity of approximately 40% of the selected area, as shown in Figure 4.9c. It is vital to note that if two pores overlap on the surface of a composite filament, ImageJ considers them a single pore. Thus, the variation in porosity content is related to CPO concentration and may allow for even finer-tuned and controlled porosities in the introduced biomaterial.

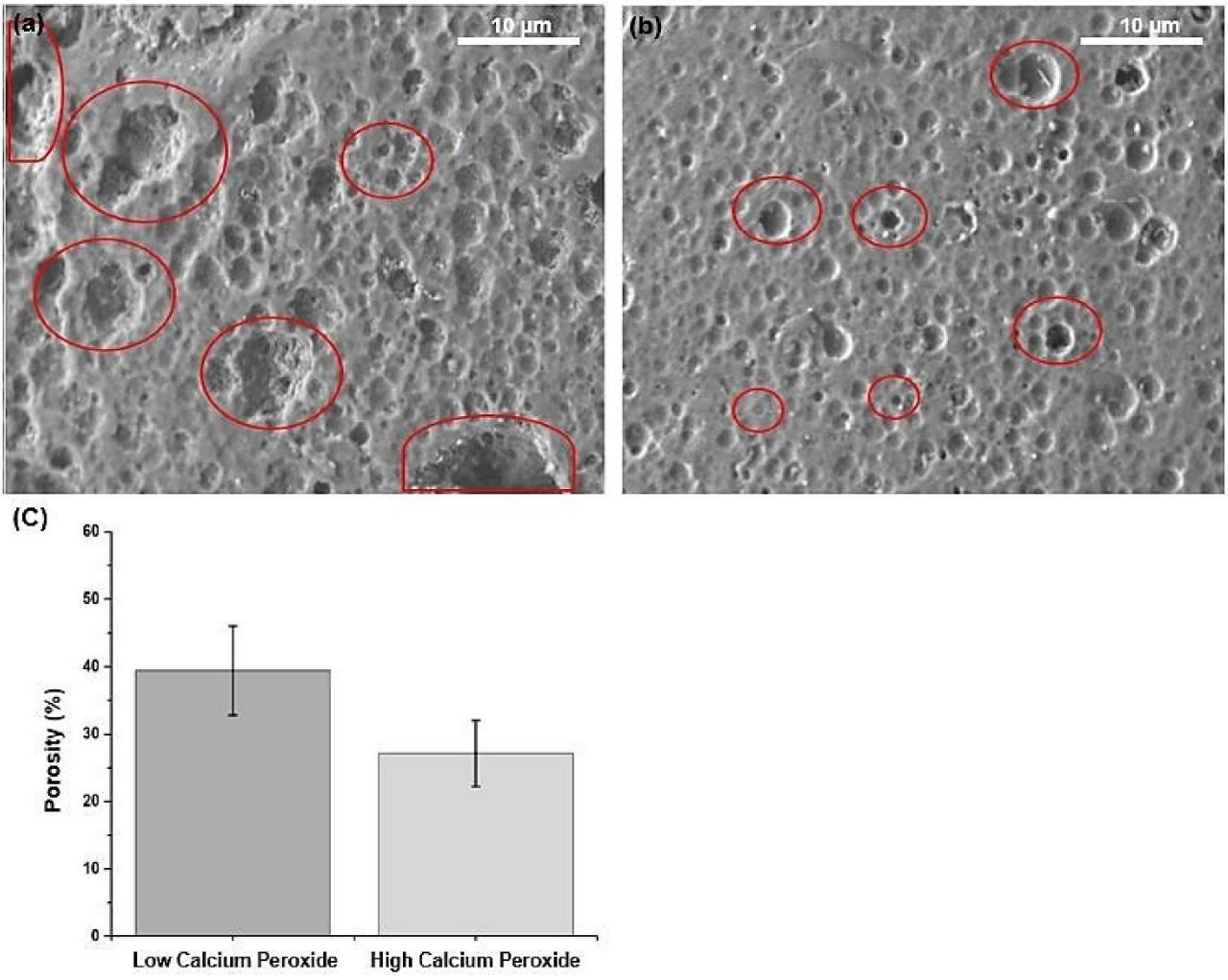

Figure 4.9. The effect of calcium peroxide on polylactic acid porosity. SEM images of the filament sur- face after degradation, showing porosities at (a) high above 6% and (b) low below 6% calcium peroxide at a magnification of ×2500 and an energy of 5.0 keV. (c) a semi-quantitative analysis of filament porosity based on image analysis (n = 3).

In Figure 4.10a,b, the samples were investigated under the microscope using SEM with red circles representing the CPO particles. These images collectively show the CPO particles embedded within the PLA matrix. CPO particles are observed in the images of the samples as white spots. Unexpectedly, we found that 9% CPO released less oxygen and less calcium than the other CPO concentrations. We anticipated observing the opposite result as the outcomes of the antibacterial and red staining methodology contradicts these findings and confirm the presence of calcium within the sample. The SEM images in Figure 4.10a,b show a large number of CPO

particles that are agglomerated together and not dispersed within the composite solution. These particles are relatively large in size, indicating that there is insufficient dispersion of the CPO within the composite solution. Moreover, Figure 4.10c,d highlights a larger number of particles of undispersed calcium peroxide (black dots) in the PLA polymer. Therefore, we estimated that at 9% CPO, the composite was already saturated, with saturation reached after 6% CPO.

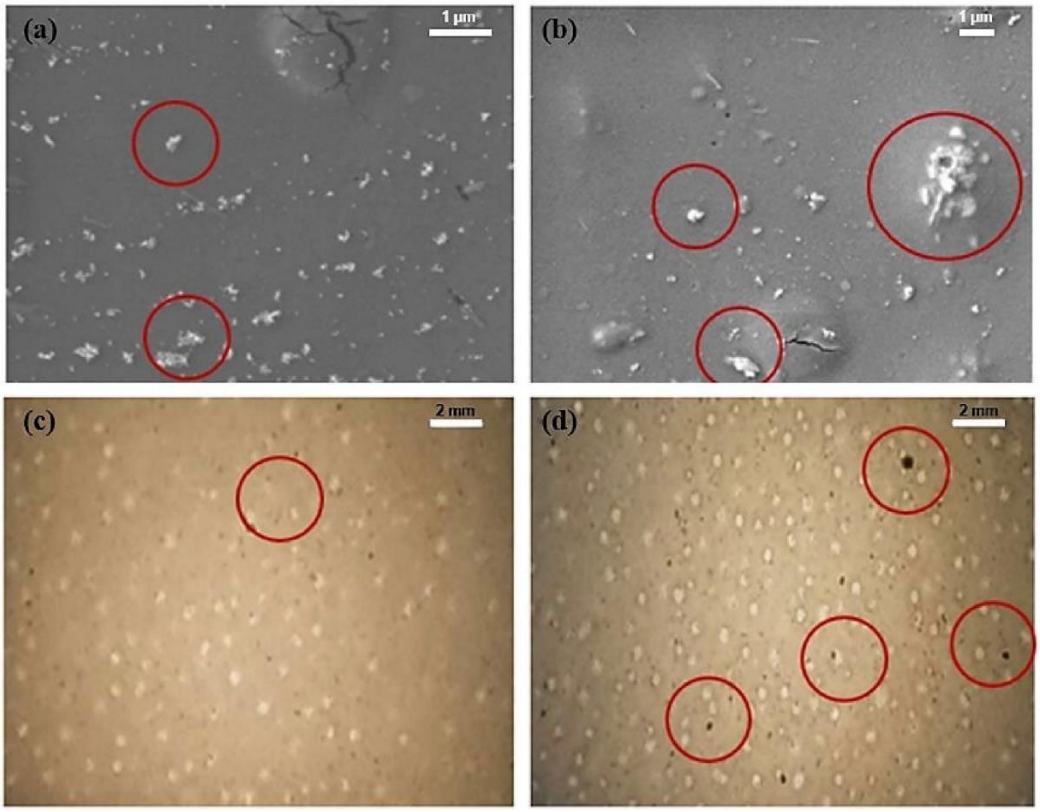

Figure 4.10. Undissolved calcium peroxide particles: (a) SEM image of low calcium peroxide concentration at a magnification of ×15,000 and an energy of 5.0 keV; (b) SEM image of high calcium peroxide concentration at a magnification of ×7500 and an energy of 5.0 keV. Optical image of the composite at (c) low and (d) high calcium peroxide concentration at a magnification of ×15.

4.5 Conclusions

The field of bone tissue engineering is expanding and focuses on developing new techniques and materials to repair or replace damaged or diseased bones. One promising area of research in this field is the use of 3D printing techniques to create composite filaments for use in bone

tissue engineering. PLA is a biodegradable and popular polymer for tissue engineering applications due to its preferable biocompatibility and mechanical properties. CPO, on the other hand, is a material that can release oxygen and calcium ions when it comes into contact with water. This property makes it a useful component in bone tissue engineering, as the increased oxygen levels and calcium ions can help to promote bone growth and healing. This study introduces a novel PLA/CPO composite filament created through wet solution mixing and hot melt extrusion, a process that can control the composition and morphology of the filament. The study examined the effect of varying CPO content on filament performance. The results showed that a 6% CPO ratio provides optimal calcium and oxygen release. However, when increasing CPO content, the composite filament displays poor dispersion of large, agglomerated particles, which can affect its mechanical properties. The composite filament with CPO content above 6% showed excellent antibacterial activity, which can be useful in preventing infections in bone tissue engineering applications. Furthermore, an in-depth study about cytocompatibility is currently being performed and will be published in a separate paper.

4.6 References

[1] United States Department of Health and Human Services. Organ Donation Statistics. Available online: https://www.organdonor. gov/learn/organ-donation-statistics (accessed on 15 January 2023).

[2] Centers for Disease Control and Prevention. Available online: https://www.cdc.gov/transplantsafety/overview/key-facts.html#:~:text=In%20the%20U.S%2C%20the%20most,1%20million%20grafts%20are%20transplanted (accessed on 27 December 2022).

[3] Sharifi, M.; Kheradmandi, R.; Salehi, M.; Alizadeh, M.; Ten Hagen, T.L.; Falahati, M. Criteria, Challenges, and Opportunities for Acellularized Allogeneic/Xenogeneic Bone Grafts in Bone Repairing. *ACS Biomater. Sci. Eng.* 2022, *8*, 3199–3219. [CrossRef] [PubMed]

[4] Kazimierczak, P.; Przekora, A. Osteoconductive and Osteoinductive Surface Modifications of Biomaterials for Bone Regeneration: A Concise Review. *Coatings* 2020, *10*, 971. [CrossRef]

[5] Barua, S.; Chattopadhyay, P.; Aidew, L.; Buragohain, A.K.; Karak, N. Infection-resistant hyperbranched epoxy nanocomposite as a scaffold for skin tissue regeneration. *Polym. Int.* 2014, *64*, 303–311. [CrossRef]

[6] Suvarnapathaki, S.; Wu, X.; Lantigua, D.; Nguyen, M.; Camci-Unal, G. Breathing life into engineered tissues using oxygen- releasing biomaterials. *NPG Asia Mater.* 2019, *11*, 65. [CrossRef]

[7] Xiao, Y.; Ahadian, S.; Radisic, M. Biochemical and Biophysical Cues in Matrix Design for Chronic and Diabetic Wound Treatment. *Tissue Eng. Part B Rev.* 2017, *23*, 9–26. [CrossRef] [PubMed]

[8] Bose, S.; Ke, D.; Sahasrabudhe, H.; Bandyopadhyay, A. Additive manufacturing of biomaterials. *Prog. Mater. Sci.* 2018, *93*, 45–111. [CrossRef] [PubMed]

[9] Ferrari, A.; Baumann, M.; Coenen, C.; Frank, D.; Hennen, L.; Moniz, A.; Torgersen, H.; Torgersen, J.; van Bodegom, L.; van Duijne, F.; et al. *Additive Bio-Manufacturing: 3D Printing for Medical Recovery and Human Enhancement*; European Parliament: Strasburg, France, 2018.

[10] Felfel, R.M.; Poocza, L.; Gimeno-Fabra, M.; Milde, T.; Hildebrand, G.; Ahmed, I.; Scotchford, C.; Sottile, V.; Grant, D.M.; Liefeith, K. In vitro degradation and mechanical properties of PLA-PCL copolymer unit cell scaffolds generated by two-photon polymerization. *Biomed. Mater.* 2016, *11*, 015011. [CrossRef]

[11] Chia, H.N.; Wu, B.M. Recent advances in 3D printing of biomaterials. *J. Biol. Eng.* 2015, *9*, 4. [CrossRef] [PubMed]

[12] Raeisdasteh Hokmabad, V.; Davaran, S.; Ramazani, A.; Salehi, R. Design and fabrication of porous biodegradable scaffolds: A strategy for tissue engineering. *J. Biomater. Sci. Polym. Ed.* 2017, *28*, 1797–1825. [CrossRef]

[13] Elmowafy, E.M.; Tiboni, M.; Soliman, M.E. Biocompatibility, biodegradation and biomedical applications of poly (lactic acid)/poly (lactic-co-glycolic acid) micro and nanoparticles. *J. Pharm. Investig.* 2019, *49*, 347–380. [CrossRef]

[14] DeStefano, V.; Khan, S.; Tabada, A. Applications of PLA in modern medicine. *Eng. Regen.* 2020, *1*, 76–87. [CrossRef]

[15] Tyler, B.; Gullotti, D.; Mangraviti, A.; Utsuki, T.; Brem, H. Polylactic acid (PLA) controlled delivery carriers for biomedical applications. *Adv. Drug Deliv. Rev.* 2016, *107*, 163–175. [CrossRef] [PubMed]

[16] Zhang, B.; Wang, L.; Song, P.; Pei, X.; Sun, H.; Wu, L.; Zhou, C.; Wang, K.; Fan, Y.; Zhang, X. 3D printed bone tissue regenerative PLA/HA scaffolds with

comprehensive performance optimizations. *Mater. Des.* 2021, *201*, 109490. [CrossRef]

[17] Radwan-Pragłowska, J.; Janus, Ł.; Pią tkowski, M.; Bogdał, D.; Matysek, D. 3D hierarchical, nanostructured chi-tosan/PLA/HA scaffolds doped with TiO_2/Au/Pt NPs with tunable properties for guided bone tissue engineering. *Polymers* 2020, *12*, 792. [CrossRef]

[18] Gholipourmalekabadi, M.; Zhao, S.; Harrison, B.S.; Mozafari, M.; Seifalian, A.M. Oxygen-Generating Biomaterials: A New, Viable Paradigm for Tissue Engineering? *Trends Biotechnol.* 2016, *34*, 1010–1021. [CrossRef]

[19] Augustine, R.; Gezek, M.; Bostanci, N.S.; Nguyen, A.; Camci-Unal, G. Oxygen-generating scaffolds: One step closer to the clinical translation of tissue engineered products. *Chem. Eng. J.* 2023, *455*, 140783. [CrossRef]

[20] Javid, N.; Honarmandrad, Z.; Malakootian, M. Ciprofloxacin removal from aqueous solutions by ozonation with calcium peroxide. *Desalination Water Treat.* 2020, *174*, 178–185. [CrossRef]

[21] Mallepally, R.R.; Parrish, C.C.; Mc Hugh, M.A.; Ward, K.R. Hydrogen peroxide filled poly(methyl methacrylate) microcapsules: Potential oxygen delivery materials. *Int. J. Pharm.* 2014, *475*, 130–137. [CrossRef]

[22] Abdullah, T.; Gauthaman, K.; Hammad, A.H.; Navare, K.J.; Alshahrie, A.A.; Bencherif, S.A.; Tamayol, A.; Memic, A. Oxygen- Releasing Antibacterial Nanofibrous Scaffolds for Tissue Engineering Applications. *Polymers* 2020, *12*, 1233. [CrossRef]

[23] Steg, H.; Buizer, A.T.; Woudstra, W.; Veldhuizen, A.G.; Bulstra, S.K.; Grijpma, D.W.; Kuijer, R. Control of oxygen release from peroxides using polymers. *J. Mater. Sci. Mater. Med.* 2015, *26*, 207. [CrossRef] [PubMed]

[24] Alemdar, N.; Leijten, J.; Camci-Unal, G.; Hjortnaes, J.; Ribas, J.; Paul, A.; Mostafalu, P.; Gaharwar, A.K.; Qiu, Y.; Sonkusale, S.; et al. Oxygen-Generating Photo-Cross-Linkable Hydrogels Support Cardiac Progenitor Cell Survival by Reducing Hypoxia-Induced Necrosis. *ACS Biomater. Sci. Eng.* 2016, *3*, 1964–1971. [CrossRef]

[25] Feng, P.; Jia, J.; Liu, M.; Peng, S.; Zhao, Z.; Shuai, C. Degradation mechanisms and acceleration strategies of poly (lactic acid) scaffold for bone regeneration. *Mater. Des.* 2021, *210*, 110066. [CrossRef]

[26] Donate, R.; Monzón, M.; Alemán-Domínguez, M.E.; Ortega, Z. Enzymatic degradation study of PLA-based composite scaffolds. *Rev. Adv. Mater. Sci.* 2020, *59*, 170–175. [CrossRef]

[27] Touri, M.; Moztarzadeh, F.; Abu Osman, N.A.; Dehghan, M.M.; Mozafari, M. 3D–printed biphasic calcium phosphate scaffolds coated with an oxygen generating system for enhancing engineered tissue survival. *Mater. Sci. Eng. C* 2018, *84*, 236–242. [CrossRef] [PubMed]

[28] Zhang, M.; Kiratiwongwan, T.; Shen, W. Oxygen-releasing polycaprolactone/calcium peroxide composite microspheres. *J. Biomed. Mater. Res. Part B Appl. Biomater.* 2019, *108*, 1097–1106. [CrossRef] [PubMed]

[29] Seekell, R.P.; Lock, A.T.; Peng, Y.; Cole, A.R.; Perry, D.A.; Kheir, J.N.; Polizzotti, B.D. Oxygen delivery using engineered microparticles. *Proc. Natl. Acad. Sci. USA* 2016, *113*, 12380–12385. [CrossRef]

[30] Ward, C.L.; Corona, B.T.; Yoo, J.J.; Harrison, B.S.; Christ, G.J. Oxygen Generating Biomaterials Preserve Skeletal Muscle Homeostasis under Hypoxic and Ischemic Conditions. *PLoS ONE* 2013, *8*, e72485. [CrossRef]

[31] Cook, C.A.; Hahn, K.C.; Morrissette-McAlmon, J.B.; Grayson, W.L. Oxygen

delivery from hyperbarically loaded microtanks extends cell viability in anoxic environments. *Biomaterials* 2015, *52*, 376–384. [CrossRef] [PubMed]

[32] Montazeri, L.; Hojjati-Emami, S.; Bonakdar, S.; Tahamtani, Y.; Hajizadeh-Saffar, E.; Noori-Keshtkar, M.; Najar-Asl, M.; Ash- tiani, M.K.; Baharvand, H. Improvement of islet engrafts by enhanced angiogenesis and microparticle-mediated oxygenation. *Biomaterials* 2016, *89*, 157–165. [CrossRef]

[33] Lee, H.-Y.; Kim, H.-W.; Lee, J.H.; Oh, S.H. Controlling oxygen release from hollow microparticles for prolonged cell survival under hypoxic environment. *Biomaterials* 2015, *53*, 583–591. [CrossRef]

[34] Fair, R.J.; Tor, Y. Antibiotics and Bacterial Resistance in the 21st Century. *Perspect. Med. Chem.* 2014, *6*, S14459. [CrossRef] [PubMed]

[35] Sladdin, M.; Lynch, J.M. Antimicrobial Properties of Calcium Peroxide in Relation to Its Potential Use as a Seed Dressing. *Microbiology* 1983, *129*, 2307–2314. [CrossRef]

[36] Siqueira, J.F., Jr.; Lopes, H.P. Mechanisms of antimicrobial activity of calcium hydroxide: A critical review. *Int. Endod. J.* 1999, *32*, 361–369. [CrossRef] [PubMed]

5 Chapter Five: Preparation and Characterisation of Poly Lactic Acid/Calcium Peroxide Composite 3D printed scaffold for Bone Tissue Engineering

Abdullah Mohammed [1], Alice Tirnoveanu [4], Richard Webb [4], Mohammad Aslam [5], Amr Elshaer [2], Hany Hassanin [1, 3], Khamis Essa [1,*]

1. School of Engineering, University of Birmingham, Birmingham B15 2TT
2. Drug Discovery, Delivery and Patient Care, School of Life Sciences, Pharmacy and Chemistry, Kingston University London, Kingston Upon Thames, Surrey, KT1 2EE
3. School of Engineering, Canterbury Christ Church University, Canterbury, CT1 1QU
4. Institute of Medical Sciences, Faculty of Medicine, Health and Social Care, Canterbury Christ Church University, CT1 1QU, UK
5. Centre of Excellence in Environmental Studies, King Abdulaziz University, Jeddah, Saudi Arabia

Authorship contribution statement

Conceptualization, H.H., A.E. and K.E.; Methodology, **A.M. (Abdullah Mohammed)**, A.T., R.W., M.A., H.H. and K.E.; Formal analysis, **A.M. (Abdullah Mohammed)**, A.E., H.H. and K.E.; Investigation (Conducting Cells Culturing Test and operating SEM and Tensile Test machines) **A.M. (Abdullah Mohammed),** M.A and A.T.; Resources R.W. and K.E. Writing—original draft, **A.M. (Abdullah Mohammed)** and H.H.; Writing—review & editing, A.E., H.H. and K.E.; Visualization, **A.M. (Abdullah Mohammed)**; Supervision, H.H. and K.E.; Project administration, H.H. and K.E.

5.1 Abstract

The latest advancements in bone scaffold technology have introduced novel biomaterials that have the ability to generate oxygen when implanted, improving cell viability and tissue maturation. In this paper, we present a new oxygen-generating polylactic acid (PLA)/calcium peroxide (CPO) composite filament that can be used in 3D printing scaffolds. The composite material was prepared using a wet solution mixing method, followed by drying and hot melt extrusion. The prepared composite filament had a 6% CPO concentration and was used for Fused Deposition Modelling (FDM) 3D printing.

The FDM printer parameters were optimized and evaluated to fabricate a square-shaped scaffold with high printing quality that matches the CAD module and 25% porosity with a pore size of 0.60mm. The fabricated scaffold was characterized in terms of its printing quality, cell culturing, and mechanical properties after cell culturing. The highest printing quality was achieved at a speed of 75 mm/s, while maintaining the printing nozzle temperature at 200°C. The samples exhibited differentiation to bone, which was further enhanced when supplemented with osteogenic media. The differentiation media samples showed upregulation of bone markers.

The mechanical properties of the samples were enhanced after cell culturing, with an increase of approximately 2 MPa stress and 0.7% strain. These findings suggest that the fabricated bone scaffold has significant potential in enhancing the regeneration of bone tissues, along with improved mechanical properties.

5.2 Introduction

The increasing need for tissue and organ transplants has resulted in a significant imbalance between the availability of organ donors and the demand for transplants. This presents a major biomedical issue, with over 106,000 people in the United States alone waiting for organ transplants [1]. According to recent statistics from March 2022, there are 17 deaths every day due to delays in transplant surgeries [1]. Bones are among the most highly sought-after tissues for transplantation in the United States, and finding a donor match is a significant challenge for bone graft procedures [2]. Autografts, in which tissues are taken from the patient's own body, are currently the preferred method for bone fracture healing and regeneration. However, there are some cases where this is not possible, such as when the fractured bone is too large or requires a high degree of precision in shaping, such as in facial bone surgery [3]. Tissue engineering has become a viable alternative to bone grafting for bone regeneration. This method involves the creation of a bone scaffold that includes growth factors, stem cells, and biocompatible and biodegradable materials, which can aid in bone fracture healing and enhance the incorporation of the graft [4, 5]. The scaffolds are designed to offer physical support and promote tissue regeneration, thereby helping the tissue to recover its functionality [6-8].

In recent times, the use of 3D printing technologies for fabricating bone scaffolds has gained considerable attention. This technique enables the creation of porous scaffolds with a specific exterior design and porous internal structure to produce scaffolds with tailored functionality [9]. Among the various 3D printing techniques, fused deposition modelling (FDM) is often employed in tissue engineering due to its low cost, accessibility, and availability [10]. Furthermore, this technique has a printing accuracy that can reach +/-0.5 mm, and a broad range of biocompatible and biodegradable polymeric materials suitable for tissue engineering can be used [10, 11].

Tissue engineering makes use of a variety of materials to repair bone, tendon, and skin. Among these, polylactic acid (PLA), polycaprolactone (PCL), and polyglycolide or poly-glycolic acid (PGA) are particularly useful due to their favourable mechanical and biochemical properties [12, 13]. PLA is a material that possesses desirable physical and mechanical properties, biocompatibility, and biodegradability, which are significantly affected by its molecular weight and stereochemistry [14]. These features make PLA a suitable material for a wide range of industrial applications, including medical devices [15]. Furthermore, PLA is compatible with fused deposition modelling (FDM) 3D printers and is approved by the US Food and drug administration (FDA) for several biomedical applications [16]. Although tissue engineering has shown promising outcomes in laboratory experiments, its clinical application has only benefited small tissue defects less than a few millimetres in size. The reason behind this limitation is the lack of vascularization, which leads to inadequate oxygen supply [17, 18]. The shortage of oxygen in engineered tissues represents a significant obstacle to bone regeneration and scaffold functionality because it hinders the growth of cells attached to the scaffold [19].

Researchers have created scaffolds that produce oxygen from different solid peroxide particles, such as magnesium peroxide, calcium peroxide, and sodium percarbonate. The usual process involves the disintegration of these particles in water, resulting in the release of oxygen through hydrolysis, as displayed in Equation (1) and Equation (2) [7, 20]. Among other materials, CPO is preferred as an oxygen-releasing agent due to its low cost and commercial availability [21, 22].

$$CaO_2 + 2H_2O \rightarrow Ca(OH)_2 + H_2O_2 \qquad \text{Eq1}$$

$$2H_2O_2 \rightarrow O_2 + 2H_2O \qquad \text{Eq2}$$

Literature shows that fabricating a bone scaffold with 3D-printed oxygenation filaments can improve bone tissue regeneration and healing. The incorporation of an oxygen source within

the scaffold has been found to promote vascularization and enhance the scaffold's efficacy [18]. The aim of the current study is to designed a novel bone scaffold from PLA/CPO composite filament using fused deposition modelling (FDM) 3D printers.

5.3 Materials and Methods

5.3.1 Materials

PLA filament 1.75mm was purchased from (Shenzhen eSUN Industrial Co., Ltd.), calcium peroxide (CPO) CaO_2 (-200 mesh size, 75% purity) was purchased from Sigma-Aldrich (St. Louis, MO, USA), catalase (from bovine serum, 5000 unit/mg), dichloromethane (DCM) was purchased from Sigma-Aldrich (St. Louis, MO, USA). And deionised water.

5.3.2 Preparation of composite filament

PLA filaments (20g) were cut into small pieces and dissolved in 100ml of DCM for 30 minutes at room temperature using a magnetic stirrer at a speed of 700rpm. Once the PLA was completely dissolved, the CPO powder was added to the solution at 6% under magnetic vigorous stirring for 90 minutes before pouring into a large plate to dry for 24 hours. After the prepared composites dried, it was cut into small pieces for loading into the hot melt extruder. A customised single screw extruder with a nozzle diameter of 2 mm was used to extrude the composite materials at a nozzle temperature of 140 ◦C and an extruding speed of 2.5 cm/s.

5.3.3 3D printing of bone scaffolds

A commercial Fused Deposition Modelling (FDM) 3D printer, Creality, model Ender 3 Pro manufactured by (Shenzhen Creality 3D Technology Co.,LTD., China) was used to fabricates the bone scaffold at different parameters (Table 5.1) scaffolds were printed in a square shape with length and width of 8x8 mm and height of 1.5mm and had a 25% porosity with pore size of 0.60mm.

Table 5.1. 3D printer parameters used to print PLA scaffolds with 6% CPO.

Sample No.	Printing temperature (ºC)	Building platform temperature (ºC)	Printing speed (mm/s)
1	200	70	25
2	200	70	50
3	200	70	75

5.3.4 Characterisations

5.3.4.1 Morphological analysis

Micrographs of the printed scaffold surfaces were captured with field emission scanning electron microscopy (FESEM) using a JEOL JSM-IT700HR instrument from JEOL USA, Inc. Scaffolds were sputter-coated with a thin layer of gold using a JFC-1600 auto fine coater from JEOL, Tokyo, Japan prior to SEM analysis. The micrograph images were used for morphological analysis using ImageJ 1.53f51, an open-source image analysis software developed by The National Institutes of Health (NIH) in the USA. The surface roughness of the printed scaffolds was evaluated using water contact angle measured with a KRUSS DSA30E drop shape analyser from Hamburg, Germany. Before testing the surface of all samples were cleaned, and deionised water was used as the test liquid.

5.3.4.2 *In-vitro* osteogenic differentiation

Cell culture

Human Mesenchymal stem cells (Lonza) were expanded in Dulbecco's Modified Eagle's Medium - GlutaMax supplemented with 5% (v/v) Human PRP , 1% (v/v) Non-Essential Amino Acids, 1% (v/v) Penicillin-Streptomycin-Amphotericin for 2 weeks prior to seeding.

Post expansion the PLA rods were sterilised for 24hrs in 100% ethanol and 1 hr Post sterilisation the PLA rods were pretreated by soaking in PBS containing 10ng/mL fibronectin at 37^{o}C. After 1 hr had elapsed the rods were then washed twice with sterile PBS and cells were seeded at 4 x 10^5 cells per rod and placed for 20 minutes in the incubator model ST180 PLUS CO2 from (Benchmark Scientific, Darmstadt, Germany) to enable the cells attachment. After 20 mins had elapsed all the rods were then submerged in KOSR media for 24 hrs Dulbecco's Modified Eagle's Medium - GlutaMax supplemented with 10% (v/v) KnockOut™ Serum Replacement, 1% (v/v) Non-Essential Amino Acids, 1% (v/v) Penicillin-Streptomycin-Amphotericin. After 24 hrs the rods were separated into two groups: Control Group (KOSR without vitamin D), and experimental differentiation group (where the media was supplemented with vitamin D, Beta-glysophosphate and ascorbic-2-phosphate).

In the negative control plate, the medium did not contain vitamin D. The media were changed twice weekly for both the control and differentiation group.

Total RNA Extraction:

RNA was extracted from the cell population of the polymer rods using Qiagen RNeasy MiniPrep Kit. The rods were incubated with the RLT Lysis Buffer, and the extraction procedures was carried out as instructed by the manufacturer's guidelines.

RNA quantification:

The extracted RNA was quantified by absorbance reading at 260/280 nm ration with Tecan i-200-Pro. The measurements were performed in triplicate. The mean concentration value per sample was used for further calculation in the qRT-PCR set-up.

Real-Time Reverse Transcriptase Polymerase Chain Reaction (qRT-PCR)

For the gene expression analysis of Glyceraldehyde 3-phosphate dehydrogenase (GAPDH), Runt-related transcription factor 2 (RUNX2), Collagen type I alpha 1 chain (COL1A1), Secreted Phosphoprotein 1 (SPP1) and Sp7 transcription factor (SP7), the Qiagen QuantiNova SYBR Green RT-PCR kit was used, according to the supplier's guidelines.

Customised primer sets for GAPDH, RUNX2, COL1A1, SPP1 and SP7 were previously designed and verified against the human cell line MG63 (Osteosarcoma) supplied by ATCC. All primers sequences were designed using human genes data from the Ensemble genome browser and the NCBI Gene database. The specificity of alignment was assessed with NCBI Primer-BLAST tool. The RT-PCR reaction was set-up as following:

The fold change value was further analysed against the GAPDH expression and vitamin D was normalised utilising delta-delta Ct to calculate fold change against control sample KOSR.

5.3.4.3 Mechanical properties

To determine the mechanical properties of the samples, a universal Instron 3367 testing machine (Norwood, MA, USA) equipped with a 30 kN load cell was used. The testing involved subjecting filament samples of varying diameters (ranging from 1.75 mm to 1.95 mm) and a length of 90 mm to tensile testing. The samples were securely held in place by manual grips, and the machine's crosshead speed was set at a constant rate of 5 mm/min. The experiments were conducted three times, and the average values were calculated to ensure accuracy. The results are presented as the average ± standard deviation (SD).

5.3.4.4 Statistical analysis

Each experiment was conducted in triplicate, and a mean value was calculated. The information is presented as the average with a ± standard deviation (SD). Origin software (OriginPro 8.0, Origin Lab Inc., Northampton, MA, USA) was used to analyse and present the data in a graphical format.

5.4 Results & discussion

5.4.1 3D Printing of bone scaffolds

The 3D printing of bone scaffolds using PLA/CPO composite material (Figure 5.1) was investigated to achieve the highest accuracy and quality. The 3D printer parameters were mainly determined by two variables: temperature and speed of printing. While maintaining the temperature constant at ~200 ºC, the printing speed was set to three different levels (Table 5.1). The dimensional accuracy of the printed scaffolds at different speeds was determined based on the number of pores fabricated without overlapping or defacing the original design. The graph in (Figure 5.2a) shows a linear relationship between accuracy and printing speed. As the speed increased, the accuracy also increased, with the highest accuracy of 98.33% being achieved at a speed of 75 mm/s. At a speed of 25 mm/s, the accuracy was very poor at about 48%. It is important to note that the temperature of the printer nozzle and the build plate were held constant during testing. This suggests that the temperature settings were not a limiting factor in the accuracy of the 3D printing process.

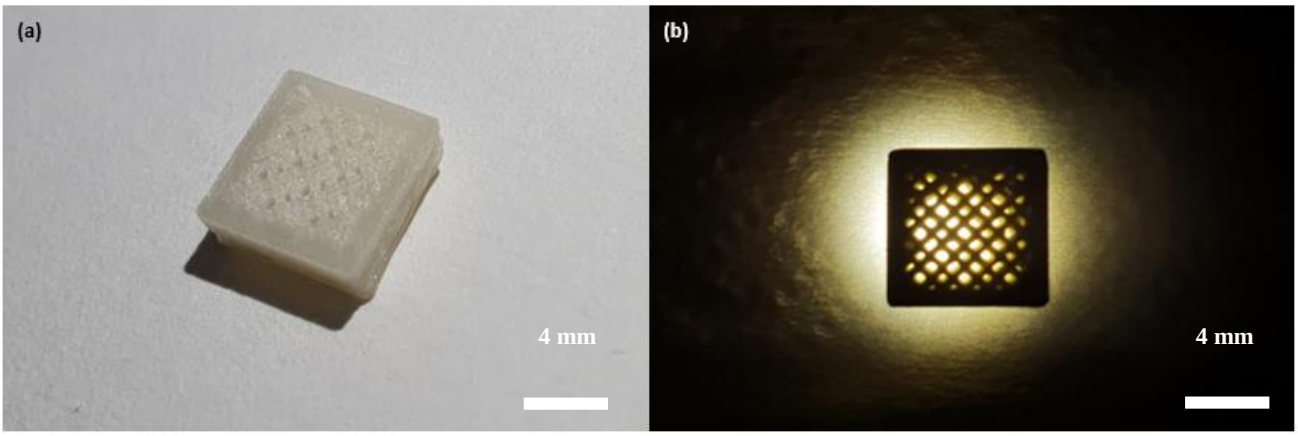

Figure 5.1. Optical images of the 3D printed scaffolds a) side image and b) top image with lighting source showing porosity.

In addition to the enhanced accuracy at higher printing speeds, the quality of the printed scaffolds was also found to be better at higher speeds. The quality of the printing was evaluated by measuring the layer line width and slope angle, as shown in (Figure 5.2f). The layer line width at low speeds of 25 mm/s and 50 mm/s was found to be small and highly irregular, with large slope angles of about 18º as shown in (Figure 5.2b). In contrast, at higher speeds of 75 mm/s, the layer line width was about 0.40 mm and the slope angle was approximately 11.5º (Figure 5.2d-f). Overall, the quality of the printing increased with the increase of the printing speed.

Furthermore, the water contact angle and SEM images of the printed scaffolds indicate the effect of printing speed on surface roughness. In (Figure 5.2c), at low speeds of 25 mm/s and 50 mm/s, the scaffolds had a contact angle of around 96.5º and 97º, respectively. However, at a speed of 75 mm/s, there was a major increase in the contact angle of approximately 6º compared to scaffolds printed at lower speeds. Generally, a smoother surface will have a higher contact angle, while a rougher surface will have a lower contact angle [23]. Furthermore, it is clear from (Figure 5.2d-f) that the surface roughness becomes smoother and more symmetrical as the printing speed is increased. It was reported by Wangwang while printing an object with 100% infill, that printing at high speed can cause cavities and delamination at the interface between different layers [24], which is opposite to our findings. It can be argued that our case is different from what has been reported in the literature because our composite material has a higher viscosity compared to pure PLA, making it more viscous due to the embedded CPO particles within the PLA matrix [25, 26]. Hence, printing parameters for high accuracy and quality can vary depending on the materials used, as they are highly influenced by the materials' properties. As a result with the PLA/CPO composite, a higher extruding speed is required to achieve the desired accuracy and quality.

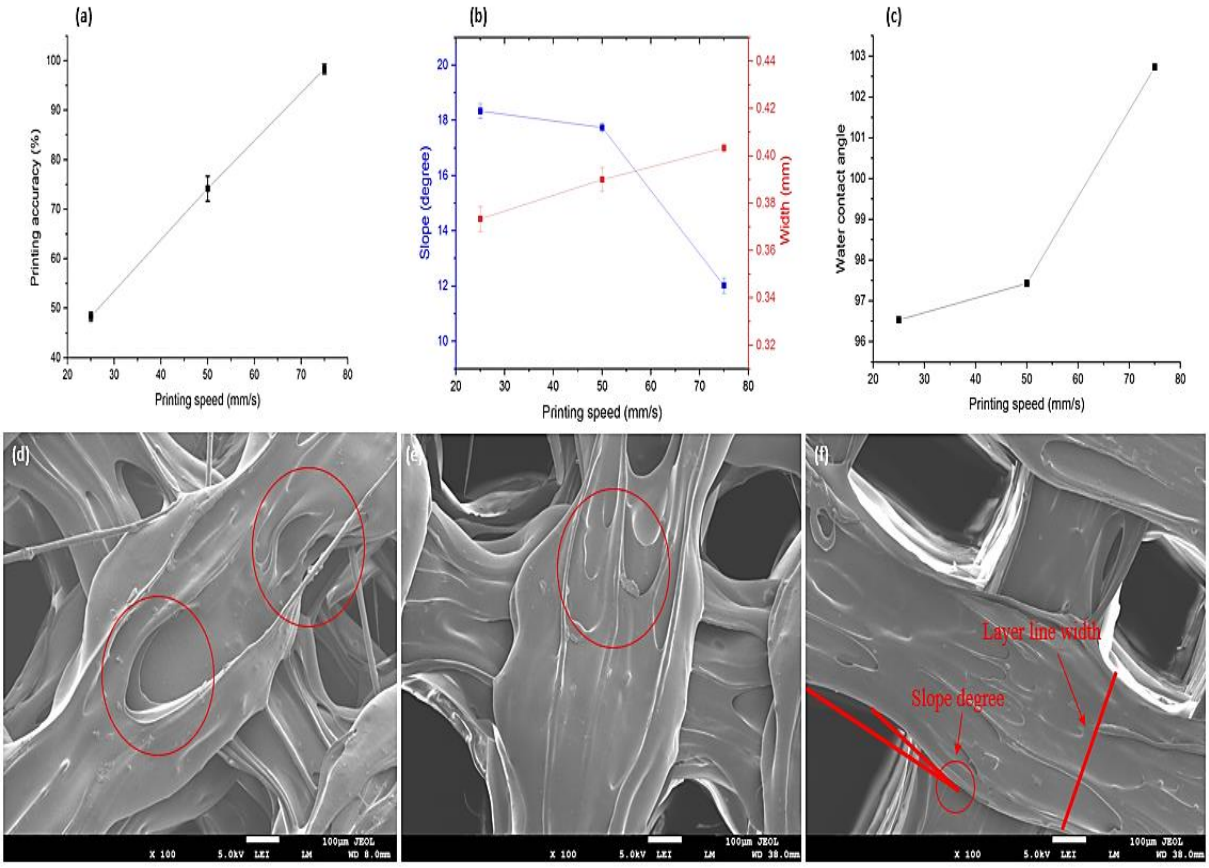

Figure 5.2. Evaluation of 3D printing accuracy and quality, (a) accuracy percentages of printed scaffolds at different printing speeds, (b) slope degree and width of scaffolds layer line at different printing speeds, and (c) water contact angles of printed scaffolds surface at different printing speeds. SEM images of printed scaffolds layer at different printing speed of: (d) 25 mm/s, (e) 50 mm/s, and (f) 75 mm/s. (n= 3).

5.4.2 Gene expression

Skeleton can be either formed by endochondral ossification or intramembranous ossification. Mesenchymal cells directly differentiate into osteoblasts which forms intramembranous bones [27]. On the other hand, the replacement of cartilaginous structure by bone will form endochondral bones. Around 90% of bone is made of type 1 collagen [28]. The latter is a triple helix structure made of 2 type 1 collagen strand (Col1a1) and on Col1a2 strand [29]. Besides, Col1a1 and Col1a2, various transcription factors are involved in bone development and maintenance. One important transcription factor is RUNX2, which is essential for osteoblast differentiation and bone formation [30]. Another significant factor is phosphoprotein 1 (Spp1),

also known as osteopenia, produced by osteoblasts. Spp1 plays a crucial role in regulating bone mineralization and remodelling processes [31]. SP7, another transcription factor, is involved in osteoblast differentiation and mineralization [32]. In the present experimental configuration, the combination of scaffold composition and culture conditions led to an enhancement in the gene expression of Human Mesenchymal stem cells (hMSCs) cells associated with bone development in contrast to those grown in a monolayer.

On Figure 5.3, the gene expression results were normalised to the control samples which were cultured in the absence of vitamin D. When Human Mesenchymal stem cells (hMSCs) were differentiated in the presence of vitamin D upregulation of the bone transcription factors essential for bone differentiation (RUNX2, SPP1 and SP7) were observed. Conversely, a downregulation of COL1A1 was noted (Figure 5.3). Notably, distinct increase was detected in the expression of RUNX2 genes in hMSC cells cultured, in contrast to the expression levels of COL1a1, SPP1, and SP7 genes, as well as literature [33].

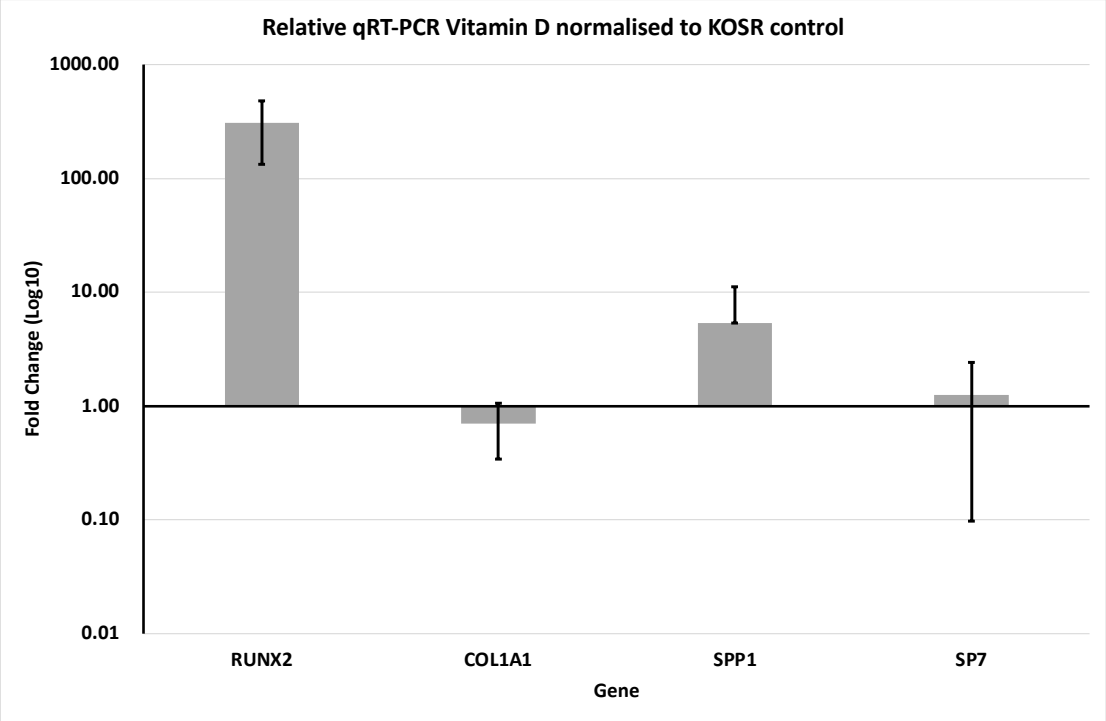

Figure 5.3. Delta-Delta Ct values for hMSCs differentiated in the presence of vitamin D (n = 3).

5.4.3 Mechanical properties

The tensile properties of the samples after cells culturing were evaluated to investigate the impact of cells on the mechanical behaviour of the PLA/CPO composite matrix. Figure 5.4 shows the stress–strain curves of the PLA/CPO composites with varying cells culturing conditions. It is evident from the graph that the ductility of scaffold has doubled when cells were attached into the scaffolds. The tensile strength of KOSR scaffolds was higher than those with vitamin D by approximately 1.2MPa and no mesenchymal cells by approximately 2MPa. Both samples of KOSR and vitamin D had a strain of about 1.5%, whereas the no cells (Control) sample has a strain of 0.7%. Apart from the KOSR all the samples showed a plastic deformation in the region of about a 0.5% strain. The high strength of KOSR can be attributed to the observation during the cells culturing, cells differentiated and expanded faster comparing to the one with vitamin D. The no cells (Control) samples were exposed to the same process and conditions but with no cells, thus it is weaker when comparing it to the pure sample with

6% CPO in our previous study this can be attributed to the CPO decomposing [25]. **Also once cells…**

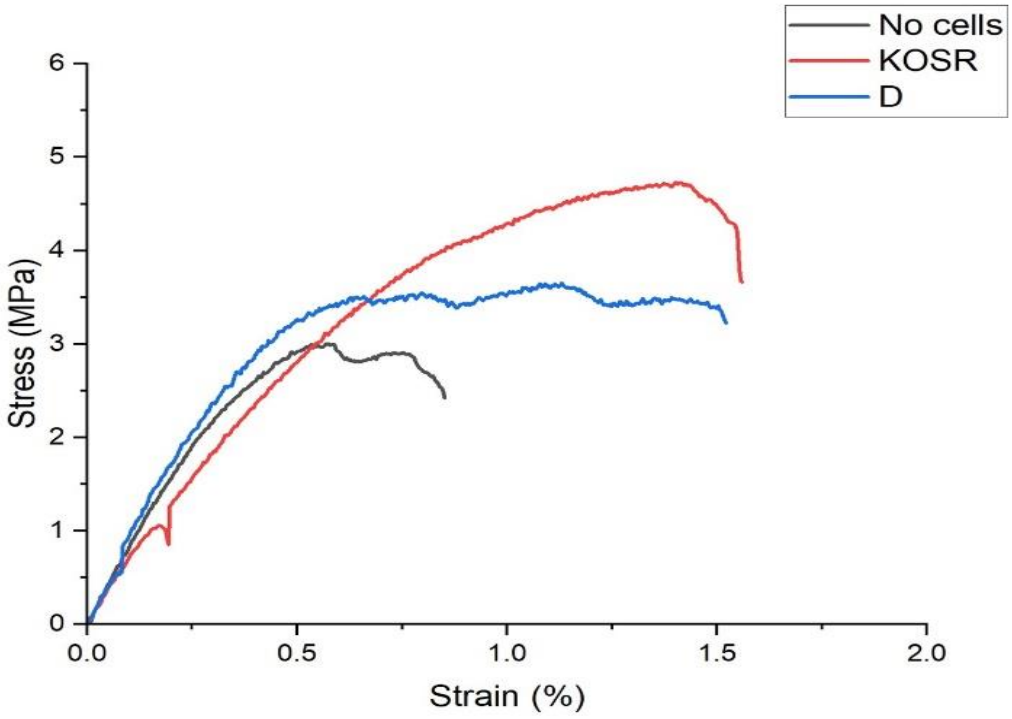

Figure 5.4. Stress strain diagram of samples containing no cells (grey), with KOSR (blue) and with vitamin D (blue). (n=3) results are represented in average ± 5% SD.

5.5 Conclusion

The area of bone tissue engineering is expanding and its primary focus is to develop innovative methods and materials for the repair or replacement of bones that have been damaged or affected by disease. A promising avenue of investigation in this field involves utilizing 3D printing methods to create porous bone scaffolds using distinct materials that possess specific properties, intended for application in tissue engineering. PLA, known as a biodegradable polymer, is widely utilized in tissue engineering due to its excellent biocompatibility, mechanical characteristics, and ability to naturally degrade over time. Conversely, CPO is a substance that has the ability to release oxygen and calcium ions upon interaction with water. This characteristic renders it a valuable element in bone tissue engineering since the elevated

levels of oxygen and calcium ions it releases can facilitate the stimulation of bone growth and enhance the healing process.

This research presents an approach to developing a bone scaffold using the FDM technique. The scaffold is constructed using a PLA/CPO composite filament material, which is produced through a combination of wet solution mixing and hot melt extrusion. The study evaluated the FDM printer parameters for achieving the required quality scaffold. Different printing speeds were examined while maintaining the printing temperature to what is suitable for the material. The printing quality were found to be enhanced with higher printing speed, this finding is the opposite to what has been reported by literature. This has lead us to hypothesised that the printing speed can be attributed to the material properties. In our case the highest quality square-shaped scaffold was fabricated at a speed of 75 mm/s and printing nozzle temperature at 200°C. The scaffold was fabricated with a 25% porosity and a pore size of 0.60mm. The samples demonstrated differentiation to bone, which was boosted even more when supplemented with osteogenic media for bone formation. The differentiation media samples exhibited upregulation of bone markers, with the most significant increase observed in the case of RUNX2. After being cultured with cells, the mechanical characteristics of the samples were improved, with a stress increase of around 2 MPa and a strain increase of 0.7%. These results indicate that the created bone scaffold has considerable promise in enhancing the regeneration of bone tissues, while also displaying improved mechanical properties.

5.6 References

[1] "United States Department of Health And Human Services (U. D. o. H. a. H.) Organ Donation Statistics." https://www.organdonor.gov/learn/organ-donation-statistics (accessed.

[2] C. f. D. C. a. P. (CDC). https://www.cdc.gov/transplantsafety/overview/key-facts.html#:~:text=In%20the%20U.S%2C%20the%20most,1%20million%20grafts%20are%20transplanted. (accessed.

[3] P. Kumar, B. Vinitha, and G. Fathima, "Bone grafts in dentistry," Journal of pharmacy & bioallied sciences, vol. 5, pp. S125-7, 06/01 2013, doi: 10.4103/0975-7406.113312.

[4] A. S. Brydone, D. Meek, and S. Maclaine, "Bone grafting, orthopaedic biomaterials, and the clinical need for bone engineering," (in eng), Proc Inst Mech Eng H, vol. 224, no. 12, pp. 1329-43, Dec 2010, doi: 10.1243/09544119jeim770.

[5] R. Dimitriou, E. Jones, D. McGonagle, and P. V. Giannoudis, "Bone regeneration: current concepts and future directions," (in eng), BMC Med, vol. 9, p. 66, May 31 2011, doi: 10.1186/1741-7015-9-66.

[6] S. Barua, P. Chattopadhyay, L. Aidew, A. K. Buragohain, and N. Karak, "Infection-resistant hyperbranched epoxy nanocomposite as a scaffold for skin tissue regeneration," Polymer International, https://doi.org/10.1002/pi.4790 vol. 64, no. 2, pp. 303-311, 2015/02/01 2015, doi: https://doi.org/10.1002/pi.4790.

[7] S. Suvarnapathaki, X. Wu, D. Lantigua, M. A. Nguyen, and G. Camci-Unal, "Breathing life into engineered tissues using oxygen-releasing biomaterials," NPG Asia Materials, vol. 11, no. 1, p. 65, 2019/11/08 2019, doi: 10.1038/s41427-019-0166-2.

[8] Y. Xiao, S. Ahadian, and M. Radisic, "Biochemical and Biophysical Cues in Matrix Design for Chronic and Diabetic Wound Treatment," (in eng), Tissue Eng Part B Rev, vol. 23, no. 1, pp. 9-26, Feb 2017, doi: 10.1089/ten.TEB.2016.0200.

[9] S. Bose, D. Ke, H. Sahasrabudhe, and A. Bandyopadhyay, "Additive manufacturing of biomaterials," (in eng), Prog Mater Sci, vol. 93, pp. 45-111, Apr 2018, doi: 10.1016/j.pmatsci.2017.08.003.

[10] A. Ferrari et al., Additive bio-manufacturing: 3D printing for medical recovery and human enhancement. 2018.

[11] R. M. Felfel et al., "In vitro degradation and mechanical properties of PLA-PCL copolymer unit cell scaffolds generated by two-photon polymerization," Biomedical Materials, vol. 11, no. 1, p. 015011, 2016/02/02 2016, doi: 10.1088/1748-6041/11/1/015011.

[12] H. N. Chia and B. M. Wu, "Recent advances in 3D printing of biomaterials," Journal of Biological Engineering, vol. 9, no. 1, p. 4, 2015/03/01 2015, doi: 10.1186/s13036-015-0001-4.

[13] V. Raeisdasteh Hokmabad, S. Davaran, A. Ramazani, and R. Salehi, "Design and fabrication of porous biodegradable scaffolds: a strategy for tissue engineering," Journal of Biomaterials Science, Polymer Edition, vol. 28, no. 16, pp. 1797-1825, 2017/11/02 2017, doi: 10.1080/09205063.2017.1354674.

[14] I. Armentano et al., "Multifunctional nanostructured PLA materials for packaging and tissue engineering," Progress in Polymer Science, vol. 38, no. 10, pp. 1720-1747, 2013/10/01/ 2013, doi: https://doi.org/10.1016/j.progpolymsci.2013.05.010.

[15] A. J. R. Lasprilla, G. A. R. Martinez, B. H. Lunelli, A. L. Jardini, and R. M. Filho, "Poly-lactic acid synthesis for application in biomedical devices — A review," Biotechnology Advances, vol. 30, no. 1, pp. 321-328, 2012/01/01/ 2012, doi: https://doi.org/10.1016/j.biotechadv.2011.06.019.

[16] B. Tyler, D. Gullotti, A. Mangraviti, T. Utsuki, and H. Brem, "Polylactic acid (PLA) controlled delivery carriers for biomedical applications," Advanced Drug Delivery Reviews, vol. 107, pp. 163-175, 2016/12/15/ 2016, doi: https://doi.org/10.1016/j.addr.2016.06.018.

[17] M. Gholipourmalekabadi, S. Zhao, B. S. Harrison, M. Mozafari, and A. M. Seifalian, "Oxygen-Generating Biomaterials: A New, Viable Paradigm for Tissue Engineering?," Trends in Biotechnology, vol. 34, no. 12, pp. 1010-1021, 2016/12/01/ 2016, doi: https://doi.org/10.1016/j.tibtech.2016.05.012.

[18] S. H. Oh, C. L. Ward, A. Atala, J. J. Yoo, and B. S. Harrison, "Oxygen generating scaffolds for enhancing engineered tissue survival," Biomaterials, vol. 30, no. 5, pp. 757-762, 2009/02/01/ 2009, doi: https://doi.org/10.1016/j.biomaterials.2008.09.065.

[19] G. Camci-Unal, N. Alemdar, N. Annabi, and A. Khademhosseini, "Oxygen Releasing Biomaterials for Tissue Engineering," (in eng), Polym Int, vol. 62, no. 6, pp. 843-848, Jun 1 2013, doi: 10.1002/pi.4502.

[20] E. Pedraza, M. M. Coronel, C. A. Fraker, C. Ricordi, and C. L. Stabler, "Preventing hypoxia-induced cell death in beta cells and islets via hydrolytically activated, oxygen-generating biomaterials," (in eng), Proc Natl Acad Sci U S A, vol. 109, no. 11, pp. 4245-4250, 2012, doi: 10.1073/pnas.1113560109.

[21] D. P. Cassidy and R. L. Irvine, "Use of calcium peroxide to provide oxygen for contaminant biodegradation in a saturated soil," Journal of Hazardous Materials, vol.

69, no. 1, pp. 25-39, 1999/09/01/ 1999, doi: https://doi.org/10.1016/S0304-3894(99)00051-5.

[22] A. J. Waite, J. S. Bonner, and R. Autenrieth, "Kinetics and Stoichiometry of Oxygen Release from Solid Peroxides," Environmental Engineering Science, vol. 16, no. 3, pp. 187-199, 1999/05/01 1999, doi: 10.1089/ees.1999.16.187.

[23] C. Li, J. Zhang, J. Han, and B. Yao, "A numerical solution to the effects of surface roughness on water–coal contact angle," Scientific Reports, vol. 11, no. 1, p. 459, 2021/01/11 2021, doi: 10.1038/s41598-020-80729-9.

[24] W. Yu, J. Shi, L. Sun, and W. Lei, "Effects of Printing Parameters on Properties of FDM 3D Printed Residue of Astragalus/Polylactic Acid Biomass Composites," Molecules, vol. 27, no. 21, doi: 10.3390/molecules27217373.

[25] A. H. Mohammed et al., "Preparation of Polylactic Acid/Calcium Peroxide Composite Filaments for Fused Deposition Modelling," Polymers, vol. 15, no. 9, doi: 10.3390/polym15092229.

[26] J. Y. Lee, S. H. Kwon, I.-J. Chin, and H. J. Choi, "Toughness and rheological characteristics of poly(lactic acid)/acrylic core–shell rubber blends," Polymer Bulletin, vol. 76, no. 11, pp. 5483-5497, 2019/11/01 2019, doi: 10.1007/s00289-018-2662-x.

[27] G. Breeland, M. A. Sinkler, and R. G. Menezes, "Embryology, bone ossification," in StatPearls [Internet]: StatPearls Publishing, 2021.

[28] X. Feng, "Chemical and Biochemical Basis of Cell-Bone Matrix Interaction in Health and Disease," (in eng), Curr Chem Biol, vol. 3, no. 2, pp. 189-196, May 1 2009, doi: 10.2174/187231309788166398.

[29] I. Boraschi-Diaz, J. Wang, J. S. Mort, and S. V. Komarova, "Collagen Type I as a Ligand for Receptor-Mediated Signaling," (in English), Frontiers in Physics, Review vol. 5, 2017-May-16 2017, doi: 10.3389/fphy.2017.00012.

[30] T. Komori, "Regulation of osteoblast differentiation by Runx2," (in eng), Adv Exp Med Biol, vol. 658, pp. 43-9, 2010, doi: 10.1007/978-1-4419-1050-9_5.

[31] J. U. A. Choi, A. W. Kijas, J. Lauko, and A. E. Rowan, "The Mechanosensory Role of Osteocytes and Implications for Bone Health and Disease States," (in English), Frontiers in Cell and Developmental Biology, Review vol. 9, 2022-February-21 2022, doi: 10.3389/fcell.2021.770143.

[32] Q. Liu, M. Li, S. Wang, Z. Xiao, Y. Xiong, and G. Wang, "Recent Advances of Osterix Transcription Factor in Osteoblast Differentiation and Bone Formation," (in English), Frontiers in Cell and Developmental Biology, Review vol. 8, 2020-December-15 2020, doi: 10.3389/fcell.2020.601224.

[33] A. Luca et al., "Improvement of osteogenic differentiation of human mesenchymal stem cells on composite poly l-lactic acid/nano-hydroxyapatite scaffolds for bone defect repair," Journal of Bioscience and Bioengineering, vol. 129, 09/01 2019, doi: 10.1016/j.jbiosc.2019.08.001.

6 Chapter Six: Conclusion and Future Research

6.1 Conclusion

Bone injuries and fractures are common and require a complex and intricate healing process that involves both biological and mechanical aspects. Tissue engineering of bone scaffolds holds great promise for future treatments of these injuries. However, conventional manufacturing techniques cannot provide the required structural properties of human bones. In recent years, three-dimensional printing or additive manufacturing technologies have enabled control over the creation of bone scaffolds with personalized geometries, appropriate materials, and tailored pores. This advancement has led to the development of new biomaterial filaments that can be used to fabricate 3D printable composite bone scaffolds. This thesis investigated and developed a novel FDM biodegradable PLA/CPO composite filament for the fabrication of a bone scaffold with the ability to generate oxygen. The aim of this composite filament is to provide effective and sustainable 3D-printed bone scaffolds for use in bone regeneration. The fabrication of the biodegradable and oxygen-generating bone scaffold was achieved through several stages. These stages outline a systematic approach to advancing bone fracture healing. Firstly, understanding the mechanism of bone fracture healing processes is crucial for designing effective treatments. This knowledge provides insights into the natural healing mechanisms and helps identify potential targets for intervention. Once the requirements for bone scaffold fabrication are defined, including materials, growth factors, designs, and manufacturing processes, the next step involves selecting suitable bone scaffold materials and growth factor agents. These choices are crucial for promoting bone regeneration and ensuring biocompatibility. Additionally, identifying an appropriate 3D printing technique for bone scaffold fabrication offers advantages such as customization and precise control over scaffold architecture. After determining the suitable materials and printing technique, preparing the defined composite material is necessary to create a scaffold with desired properties. Subsequently, optimizing and characterizing the prepared composite material for

morphological and mechanical properties ensures that it meets the required standards. Additionally, optimizing the 3D printing process for fabricating bone scaffold using the composite material enhances efficiency and accuracy. Lastly, characterizing the printed scaffold for release, antibacterial activities, and cell culturing confirms its functionality and biocompatibility. Overall, this multi-step process demonstrates the complexity and meticulousness required to develop advanced bone fracture healing solutions.

The main findings can be summarized as follow: In the first research study, the main findings encompassed the demonstration of bone properties and the mechanisms governing fracture healing. Additionally, the research shed light on the current treatments employed in bone fracture repair. It delved into discussions surrounding bone scaffold design, materials, and the necessary growth factors. Furthermore, the study critically reviewed and compared conventional and additive manufacturing technologies for bone scaffold fabrication, while highlighting their respective limitations. In the second research, a novel Fused Deposition Modelling (FDM) biomaterial filament was successfully developed through a process that entailed preparing a composite of polylactic acid (PLA) and calcium peroxide (CPO) using wet solution mixing and hot melt extrusion. This study also optimized the parameters of the hot melt extruder to ensure the fabrication of 3D printable composite filaments. The research involved a rheological examination, revealing that an increase in CPO content led to increased viscosity at 200 ºC. Additionally, microstructural analysis showed a transition from crystalline to amorphous structures in the PLA/CPO samples. Notably, the mechanical strength and ductility of the composite filaments experienced a decrease, except for the 6% CPO filament, which demonstrated an exception. The 6% CPO filament made of PLA/CPO stood out by exhibiting superior printing quality and improved mechanical properties when compared to other CPO ratios. In the third research phase, the prepared filaments underwent comprehensive characterization, focusing on various aspects, including the presence of calcium peroxide, the

release of oxygen, porosity, and antibacterial properties. Notably, data obtained from scanning electron microscopy and X-ray diffraction illustrated the stability of calcium peroxide within the composite. Furthermore, the study unveiled that CPO ratios of 6% and below exhibited a more favorable release profile in comparison to higher ratios. This outcome could be attributed to the homogeneous distribution of CPO particles within the PLA matrix. Filaments containing CPO ratios lower than 6% also displayed increased and symmetrical porosity, a result of the dissolution of CPO particles. Impressively, CPO ratios of 6% and higher exhibited antibacterial activity against Gram-positive bacteria. In the fourth research phase, an in-depth exploration of Fused Deposition Modelling (FDM) 3D printing processes was conducted, with a specific focus on optimizing these processes for the 6% CPO composite filament to achieve the high-quality fabrication of bone scaffolds. The scaffolds produced were in a square shape, measuring 8x8 mm in length and width, and with a height of 1.5 mm. The scaffolds had a 25% porosity and pores with a size of 0.60 mm. The study determined that the highest printing quality was attained at a printing speed of 75 mm/s, while maintaining a printing nozzle temperature of 200°C. Additionally, the research observed that the produced samples underwent differentiation into bone, which was further augmented when supplemented with osteogenic media. In the presence of vitamin D, the study identified the upregulation of critical bone transcription factors essential for bone differentiation, including RUNX2, SPP1, and SP7, while simultaneously noting the downregulation of COL1A1. Furthermore, a distinct increase in the expression of RUNX2 genes was detected in human mesenchymal stem cells (hMSC) cultured within these scaffolds. Mechanical properties were significantly enhanced following cell culturing, with an approximate increase of 2 MPa in stress and 0.7% in strain when compared to samples without mesenchymal cells. Interestingly, the tensile strength of scaffolds lacking vitamin D was found to be higher than those with vitamin D by approximately 1.2 MPa, and even greater when compared to samples without mesenchymal cells, displaying an increase

of approximately 2 MPa. These findings highlight the remarkable potential of the 6% CPO composite filament in producing enhanced bone scaffolds with impressive mechanical and biological attributes.

6.2 Future research

The studies undertaken in this thesis have focused on the development of a biomedical printable PLA/CPO composite filament tailored for use in fused deposition modelling (FDM) for 3D printing bone scaffolds capable of oxygen generation. The effect of different ratios of calcium peroxide (CPO) and manufacturing parameters were assessed in terms of manufacturing process, mechanical properties, and biological activities.

In future research, there is room for further investigation into several key areas. These areas include investigating the precise oxygen levels necessary to facilitate the most favorable conditions for optimal bone cell proliferation, along with the growth of surrounding cells associated with vasculature, which is a critical endeavor. Furthermore, it is important to delve into the repercussions of oxygen levels that are either excessively abundant or grossly inadequate on the viability and expansion of these cells. An additional avenue for exploration involves fine-tuning the degradation timeline of the PLA/CPO bone scaffold to synchronize it with natural bone growth. This innovative approach offers a promising opportunity to further enhance the efficacy of bone tissue engineering. The degradation period of a scaffold is a crucial factor in the success of regenerative treatments. In the context of PLA/CPO scaffolds, this refers to the rate at which the scaffold material breaks down within the body. By strategically adjusting this degradation period, researchers can align it more closely with the intricacies of the bone growth process, ensuring that the scaffold provides necessary support during the entire duration of bone tissue regeneration.

Moreover, the mechanical properties of a scaffold, such as its strength, stiffness, and flexibility, play an integral role in its performance within the body. Understanding how these properties transform over time is vital for ensuring that the scaffold maintains its structural integrity and adequately supports the regenerating bone tissue. As the body's regenerative processes gradually restore and replace the scaffold with natural bone tissue, the mechanical characteristics of the scaffold are bound to evolve. Furthermore, it is fundamental to address the imperative requirement for the mechanical properties of the scaffold, with a specific emphasis on achieving the requisite strength levels tailored to the diversity of bones throughout the human body. This aspect of scaffold development represents a critical challenge in the field of regenerative bone tissue engineering.

Lastly, it is imperative to underscore the necessity for an in-depth in vivo assessment of the PLA/CPO bone scaffold in prospective research endeavors. This critical phase in the research process plays a pivotal role in bridging the gap between laboratory-based investigations and real-world clinical applications, allowing us to gain a comprehensive understanding of how the scaffold performs within a living organism. It will also allow us to examine the potential long-term side effects of PLA on the body.